# Response to the comments by Co-Editor, Referee 1 and Referee 2.

According to Co-Editor's comments, the spelling is changed from "Setchenow" to "Sechenov" through the manuscript.

The response to Referee 1 and Referee 2 follows sequence: (1) comments from Co-Editor and Referees, (2) author's response, (3) author's changes in manuscript.

The author's changes are marked in blue. In addition, I provide a marked-up manuscript version showing the changes made (using track changes in Word).

I will reply to each comment as follows.

# 1. To the comments by Referee 1:

Thank you very much for the constructive comments.

I will reply to each comment as follows.

**R1-1 ----------**

(1) comments from Referee 1

A glance at Figure 2 gives the reassuring impression that random errors are quite small for both the IGS and PRV-HS methods. However, there is a small but significant difference in the results at the one temperature where both techniques are used. This shows a systematic error in one or both of the methods.

(2) author's response

Thank you for the comment. Evaluation of systematic errors or potential systematic bias is also commented by Referee 2. Potential systematic bias of values of $K_{eq}$ determined are estimated to be within ±2% in the IGS method and within ±4% in the PRV-HS method, as described in the revised manuscript.

In the original manuscript, error bars in Fig. 2 represent statics errors (*error_S*) only. I revise Fig. 2 by plotting the data with error bars (*error_T*) representing both *error_S* and potential systematic bias (*error_B*). Values of *error_T* are calculated by (*error_S* + *error_B*) rather than $\sqrt{(error\_S)^2 + (error\_B)^2}$ because *error_B* is potential systematic bias. Tables 1, S1 and 3 list *error_T* as well as *error_S* in the revised manuscript. Fig. 4 is also revised by plotting the data with error bars (*error_T*). Error bars of values of $\frac{F}{k_1 RTV}$ in Figs. 1, 3, S5, S6, S7, and S8 are explained in the captions.

As seen in Fig. 2 in the revised manuscript, potential systematic bias in both the PRV-HS method and the IGS method could be a reason why there is the small offset between PRV-HS and IGS method at 312 K

(3) author's changes in manuscript

lines 13-17, page 5

As described in *Results and discussion* (Sect. 3.1), $CH_2F_2$ in the headspace over the test solution was not expected to be redistributed into the test solution. Hence Eq. (6) was used to deduce $K_{eq}(T)$ from $k_1$. Errors of $T$ are estimated to be within ±0.2 K. These errors of $T$ may give potential systematic bias of ca. ±1% ($\delta K_{eq}/K_{eq}$) where $\delta K_{eq}$ is error of the value of $K_{eq}$. Errors of $F$ are estimated to be less than 1.4 %, and theses errors may give potential systematic bias of less than 1.4 % ($\delta K_{eq}/K_{eq}$). Accordingly, for the IGS methods, values of $K_{eq}$ may have potential systematic bias of ca. ±2%.

lines 4-7, page 7

Errors of $T$ are estimated to be within ca. 2 K. These errors of $T$ may give potential systematic bias of ca. ±4% ($\delta K_{eq}/K_{eq}$) at 313 K and ca. ±3% ($\delta K_{eq}/K_{eq}$) at 353 K. Errors of $V_0$ are estimated to be less than 1 %, and these errors may give potential systematic bias of less than 1 % ($\delta K_{eq}/K_{eq}$). Accordingly, for the PRV-HS methods, values of $K_{eq}$ may have potential systematic bias of ca. ±4%.

lines 3-9, page 8

Figure 2 plots the average $K_H$ values for the $V$ value of 0.350 $dm^3$ against $100/T$. Error bars of the data represent both 2σ for the average and potential systematic bias (±2%). Figure 2 also displays the $K_H(T)$ values obtained by the PRV-HS method. The results of the PRV-HS experiments are described in *Supporting Information* (Fig. S3, Fig. S4 and Table S1). The $K_H$ value obtained by the PRV-HS experiments at each temperature and its error were estimated at 95% confidence level by fitting the two datasets at each temperature (Fig. S4) simultaneously by means of the nonlinear least-squares method with respect to Eq. (11). Error bars of the data by PRV-HS method in Fig. 2 represent both errors at 95% confidence level for the regression and potential systematic bias (±4%).

Caption, Fig. 1

Plots of values of $F/(k_1RTV)$ against $F$ at each temperature for 0.350 $dm^3$ and 0.300 $dm^3$ of deionized water. Error bars represent 2σ due to errors of values of $k_1$ as described in Sect. S2 in Supporting Information. Grey symbols represent the data excluded for calculating the average.

Caption, Fig. 3

Plots of values of $F/(k_1RTV)$ against $F$ at each temperature for 0.35 $dm^3$ of a-seawater at 36.074‰. Grey symbols represent the data excluded for calculating the average. Error bars represent 2σ due to errors of values of $k_1$ as described in Sect. S2 in Supporting Information. Grey symbols represent the data excluded for calculating the average.

Caption, Fig. S5

Plots of values of $F/(k_1RTV)$ against $F$ at each temperature for 0.35 $dm^3$ of a-seawater at 4.452‰. Error bars represent 2σ due to errors of values of $k_1$ as described in Sect. S2. Grey symbols represent the data excluded for calculating the average.

Caption, Fig. S6

Plots of values of $F/(k_1RTV)$ against $F$ at each temperature for 0.35 $dm^3$ of a-seawater at 8.921‰. Error bars represent 2σ due to errors of values of $k_1$ as described in Sect. S2. Grey symbols represent the data excluded for calculating the average.

Caption, Fig. S7

Plots of values of $F/(k_1RTV)$ against $F$ at each temperature for 0.35 $dm^3$ of a-seawater at 21.520‰. Error bars represent 2σ due to errors of values of $k_1$ as described in Sect. S2. Grey symbols represent the data excluded for calculating the average.

Caption, Fig. S8

Plots of values of $F/(k_1RTV)$ against $F$ at each temperature for 0.35 $dm^3$ of a-seawater at 51.534‰. Error bars represent 2σ due to errors of values of $k_1$ as described in Sect. S2. Grey symbols represent the data excluded for calculating the average.

Fig. 2

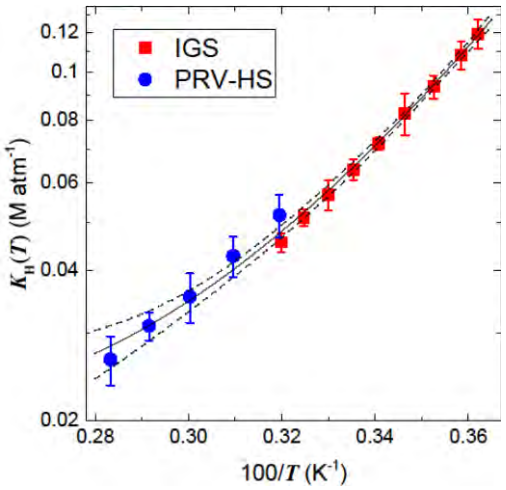


**Figure 2. van't Hoff plot of the $K_H$ values obtained by the IGS method and the PRV-HS method. Bold curve displays the fitting of the data obtained by the IGS method and the PRV-HS method (Eq. (13)). Dashed curves display upper and lower 95% confidence limit of the above fitting by Eq. (12). Error bars of the data by the IGS method represent both 2σ for the average and potential systematic bias (±2%). Error bars of the data by PRV-HS method represent both errors at 95% confidence level for the regression and potential systematic bias (±4%).**

Fig. 4

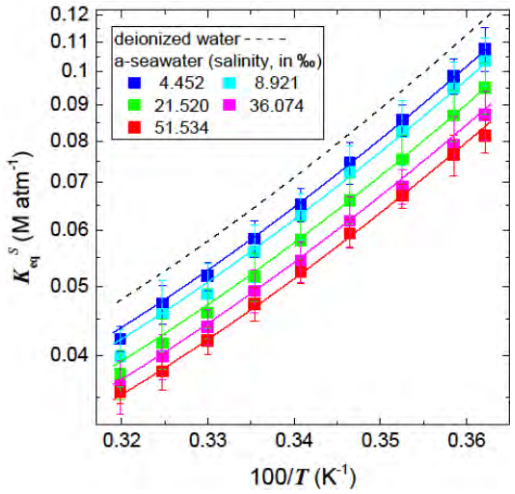


**Figure 4. van't Hoff plot of the $K_{eq}^{S}$ values for a-seawater at each salinity. Dashed curve represents the $K_H$ values by Eq. (13). Bold curves represent the fitting obtained by Eq. (23). Error bars of the data represent both 2σ for the average and potential systematic bias (±2%).**

Table 1

**Table 1. The average of values of $F/(k_1RTV)$ obtained for $V$ value of 0.350 dm$^3$ and 0.300 dm$^3$ and the $K_H(T)$ value derived from Eq. (13) at each temperature. $N$ represents number of experimental runs for the average.**

| $T$ (K) | $F/(k_1RTV)$ | | | | $K_H(T)$ (M atm$^{-1}$) |
|---|---|---|---|---|---|
| | $V$ = 0.350 | | $V$ = 0.300 | | |
| | average [a, b] | $N$ [c] | average [a] | $N$ [c] | From Eq. (13) [d, e] |
| 276.15 | 0.119 ± 0.006 (0.008) | 21 (2) | 0.117 ± 0.006 (0.008) | 11 (0) | 0.119 ± 0.003 (0.005) |
| 278.35 | 0.107 ± 0.005 (0.007) | 18 (3) | 0.110 ± 0.005 (0.007) | 14 (0) | 0.111 ± 0.002 (0.004) |
| 283.65 | 0.093 ± 0.003 (0.005) | 27 (5) | 0.092 ± 0.001 (0.003) | 5 (0) | 0.094 ± 0.002 (0.004) |
| 288.65 | 0.082 ± 0.006 (0.008) | 41 (5) | 0.084 ± 0.006 (0.008) | 12 (0) | 0.082 ± 0.002 (0.004) |
| 293.45 | 0.071 ± 0.001 (0.002) | 15 (8) | 0.071 ± 0.001 (0.002) | 5 (0) | 0.072 ± 0.002 (0.003) |
| 298.15 | 0.064 ± 0.002 (0.003) | 30 (6) | 0.067 ± 0.005 (0.006) | 12 (0) | 0.065 ± 0.002 (0.003) |
| 303.05 | 0.057 ± 0.003 (0.004) | 16 (0) | 0.056 ± 0.005 (0.006) | 4 (0) | 0.058 ± 0.002 (0.003) |
| 307.95 | 0.051 ± 0.001 (0.002) | 12 (6) | 0.054 ± 0.004 (0.005) | 10 (0) | 0.052 ± 0.002 (0.003) |
| 312.65 | 0.046 ± 0.001 (0.002) | 13 (3) | 0.047 ± 0.001 (0.002) | 4 (0) | 0.048 ± 0.001 (0.002) |

a. Errors are 2σ for the average only.; b. Number in parenthesis represents an error reflecting both 2σ for the average and potential systematic bias (±2%).; c. Number in parenthesis represents number of experimental runs excluded for the average.; d. Errors are 95% confidence level for the regression only.; e. Number in parenthesis represents an error reflecting both errors at 95% confidence level for the regression and potential systematic bias (±2%).

Table S1

**Table S1. $L_i$ values for various $V_i/V_0$ ratios at various temperatures, slopes and intercepts for linear regression with respect to Eq. (10), $K_H(T)$ values calculated from the slopes and intercepts, and $K_H(T)$ values and the errors at 95% confidence level estimated by non-linear fitting the two datasets simultaneously at each temperature (Fig. S4) with respect to Eq. (11).**

| $T$ (K) | $L_i$ (a.u.) [a] | | | | | | Eq. (10) Intercept | Eq. (10) Slope | $K_H$ (M atm$^{-1}$) | | |
|---|---|---|---|---|---|---|---|---|---|---|---|
| | $V_i/V$ = 0.421 | 0.351 | 0.280 | 0.210 | 0.140 | 0.070 | | | Eq. (10) | Eq. (11) [b, c] | Eq. (13) [b] |
| 353 | 3.226±0.002 | 3.270±0.026 | 3.330±0.004 | 3.391±0.008 | 3.462±0.014 | 3.526±0.009 | 3.581 | –0.870 | 0.026 | 0.027 ±0.002 (±0.003) | 0.028 ±0.003 |
| | 2.044±0.006 | 2.050±0.012 | 2.112±0.010 | 2.132±0.009 | 2.186±0.021 | 2.209±0.011 | 2.248 | –0.513 | 0.027 | | |
| 343 | 3.000±0.018 | 3.025±0.009 | 3.070±0.008 | 3.089±0.015 | 3.117±0.015 | 3.148±0.018 | 3.179 | –0.423 | 0.031 | 0.031 ±0.001 (±0.002) | 0.031 ±0.002 |
| | 1.949±0.004 | 1.955±0.005 | 1.968±0.003 | 1.998±0.004 | 2.020±0.002 | 2.030±0.009 | 2.050 | –0.258 | 0.031 | | |
| 333 | 3.247±0.018 | 3.234±0.018 | 3.243±0.015 | 3.241±0.010 | 3.247±0.009 | 3.223±0.013 | 3.231 | 0.034 | 0.037 | 0.036 ±0.003 (±0.004) | 0.035 ±0.002 |
| | 3.080±0.009 | 3.044±0.006 | 3.082±0.005 | 3.127±0.009 | 3.113±0.008 | 3.134±0.014 | 3.149 | –0.213 | 0.034 | | |
| 323 | 3.208±0.011 | 3.190±0.008 | 3.133±0.010 | 3.134±0.011 | 3.092±0.008 | 3.093±0.006 | 3.055 | 0.355 | 0.042 | 0.043 ±0.002 (±0.004) | 0.040 ±0.001 |
| | 3.357±0.010 | 3.289±0.014 | 3.275±0.005 | 3.233±0.004 | 3.226±0.016 | 3.160±0.001 | 3.135 | 0.496 | 0.044 | | |
| 313 | 3.245±0.018 | 3.185±0.013 | 3.100±0.015 | 3.022±0.012 | 2.995±0.012 | 2.915±0.011 | 2.848 | 0.935 | 0.052 | 0.052 ±0.003 (±0.005) | 0.047 ±0.001 |
| | 2.162±0.031 | 2.134±0.010 | 2.060±0.014 | 2.029±0.018 | 1.992±0.010 | 1.925±0.018 | 1.896 | 0.612 | 0.052 | | |

a. Errors are 2σ for the regression only.; b. Errors are those at 95% confidence level for the regression only.; c. Number in parenthesis represents both errors at 95% confidence level for the regression and potential systematic bias (±4%).

Table 3

**Table 3. The average of values of $F/(k_1RTV)$ obtained for $V$ value of 0.350 dm$^3$ and the $K_{eq}^S(T)$ value derived from Eq. (23) at each salinity and temperature. $N$ represents number of experimental runs for the average.**

| $T$ (K) | $K_{eq}^S$ (M atm$^{-1}$) | | | | | |
|---|---|---|---|---|---|---|
| | salinity, 4.452 ‰ | | | salinity, 8.921 ‰ | | |
| | average [a, b] | $N$ [c] | Eq. (23) [d, e] | average [a, b] | $N$ [c] | Eq. (23) [d, e] |
| 276.15 | 0.108 ± 0.006 (0.008) | 8 (0) | 0.107 ± 0.003 (0.005) | 0.103 ± 0.006 (0.008) | 21 (0) | 0.103 ± 0.003 (0.005) |
| 278.35 | 0.099 ± 0.004 (0.006) | 12 (0) | 0.100 ± 0.002 (0.005) | 0.095 ± 0.006 (0.008) | 26 (1) | 0.096 ± 0.002 (0.004) |
| 283.65 | 0.086 ± 0.003 (0.005) | 9 (0) | 0.085 ± 0.002 (0.004) | 0.083 ± 0.007 (0.009) | 24 (0) | 0.082 ± 0.002 (0.004) |
| 288.65 | 0.075 ± 0.004 (0.006) | 12 (0) | 0.074 ± 0.002 (0.003) | 0.072 ± 0.005 (0.006) | 33 (0) | 0.071 ± 0.001 (0.002) |
| 293.45 | 0.065 ± 0.002 (0.003) | 10 (0) | 0.066 ± 0.002 (0.003) | 0.063 ± 0.003 (0.004) | 27 (5) | 0.063 ± 0.002 (0.003) |
| 298.15 | 0.058 ± 0.002 (0.003) | 13 (0) | 0.059 ± 0.002 (0.003) | 0.056 ± 0.004 (0.005) | 26 (2) | 0.056 ± 0.002 (0.003) |
| 303.05 | 0.052 ± 0.001 (0.002) | 8 (0) | 0.053 ± 0.002 (0.003) | 0.049 ± 0.004 (0.005) | 14 (6) | 0.051 ± 0.001 (0.002) |
| 307.95 | 0.047 ± 0.002 (0.003) | 13 (1) | 0.048 ± 0.001 (0.002) | 0.046 ± 0.004 (0.005) | 23 (1) | 0.046 ± 0.001 (0.002) |
| 312.65 | 0.042 ± 0.001 (0.002) | 7 (0) | 0.044 ± 0.001 (0.002) | 0.040 ± 0.003 (0.004) | 12 (8) | 0.042 ± 0.001 (0.002) |

| $T$ (K) | $K_{eq}^S$ (M atm$^{-1}$) | | | | | |
|---|---|---|---|---|---|---|
| | salinity, 21.520 ‰ | | | salinity, 36.074 ‰ | | |
| | average [a, b] | $N$ [c] | Eq. (23) [d, e] | average [a, b] | $N$ [c] | Eq. (23) [d, e] |
| 276.15 | 0.095 ± 0.006 (0.008) | 20 (0) | 0.095 ± 0.003 (0.005) | 0.088 ± 0.005 (0.007) | 21 (0) | 0.089 ± 0.002 (0.004) |
| 278.35 | 0.087 ± 0.005 (0.007) | 22 (0) | 0.088 ± 0.002 (0.004) | 0.079 ± 0.006 (0.008) | 20 (3) | 0.083 ± 0.002 (0.004) |
| 283.65 | 0.075 ± 0.004 (0.006) | 15 (1) | 0.076 ± 0.001 (0.003) | 0.069 ± 0.002 (0.003) | 18 (2) | 0.071 ± 0.001 (0.002) |
| 288.65 | 0.066 ± 0.004 (0.005) | 20 (0) | 0.066 ± 0.001 (0.002) | 0.062 ± 0.004 (0.005) | 19 (4) | 0.062 ± 0.001 (0.002) |
| 293.45 | 0.058 ± 0.003 (0.004) | 14 (0) | 0.058 ± 0.001 (0.002) | 0.054 ± 0.002 (0.003) | 19 (4) | 0.055 ± 0.001 (0.002) |
| 298.15 | 0.052 ± 0.003 (0.004) | 20 (0) | 0.052 ± 0.001 (0.002) | 0.049 ± 0.002 (0.003) | 24 (4) | 0.049 ± 0.001 (0.002) |
| 303.05 | 0.046 ± 0.003 (0.004) | 16 (0) | 0.047 ± 0.001 (0.002) | 0.044 ± 0.002 (0.003) | 16 (0) | 0.044 ± 0.001 (0.002) |
| 307.95 | 0.042 ± 0.003 (0.004) | 16 (0) | 0.043 ± 0.001 (0.002) | 0.040 ± 0.002 (0.003) | 15 (2) | 0.040 ± 0.001 (0.002) |
| 312.65 | 0.038 ± 0.002 (0.003) | 16 (0) | 0.039 ± 0.001 (0.002) | 0.036 ± 0.002 (0.003) | 16 (0) | 0.037 ± 0.001 (0.002) |

| $T$ (K) | $K_{eq}^S$ (M atm$^{-1}$) | | |
|---|---|---|---|
| | salinity, 51.534 ‰ | | |
| | average [a, b] | $N$ [c] | Eq. (23) [d, e] |
| 276.15 | 0.081 ± 0.003 (0.005) | 10 (0) | 0.084 ± 0.002 (0.004) |
| 278.35 | 0.077 ± 0.003 (0.005) | 15 (0) | 0.078 ± 0.002 (0.004) |
| 283.65 | 0.067 ± 0.001 (0.003) | 9 (1) | 0.067 ± 0.001 (0.002) |
| 288.65 | 0.059 ± 0.002 (0.003) | 14 (1) | 0.059 ± 0.001 (0.002) |
| 293.45 | 0.052 ± 0.001 (0.002) | 7 (3) | 0.052 ± 0.001 (0.002) |
| 298.15 | 0.047 ± 0.002 (0.003) | 15 (0) | 0.047 ± 0.001 (0.002) |
| 303.05 | 0.042 ± 0.001 (0.002) | 8 (0) | 0.042 ± 0.001 (0.002) |
| 307.95 | 0.038 ± 0.002 (0.003) | 12 (0) | 0.038 ± 0.001 (0.002) |
| 312.65 | 0.036 ± 0.001 (0.002) | 7 (1) | 0.035 ± 0.001 (0.002) |

a. Errors are 2σ for the average only.; b. Number in parenthesis represents an error reflecting both 2σ for the average and potential systematic bias (±2%).; c. Number in parenthesis represents number of experimental runs excluded for the average.; d. Errors are 95% confidence level for the regression only.; e. Number in parenthesis represents an error reflecting both errors at 95% confidence level for the regression and potential systematic bias (±2%).

**R1-2 ----------**

(1) comments from Referee 1

In the fitting equation, equation 13, the number of significant figures reported is much higher than justified for the relatively small number of data points. In nonlinear fitting of this type, most programs report the variance associated with each of the fitting coefficients. If the square-root-of-variance is not small compared to the fitting coefficient, that means that the inclusion of that coefficient is probably not justified.

(2) author's response

Thank you for the comments. According to Referee 1's comment, I revise the significant figure of each fitting coefficient in Eq. (13). I set the least digit of the significant figure to the second decimal place so that the values calculated by Eq. (13) are consistent with the significant figure of $K_H$.

Thank you for the suggestion that the square-root-of-variance of the fitting coefficient should be checked for justifying whether the coefficient should be included in the van't Hoff equation.

The square-root-of-variance, that is, standard deviation for each fitting coefficient in Eq. (12) justifies the three-term van't Hoff equation. The standard deviation for each fitting coefficient is described in the revised manuscript. Because the ratio of $2\times\delta a_3/a_3$ is 0.293, the three-term van't Hoff equation is thus justified.

In addition, even if the data only in the IGS method is fitted separately, a three-term fit to the data in the IGS method would be justified as Eq. (A1), although errors of the fitting coefficients are larger than those in Eq. (13).

$$\ln(K_H(T)) = (-41.7 \pm 7.2) + (66.8 \pm 10.5) \times \left(\frac{100}{T}\right) + (15.1 \pm 3.7) \times \ln\left(\frac{T}{100}\right) \quad \text{(A1)}$$

where errors of the fitting coefficients represent standard deviation only for non-linear fitting.

(3) author's changes in manuscript

lines 14-16, page 8

$$\ln\left(K_H(T)\right) = -49.71 + 77.70 \times \left(\frac{100}{T}\right) + 19.14 \times \ln\left(\frac{T}{100}\right) \quad (13).$$

The square-root-of-variance, that is, standard deviation for each fitting coefficient in Eq. (12) is as follows:

$\delta a_1 = 5.5$; $\delta a_2 = 8.3$; $\delta a_3 = 2.8$.

**R1-3 ----------**

(1) comments from Referee 1

The treatment of the salting-out effect is overworked. In Referee 1's opinion, lines 9-26, page 9 should be eliminated and the author should simply state that $\ln(K_H/K_{eq})$ varies close to the 0.5 power of salinity, in contrast to the Sechenov.

(2) author's response

Thank you for the constructive comments. I agree the comment that the treatment of the salting-out effect is overworked. I followed the referee's opinion and found that all the data in Fig. 5 could be fitted using only one parameter (Eq. (22)) as described in the revised manuscript.

In the revised manuscript, error bars in Fig. 5 reflect *error_T* (R1-1) and Figs. 4 (shown in R1-2) and 6 are redrawn according to Eq. (23).

(3) author's changes in manuscript

lines 10-12, page 1, Abstract

The salinity dependence of $K_{eq}^{S}$ (the salting-out effect), $\ln(K_H/K_{eq}^{S})$, did not obey the Sechenov equation but was proportional to $S^{0.5}$. Overall, the $K_{eq}^{S}(T)$ value was expressed by $\ln(K_{eq}^{S}(T)) = -49.71 + (77.70 - 0.134 \times S^{0.5}) \times (100/T) + 19.14 \times \ln(T/100)$.

lines 2-17, page 10

This result suggests that $\ln(K_H(T)/K_{eq}^{S}(T))$ varied according to Eq. (18):

$$\ln(K_H(T)/K_{eq}^{S}(T)) = k_{s1} S^{0.5} \quad (18)$$

Values of $k_{s1}$ may be represented by the following function of $T$:

$$k_{s1} = b_1 + b_2 \times (100/T) \quad (19)$$

Parameterizations of $b_1$ and $b_2$ obtained by fitting all the $\ln(K_H(T)/K_{eq}^{S}(T))$ and $S$ data at each temperature simultaneously by means of the nonlinear least-squares method gives Eq. (20).

$$\ln(K_H(T)/K_{eq}^{S}(T)) = (0.0127 + 0.0099 \times (100/T)) \times S^{0.5} \quad (20)$$

The standard deviation for each fitting coefficient in Eq. (19) is as follows:

$\delta b_1 = 0.0106$; $\delta b_2 = 0.0031$.

Since $2 \times \delta b_1 > b_1$, the parameterization by Eq. (19) may be overworked. Accordingly, all the $\ln(K_H(T)/K_{eq}^{S}(T))$ and $S$ data at each temperature are fitted simultaneously using Eq. (21) instead of Eq. (19). The nonlinear least-squares method gives Eq. (22).

$$k_{s1} = b_2 \times (100/T) \quad (21)$$

$$\ln(K_H(T)/K_{eq}^{S}(T)) = 0.134 \times (100/T) \times S^{0.5} \quad (22)$$

The standard deviation for the fitting coefficient in Eq. (21) is as follows: $\delta b_2 = 0.001$. As seen in Fig. 5, Eqs. (21) and (22) reproduced the data well.

lines 25-26, page 10

In Eq. (22), $K_H(T)$ is represented by Eq. (13), as described in Sect. 3.1. Therefore ${K_{eq}}^S(T)$ is represented by Eq. (23):

$$\ln({K_{eq}}^S) = -49.71 + (77.70 - 0.134 \times S^{0.5}) \times \left(\frac{100}{T}\right) + 19.14 \times \ln\left(\frac{T}{100}\right) \quad (23)$$

Fig 6

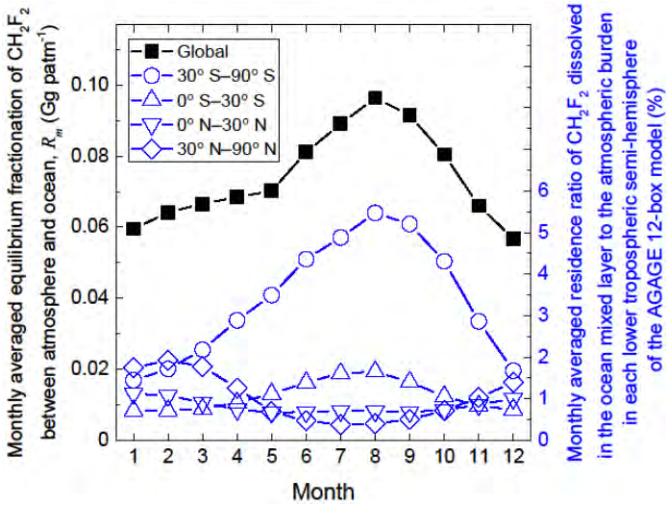


**Figure 6. Plots of monthly averaged equilibrium fractionation of $CH_2F_2$ between atmosphere and ocean, $R_m$ (Gg patm$^{-1}$) in the global and the semi-hemispheric atmosphere. Right vertical axis represents monthly averaged residence ratio of $CH_2F_2$ dissolved in the ocean mixed layer to the atmospheric burden for each lower tropospheric semi-hemisphere of the AGAGE 12-box model.**

**R1-4** ----------

(1) comments from Referee 1

On page 3, lines11-12 (in the revised manuscript), the water quality should be indicated as (resistivity > 18 megohm-cm).

(2) author's response

Thank you for the comment. I correct the text according to the comment.

(3) author's changes in manuscript

lines 11-12, page 3

Water was purified with a Milli-Q Gradient A10 system (resistivity > 18 megohm-cm).

**R1-5** ----------

(1) comment from Referee 1

On page 7, line 1 (in the revised manuscript), "non-linear" is misspelled.

(2) author's response

Thank you for the comment. I correct the text according to the comment.

(3) author's changes in manuscript

lines 1-2, page 7

Furthermore, values of $K_{eq}(T)$ and errors of them were determined by nonlinear fitting of the data of $L_i$ and $V_i/V$ by means of Eq. (11), which was obtained from Eq. (10):

## 2. To the comments by Referee 2:

Thank you very much for the constructive comments.

I will reply to each comment as follows.

**R2-1** ----------

(1) comments from Referee 2

The manuscript would benefit from an explicit discussion of experimental error. What are the parameters that limit the accuracy of the inert-gas stripping (IGS) method? Of the stripping column apparatus? And of the phase ratio variation headspace method (PRV-HS)? Do error bars reflect statics only, or also potential sources of systematic bias?

(2) author's response

Thank you for the comment. I reply to the comments in the sequence: (i) on the parameters that limit the accuracy of the IGS method; (ii) on the parameters that limit the accuracy of the PRV-HS method; and (ii) on error bars.

(i) the parameters that limit the accuracy of the IGS methods

The parameters that limit the accuracy of the IGS methods are temperature of the test solution ($T$) and flow rate of purge gas ($F$).

The accuracy of $T$ ($\delta T$) are within 0.2 K and may give potential systematic bias of ±0.5 to ±0.6 % ($\delta K_{eq}/K_{eq}$), where $\delta K_{eq}$ indicates an error of $K_{eq}$.

For $F$, the accuracy of $F_{meas}$ is estimated to be within 1% from the accuracy of the high-precision film flow meter SF-1U with VP-2U used for calibrating the soap flow meter. Errors in the term of $\frac{P_{\mathrm{meas}}-h_{\mathrm{meas}}}{P_{\mathrm{hs}}-h} \times \frac{T}{T_{\mathrm{meas}}}$ in Eq (3) are estimated at ca. ±1 %. Hence, the accuracy of $F$ ($\delta F$) are estimated to be within 1.4 % and may give potential systematic bias of ±1.4 % of $\delta K_{eq}/K_{eq}$.

Values of $\delta K_{eq}/K_{eq}$ due to both $\delta T$ and $\delta F$ may thus have potential systematic bias of ca. ±2%.

(ii) the parameters that limit the accuracy of the PRV-HS methods

The parameters that limit the accuracy of the PRV-HS methods are temperature of the test solution ($T$) and volume of the vials used ($V$).

Although the apparatus used (Agilent, HP7694) was expected to keep $T$ constant, the accuracy of $T$ may not be certified. I have applied the same apparatus to determination of the $K_H$ values for some HCFCs such as HCFC-123 using the PRV-HS methods [Kutsuna, S. *Int. J. Chem. Kinet.*, 45, 440-451, 2013]. On the basis of the $K_H$ values thus determined and comparison between them and the reported values for HCFC-123, errors of $T$ are estimated to be within ca. 2 K. These errors of $T$ may give potential systematic bias of ca. ±4 % ($\delta K_{eq}/K_{eq}$) at 313 K and ca. ±3 % ($\delta K_{eq}/K_{eq}$) at 353 K.

Errors for $V$ ($\delta V$) are estimated to be less than 1 %, and these errors may give potential systematic bias of less than 1 % of $\delta K_{eq}/K_{eq}$.

Accordingly, for the PRV-HS methods, values of $\delta K_{eq}/K_{eq}$ due to both $\delta T$ and $\delta V$ may have potential systematic bias of ca. ±4%.

(iii) Error bars in Figure 2

Error bars in Figure 2 reflect statics only (*error_S*) in the original manuscript. Error bars in Figure 2m represent errors (*error_T*) reflecting both *error_S* and potential systematic bias (*error_B*). Values of *error_T* are also indicated in Tables 1m, S1m and 3m. Values of *error_T* are calculated by (*error_S* + *error_B*) rather than $\sqrt{(error\_S)^2 + (error\_B)^2}$ because *error_B* is potential systematic bias.

(3) author's changes in manuscript

The change in manuscript is the same as described in R1-1.

**R2-2 ----------**

(1) comments from Referee 2

There does appear to be a small -yet significant- offset between PRV-HS and IGS method in Figure 2. Why IGS is believed to be more accurate?

(2) author's response

Thank you for the comment. There appears to be a small - yet significant - offset between PRV-HS and IGS method at 312 K. This point is also commented by Referee 1. For the PRV-HS methods, values of $\delta K_{eq}/K_{eq}$ may have potential systematic bias of ca. ±4%, which results mostly from the accuracy of temperature of the test solution, as aforementioned (R2-1). For the IGS method, values of $\delta K_{eq}/K_{eq}$ may have potential systematic bias of ca. ±2%. The IGS method is thus believed to be more accurate. Potential systematic bias in both the PRV-HS method and the IGS method could be a reason why there is the small offset between PRV-HS and IGS method at 312 K.

(3) author's changes in manuscript

The change in manuscript related to this comment is included in the changes described in R1-1.

**R2-3 ----------**

(1) comments from Referee 2

Does the fit according to (Eq (13)) take into account the relative weight of error bars?

(2) author's response

Thank you for the comment. The fit according to Eq. (13) does not take into account the relative weight of error bars. This is clearly described in the revised manuscript.

(3) author's changes in manuscript

lines 10-11, page 8:

All the $K_H$ values were regressed with respect to the van't Hoff equation (Eq. (12)) with no weighting (Clarke and Glew, 1965; Weiss, 1970):

**R2-4 ----------**

(1) comments from Referee 2

What is the reason for the large variation in the size of error bars in Fig. 5?

(2) author's response

Thank you for the comment. As Referee 2 comments, there are the large variation in the size of error bars in Fig. 5. Ratio among error bars of the data at the same temperature is up to maximum value of 4.5: error bars are 0.084 for 8.921‰ and 0.019 for 51.534‰ at 10.5 °C. Error bars for the data at 8.921‰ tend to be large and error bars for the data at 51.534‰ tend to be small: this reflects statics errors of the data at 8.921‰ and 51.534‰.

Errors of the data in Fig. 5 represents statics only (*error_S*, as shown in R2-1). As replied in R2-1, errors from both statics (*error_S*) and potential systematic bias of ±2% (*error_B*) will be used as errors (*error_T*) for the data in Fig. 5: (*error_T*) = (*error_S*) + (*error_B*). In the revised manuscript, error bars of the data in Fig. 5 represent *error_T*. As seen in Fig. 5 in the revised manuscript, the ratios among error bars of the data at the same temperature are smaller than the corresponding ratios in Fig. 5 in the original manuscript. For example, the ratio of error bars between at 8.921‰ and 51.534‰ at 10.5 °C is 2.7 while it is 4.5 in the original manuscript as aforementioned.

In the revised manuscript, error bars will be represented by *error_T* in Fig. 5.

(3) author's changes in manuscript

Figure 5:

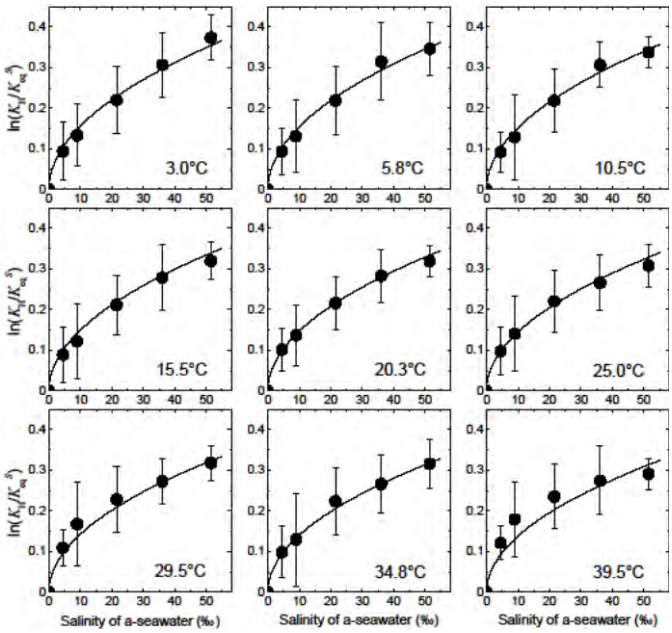


**Figure 5. Plots of $\ln(K_H(T)/K_{eq}^S(T))$ vs. salinity in a-seawater at each temperature. Bold curves represent the fitting obtained by Eq. (22). Error bars represent errors reflecting both 2σ for the average and potential systematic bias (±2%) of $K_{eq}^S$.**

**R2-5 ----------**

(1) comments from Referee 2

The $S^{0.5}$ components of the fit (deviation from Sechenov) is strongest at warm temperatures, and smallest at low temperatures. This is an interesting observation, that warrants discussion. What are possible causes? What is its relevance?

(2) author's response

Thank you for the comment. The reason why $\ln(K_H/K_{eq}{}^S)$ is proportional to $S^{0.5}$ rather than $S$ is still unclear. I will describe a potential reason for this proportionality simply in the text, and make discussion in *Supporting Information*.

(3) author's changes in manuscript

lines 22-24, page 10:

The reason for this salting-out effect of $CH_2F_2$ solubility in a-seawater is not clear. Specific properties of $CH_2F_2$ –small molecular volume, which results in small work of cavity creation (Graziano, 2004; 2008), and large solute-solvent attractive potential energy in water and a-seawater– may cause deviation from Sechenov relationship (Sect. S5, *Supporting Information*).

Sect. S5, 2nd block, page 8 - page 9 in Supporting Information:

I calculate Ben-Naim standard Gibbs energy $\Delta G^{\bullet}$, enthalpy $\Delta H^{\bullet}$, and entropy $\Delta S^{\bullet}$ changes for dissolution of $CH_2F_2$ in water because these values correspond to the values for the transfer from a fixed position in the gas phase to a fixed position in water. Values of $\Delta G^{\bullet}$, $\Delta H^{\bullet}$, and $\Delta S^{\bullet}$ are calculated on the basis of the Ostwald solubility coefficient, $L(T)$, as follows.

$$\ln(L(T)) = \ln\left(RTK_{eq}{}^S(T)\right) \quad \text{(B1)}$$

$$\Delta G^{\cdot} = R'T\ln(L(T)) \quad \text{(B2)}$$

$$\Delta H^{\cdot} = -\frac{\partial}{\partial(1/T)}\left(\frac{\Delta G^{\cdot}}{T}\right) \quad \text{(B3)}$$

$$\Delta S^{\cdot} = \frac{\Delta H^{\cdot} - \Delta G^{\cdot}}{T} \quad \text{(B4)}$$

where both $R$ and $R'$ represent gas constant but their units are different: $R$ = 0.0821 in atm dm$^3$ K$^{-1}$ mol$^{-1}$; $R'$ = 8.314 in J K$^{-1}$ mol$^{-1}$.

Combining Eqs. (B1), (B2), (B3), and (B4) with Eqs. (14) and (15), $\Delta G^{\bullet}$ (kJ mol$^{-1}$), $\Delta H^{\bullet}$ (kJ mol$^{-1}$), and $\Delta S^{\bullet}$ (J mol$^{-1}$ K$^{-1}$) are represented by $\Delta G_{sol}$ and $\Delta H_{sol}$ as follows:

$$\Delta G^{\cdot} = \Delta G_{sol} + R'T\ln(RT) \quad \text{(B5)}$$

$$\Delta H^{\cdot} = \Delta H_{sol} + R'T \quad \text{(B6)}$$

$$\Delta S^{\cdot} = \frac{\Delta H_{sol} - \Delta G_{sol}}{T} + R' - R'\ln(RT) \quad \text{(B7)}$$

Values of $\Delta G^{\bullet}$, $\Delta H^{\bullet}$, and $\Delta S^{\bullet}$ calculated at 298 K are listed in Table S2. Table S2 also lists values of $\Delta G^{\bullet}$, $\Delta H^{\bullet}$, and $\Delta S^{\bullet}$ reported for $CH_3F$ and $C_2H_6$ (Graziano, 2004) and $CH_4$ (Graziano, 2008) at 298 K. The chemicals, which having a methyl group, in Table S2 are classified into two groups ($CH_2F_2$ and $CH_3F$; $CH_4$ and $C_2H_6$) according to $\Delta G^{\bullet}$.

Table S2 lists values of $\Delta G_c$, $E_a$ and $\Delta H^h$ deduced using a scaled particle theory (Granziano, 2004; 2008). $\Delta G_c$ is the work of cavity creation to insert a solute in a solvent. $E_a$ is a solute-solvent attractive potential energy and accounts for the solute-solvent interactions consisting of dispersion, dipole-induced dipole, and dipole-dipole contributions. $\Delta H^h$ is enthalpy of solvent molecules reorganization caused by solute insertion. The solvent reorganization mainly involves a rearrangement of H-bonds.

$\Delta G_c$ is entropic in nature in all liquids, being a measure of the excluded volume effect due to a reduction in the spatial configurations accessible to liquid molecules upon cavity creation. Hence, $C_2H_6$ has larger value of $\Delta G_c$ than $CH_3F$ and $CH_4$. $\Delta G_c$, $E_a$, and $\Delta H^h$ are related to $\Delta G^{\bullet}$ and $\Delta H^{\bullet}$ as follows (Graziano, 2008):

$$\Delta G^{\cdot} = \Delta G_c + E_a \quad \text{(B8)}$$

$$\Delta H^{\cdot} = E_a + \Delta H^h \quad \text{(B9)}$$

Table S3 thus suggests that smaller value of $\Delta G^{\bullet}$ of $CH_3F$ than $CH_4$ is due to large solute-solvent attractive potential energy ($-E_a$) of $CH_3F$.

**Table S3. Ben-Naim standard hydration Gibbs energy $\Delta G^{\bullet}$, enthalpy $\Delta H^{\bullet}$, and entropy $\Delta S^{\bullet}$ changes for dissolution of $CH_2F_2$ at 298 K determined here and the corresponding values and values of $\Delta G_c$, $E_a$ and $\Delta H^h$ reported for $CH_3F$ and $C_2H_6$ (Granziano, 2004) and $CH_4$ (Graziano, 2008).**

| | $\Delta G^{\cdot}$ (kJ mol$^{-1}$) | $\Delta H^{\cdot}$ (kJ mol$^{-1}$) | $\Delta S^{\cdot}$ (J K$^{-1}$ mol$^{-1}$) | $\Delta G_c$ (kJ mol$^{-1}$) | $E_a$ (kJ mol$^{-1}$) | $\Delta H^h$ (kJ mol$^{-1}$) |
|---|---|---|---|---|---|---|
| $CH_2F_2$ | −1.1 | −14.7 | −45.4 | | | |
| $CH_3F$ | −0.9 | −15.8 | −50.0 | 23.3 | −24.3 | 8.5 |
| $CH_4$ | 8.4 | −10.9 | −64.7 | 22.9 | −14.5 | 3.7 |
| $C_2H_6$ | 7.7 | −17.5 | −84.5 | 28.4 | −20.7 | 3.2 |

Graziano (2008) definitively explained the salting-out of $CH_4$ by sodium chloride at molecular level on the basis of a scaled particle theory. He explained that $\Delta G_c$ increase was linearly related to the increase in the volume packing density of the solutions ($\xi_3$) with adding NaCl. Such an increase of $\Delta G_c$ is probably the case for salting-out of $CH_2F_2$ by a-seawater observed in this study. He also explained that $E_a$ was linearly related to the increase in $\xi_3$ assuming that a fraction of the dipole-induced dipole attractions could be taken into account by the parameterization of the dispersion contribution.

I think the possibility that $E_a$ may be nonlinearly related to the increase in $\xi_3$ because of dipole-dipole interaction between $CH_2F_2$ and solvents. Temperature dependence in Eq. (22) suggests that salting-out effect of $CH_2F_2$ by a-seawater is enthalpic. Eqs. (22) and (B9) thus suggests that the salting-out of $CH_2F_2$ is mostly related to change in $E_a$. $CH_2F_2$ has relatively small value of $\Delta G_c$ because of its small molecular volume compared to other chemicals such as $C_2H_6$. Accordingly,

$\Delta G^*$, that is, solubility of $CH_2F_2$ would depend on $E_a$ rather than $\Delta G_c$. Therefore, I think that specific properties of $CH_2F_2$ – small molecular volume, which results in small work of cavity creation (Graziano, 2004; 2008), and large solute-solvent attractive potential energy in water and a-seawater– may cause deviation from Sechenov relationship.

The following two references will be cited both in the manuscript and in *Supporting Information*.

Graziano, G.: Case study of enthalpy–entropy noncompensation. Journal of Chemical Physics, 120, 4467-4471, doi: 10.1063/1.1644094, 2004.

Graziano, G.: Salting out of methane by sodium chloride: A scaled particle theory study. Journal of Chemical Physics, 129, 084506, doi: 10.1063/1.2972979, 2008.

**R2-6 ----------**

(1) comments from Referee 2

The discussion in Sect. 3.3 assumes solubility equilibrium with the atmosphere over the full depth of the ocean mixed layer. How deep is this mixed ocean layer in the model? Does this mean the model estimates an upper limit?

(2) author's response

Thank you for the comments. The depth of the ocean mix layer in the model is 10 to 600 m. The depth distribution of $CH_2F_2$ dissolved in the ocean mixed layer in each semi-hemisphere is listed in Tables S4 (30° S–90° S), S5 (30° S–0° S), S6 (0° N–30° S) and S7 (30° N–90° N) in the revised manuscript. As seen in these tables, the $CH_2F_2$ dissolved in the ocean mixed layer resides mostly in less than 300 m depth. For example, for the southern semi-hemisphere (30° S–90° S) (Table S4), in August, when the amount of $CH_2F_2$ dissolved in the ocean mixed layer is maximum, 66% of the $CH_2F_2$ would be dissolved in the mixed layer with its depth between 100 m and 200 m, and 91 % of the $CH_2F_2$ dissolved in the ocean mixed layer is expected to reside in less than 300 m depth.

As Referee 2 pointed out, model estimates mean an upper limit of the amount of $CH_2F_2$ dissolved in the ocean mixed layer. This point will be clearly described in the revised manuscript.

(3) author's changes in manuscript

<u>line 29, page 11 - line 11, page 12:</u>

As seen in Figure 6, in the southern semi-hemispheric lower troposphere (30° S–90° S), at least 5 % of the atmospheric burden of $CH_2F_2$ would reside in the ocean mixed layer in the winter, and the annual variance of the $CH_2F_2$ residence ratio would be 4%. These ratios are, in fact, upper limits because $CH_2F_2$ in the ocean mixed layer may be undersaturated. It takes days to a few weeks after a change in temperature or salinity for oceanic surface mixed layers to come to equilibrium with

the present atmosphere, and equilibration time increases with depth of the surface mixed layer (Fine, 2011). In the estimation using the gridded data here, >90 % of $CH_2F_2$ in the ocean mixed layer would reside in less than 300 m depth (Tables S4, S5, S6 and S7).

Haine and Richards (1995) demonstrated that seasonal variation in ocean mixed layer depth was the key process which affected undersaturation and supersaturation of chlorofluorocarbon 11 (CFC-11), CFC-12 and CFC-113 by use of a one-dimensional slab mixed model. As described above, >90 % of $CH_2F_2$ in the ocean mixed layer is expected to reside in less than 300 m depth. According to the model calculation results by Haine and Richards (1995), saturation of $CH_2F_2$ would be >0.9 for the ocean mixed layer with less than 300 m depth. The saturation of $CH_2F_2$ in the ocean mixed layer is thus estimated to be at least 0.8. In the southern semi-hemispheric lower troposphere (30° S–90° S), therefore, at least 4 % of the atmospheric burden of $CH_2F_2$ would reside in the ocean mixed layer in the winter, and the annual variance of the $CH_2F_2$ residence ratio would be 3%.

The following two references will be cited in the manuscript.

Fine, R. A.: Observations of CFCs and $SF_6$ as ocean tracers. Annual Review of Marine Science, 3, 173-195, doi:10.1146/annurev.marine.010908.163933, 2011.

Haine, T. W. N. and Richards, K. J.: The influence of the seasonal mixed layer on oceanic uptake of CFCs. Journal of Geophysical Research, 100, 10727-10744, doi:10.1029/95JC00629, 1995.

Supporting Information, Tables S4, S5, S6 and S7

**Table S4. Monthly amount of $CH_2F_2$ dissolved in the ocean mixed layer at solubility equilibrium with the atmospheric $CH_2F_2$ (partial pressure, 1 atm) and the depth distribution of the $CH_2F_2$ dissolved in the southern semi-hemisphere (90°S - 30°S).**

| | Amount (Gg patm$^{-1}$) | Distribution of the amount of $CH_2F_2$ dissolved in the ocean mixed layer with respect to the ocean mixed layer depth (%) | | | | | |
|---|---|---|---|---|---|---|---|
| | | 10 - 100 m | 100 - 200 m | 200 - 300 m | 300 - 400 m | 400 - 500 m | 500 - 600 m |
| January | 0.0169 | 94.9 | 2.9 | 1.0 | 0.5 | 0.3 | 0.3 |
| February | 0.0201 | 92.1 | 3.6 | 2.9 | 1.0 | 0.3 | 0.0 |
| March | 0.0255 | 87.8 | 9.2 | 1.7 | 0.7 | 0.2 | 0.4 |
| April | 0.0338 | 66.5 | 31.8 | 1.1 | 0.2 | 0.1 | 0.2 |
| May | 0.0409 | 48.5 | 48.1 | 2.2 | 0.8 | 0.3 | 0.0 |
| June | 0.0510 | 26.8 | 62.7 | 8.0 | 1.7 | 0.8 | 0.1 |
| July | 0.0571 | 14.1 | 69.3 | 12.2 | 3.3 | 0.9 | 0.1 |
| August | 0.0640 | 8.5 | 65.8 | 17.0 | 6.2 | 2.3 | 0.2 |
| September | 0.0609 | 13.5 | 61.0 | 14.6 | 8.2 | 2.7 | 0.0 |
| October | 0.0504 | 24.7 | 58.6 | 12.1 | 2.9 | 1.4 | 0.3 |
| November | 0.0335 | 60.4 | 30.5 | 4.6 | 2.2 | 2.3 | 0.1 |
| December | 0.0196 | 95.1 | 4.3 | 0.4 | 0.2 | 0.0 | 0.0 |

**Table S5. Monthly amount of $CH_2F_2$ dissolved in the ocean mixed layer at solubility equilibrium with the atmospheric $CH_2F_2$ (partial pressure, 1 patm) and the depth distribution of the $CH_2F_2$ dissolved in the southern semi-hemisphere (30°S - 0°S).**

| | Amount (Gg patm$^{-1}$) | Distribution of the amount of $CH_2F_2$ dissolved in the ocean mixed layer with respect to the ocean mixed layer depth (%) | | | | | |
|---|---|---|---|---|---|---|---|
| | | 10 - 100 m | 100 - 200 m | 200 - 300 m | 300 - 400 m | 400 - 500 m | 500 - 600 m |
| January | 0.0084 | 99.6 | 0.4 | 0 | 0 | 0 | 0 |
| February | 0.0084 | 99.7 | 0.3 | 0 | 0 | 0 | 0 |
| March | 0.0089 | 100.0 | 0 | 0 | 0 | 0 | 0 |
| April | 0.0106 | 100.0 | 0 | 0 | 0 | 0 | 0 |
| May | 0.0131 | 100.0 | 0 | 0 | 0 | 0 | 0 |
| June | 0.0163 | 97.1 | 2.9 | 0 | 0 | 0 | 0 |
| July | 0.0189 | 80.1 | 19.9 | 0 | 0 | 0 | 0 |
| August | 0.0193 | 73.1 | 26.9 | 0 | 0 | 0 | 0 |
| September | 0.0165 | 82.2 | 17.8 | 0 | 0 | 0 | 0 |
| October | 0.0124 | 94.6 | 5.4 | 0 | 0 | 0 | 0 |
| November | 0.0097 | 99.9 | 0.1 | 0 | 0 | 0 | 0 |
| December | 0.0087 | 100.0 | 0 | 0 | 0 | 0 | 0 |

**Table S6. Monthly amount of $CH_2F_2$ dissolved in the ocean mixed layer at solubility equilibrium with the atmospheric $CH_2F_2$ (partial pressure, 1 patm) and the depth distribution of the $CH_2F_2$ dissolved in the northern semi-hemisphere (0°N - 30°N).**

| | Amount (Gg patm$^{-1}$) | Distribution of the amount of $CH_2F_2$ dissolved in the ocean mixed layer with respect to the ocean mixed layer depth (%) | | | | | |
|---|---|---|---|---|---|---|---|
| | | 10 - 100 m | 100 - 200 m | 200 - 300 m | 300 - 400 m | 400 - 500 m | 500 - 600 m |
| January | 0.0132 | 96.4 | 3.6 | 0 | 0 | 0 | 0 |
| February | 0.0126 | 95.9 | 4.1 | 0 | 0 | 0 | 0 |
| March | 0.0107 | 98.7 | 1.3 | 0 | 0 | 0 | 0 |
| April | 0.0087 | 99.8 | 0.2 | 0 | 0 | 0 | 0 |
| May | 0.0079 | 100.0 | 0 | 0 | 0 | 0 | 0 |
| June | 0.0080 | 100.0 | 0 | 0 | 0 | 0 | 0 |
| July | 0.0084 | 100.0 | 0 | 0 | 0 | 0 | 0 |
| August | 0.0082 | 100.0 | 0 | 0 | 0 | 0 | 0 |
| September | 0.0080 | 100.0 | 0 | 0 | 0 | 0 | 0 |
| October | 0.0086 | 100.0 | 0 | 0 | 0 | 0 | 0 |
| November | 0.0100 | 100.0 | 0 | 0 | 0 | 0 | 0 |
| December | 0.0118 | 100.0 | 0 | 0 | 0 | 0 | 0 |

**Table S7. Monthly amount of $CH_2F_2$ dissolved in the ocean mixed layer at solubility equilibrium with the atmospheric $CH_2F_2$ (partial pressure, 1 patm) and the depth distribution of the $CH_2F_2$ dissolved in the northern semi-hemisphere (30°N - 90°N).**

| | Amount (Gg patm$^{-1}$) | Distribution of the amount of $CH_2F_2$ dissolved in the ocean mixed layer with respect to the ocean mixed layer depth (%) | | | | | |
|---|---|---|---|---|---|---|---|
| | | 10 - 100 m | 100 - 200 m | 200 - 300 m | 300 - 400 m | 400 - 500 m | 500 - 600 m |
| January | 0.0205 | 41.3 | 50.1 | 7.0 | 1.4 | 0.2 | 0.0 |
| February | 0.0225 | 34.5 | 55.3 | 7.1 | 2.3 | 0.6 | 0.2 |
| March | 0.0208 | 49.7 | 42.3 | 4.9 | 1.7 | 0.7 | 0.6 |
| April | 0.0147 | 79.7 | 17.6 | 1.7 | 0.4 | 0.0 | 0.6 |
| May | 0.0081 | 90.1 | 9.9 | 0 | 0 | 0 | 0 |
| June | 0.0055 | 97.7 | 2.3 | 0 | 0 | 0 | 0 |
| July | 0.0045 | 96.6 | 3.4 | 0 | 0 | 0 | 0 |
| August | 0.0048 | 94.4 | 5.6 | 0 | 0 | 0 | 0 |
| September | 0.0059 | 97.7 | 2.3 | 0 | 0 | 0 | 0 |
| October | 0.0084 | 99.6 | 0.4 | 0 | 0 | 0 | 0 |
| November | 0.0121 | 89.6 | 10.4 | 0.1 | 0 | 0 | 0 |
| December | 0.0163 | 71.0 | 26.1 | 2.9 | 0 | 0 | 0 |

**R2-7 ----------**

(1) comments from Referee 2

The conclusion that 5% of the atmospheric burden of $CH_2F_2$ would reside in the ocean mixed layer in the southern semi-hemispheric lower troposphere during winter seems to be an upper limit, and should be worded as such. How much lower could this upper limit be?

(2) author's response

Thank you for the comments. As described in R2-6, it takes days to a few weeks after a change in temperature or salinity for oceanic surface mixed layers to come to equilibrium with the present atmosphere, and equilibration time increases with depth of the surface mixed layer (Fine, 2011).

Haine and Richards (1995) demonstrated that the seasonal variation in ocean mixed layer depth was the key process which affected undersaturation and supersaturation of chlorofluorocarbon 11 (CFC-11), CFC-12 and CFC-113 by use of a one-dimensional slab mixed model. Specifically, the mixed layer deepening in autumn would cause undersaturation in the mixed layer. In the estimation, >90 % of $CH_2F_2$ in the ocean mixed layer is expected to reside in less than 300 m depth (Tables S4, S5, S6 and S7). According to the report by Haine and Richards (1995), saturation of $CH_2F_2$ would be >0.9 for the ocean mixed layer with less than 300 m depth. The saturation of $CH_2F_2$ in the ocean mixed layer is thus estimated to be at least 0.8.

The manuscript will be revised, as described in R2-6, and Fine (2011) and Haine and Richards (1995) will be cited.

(3) author's changes in manuscript

lines 13-16, page 1, Abstract

By using this equation in a lower tropospheric semi-hemisphere (30° S–90° S) of the Advanced Global Atmospheric Gases Experiment (AGAGE) 12-box model, we estimated that 1 to 4 % of the atmospheric burden of $CH_2F_2$ resided in the ocean mixed layer and that this percentage was at least 4 % in the winter; dissolution of $CH_2F_2$ in the ocean may partially influence estimates of $CH_2F_2$ emissions from long-term observational data of atmospheric $CH_2F_2$ concentrations.

lines 20-24, page 12

By using the solubility of $CH_2F_2$ determined in this study, the magnitude of buffering of the atmospheric burden of $CH_2F_2$ by the additional $CH_2F_2$ in ocean surface waters is estimated to be realistically limited to only about 1 % globally; however, in a southern semi-hemispheric lower troposphere (30° S–90° S) of the AGAGE 12-box model, the atmospheric burden of $CH_2F_2$ is estimated to reside in the ocean mixed layer by at least 4 % in the winter and by 1 % in the summer.

Other changes are included in the change mentioned in R2-6.

**R2-8 ----------**

(1) comments from Referee 2

It seems surprising that the dissolution of $CH_2F_2$ into the ocean should affect estimates of $CH_2F_2$ emissions in the Southern Hemisphere and their seasonal variability, because the atmospheric concentrations that reach the Southern Hemisphere are also affected by transport, and chemical removal, and related uncertainties. This should be mentioned.

(2) author's response

Thank you for the comment. As Referee 2 pointed out, the atmospheric concentrations that reach the Southern Hemisphere are also affected by transport, chemical removal, and related uncertainties; this should be mentioned.

I will first describe how the dissolution of $CH_2F_2$ into the ocean may affect estimation of $CH_2F_2$ emissions in the Southern Hemisphere and their seasonal variability, and then I will show the revised text.

In 2012, atmospheric concentrations of $CH_2F_2$ in the Northern Hemisphere are by >30% higher than in the Southern Hemisphere (O'Doherty et al., 2014); the strong inter-hemisphere gradient indicates that emissions of $CH_2F_2$ are predominantly in the Northern Hemisphere. In the AGAGE 12 box model (Rigby et al., 2013), transport of $CH_2F_2$ is dominated by eddy diffusion between the boxes in the model. The seasonal eddy diffusion

parameters between the Northern Hemisphere and the Southern Hemisphere in the model are 187 to 568 days in lower troposphere, and 81 to 109 days in upper troposphere (Rigby et al., 2013).

The rate of increase in atmospheric concentration of $CH_2F_2$ due to the emission of $CH_2F_2$ in the Southern Hemisphere, which is denoted as $RE_{south}$ hereafter, is thus more sensitive to change in atmospheric concentrations of $CH_2F_2$ in the Southern Hemisphere than those in the Northern Hemisphere, partly because $CH_2F_2$ is removed through gas phase reactions with OH (partial atmospheric lifetime of 5.5 years). Furthermore, $RE_{south}$ would range small values such as a few % $y^{-1}$ or less because emissions of $CH_2F_2$ were predominantly in the Northern Hemisphere and because, in 2012, the rate of increase in the global mean mole fraction of $CH_2F_2$ was 17% $y^{-1}$ (O'Doherty et al., 2014). In estimation of $RE_{south}$, small value of $RE_{south}$ would be deduced from difference in the rates of increase of atmospheric concentrations of $CH_2F_2$ between hemispheres. Dissolution of $CH_2F_2$ in the ocean in the Southern Hemisphere may thus affect estimation of $RE_{south}$ and then affect estimation of $CH_2F_2$ emissions in the Southern Hemisphere and their seasonal variability.

I revise the text as follows.

(3) author's changes in manuscript

lines 12-16, page 12

In the Southern Hemisphere, $CH_2F_2$ emission rates are much lower than in the Northern Hemisphere. Hence, dissolution of $CH_2F_2$ in the ocean, even if dissolution is reversible, may influence estimates of $CH_2F_2$ emissions derived from long-term observational data on atmospheric concentrations of $CH_2F_2$; in particular, consideration of dissolution of $CH_2F_2$ in the ocean may affect estimates of $CH_2F_2$ emissions in the Southern Hemisphere and their seasonal variability because of slow rates of inter-hemispheric transport and small portion of the $CH_2F_2$ emissions in the Southern Hemisphere to the total emissions.

**R2-9 ----------**

(1) comments from Referee 2

On line 27, page 2 (in the revised manuscript), 'first' is written twice.

(2) author's response

Thank you for the comment. The text is revised.

(3) author's changes in manuscript

line 27, page 2

First, the values of $K_H$ for $CH_2F_2$ were determined over the temperature range from 276 to 313 K by means of an inert-gas stripping (IGS) method.

**R2-10----------**

(1) comments from Referee 2

On lines 9-10, page 5 (in the revised manuscript), add errors for numbers. See comments #1, #2 and add typical values, their units, and uncertainties of variables for the key equations throughout the manuscript.

(2) author's response

Thank you for the comment. If redistribution of $CH_2F_2$ in the headspace to the test solution had occurred, the $K_{eq}$ values determined in this study would be overestimated. Errors due to this redistribution are always negative values. The ratio of the errors to the $K_{eq}$ values (%) is $100 \times \frac{\left(\frac{V_{head}}{RTV}\right)}{\left(\frac{1}{k_1}\frac{F}{RTV}\right)}$, that is, $\frac{100k_1V_{head}}{F}$. Under the experimental conditions here, this ratio is calculated to be −2.0 to −2.3 % at 3.0 °C and −4.6 to −5.1 % at 39.5 °C. Values of this ratio increase as values of $K_{eq}$ decrease. This ratio is maximum (−6.5 %) for a-seawater at 51.534‰ and 39.5 °C.

Typical values, their units, and uncertainties of variables for the key equations are added in the revised manuscript.

(3) author's changes in manuscript

lines 6-8, page 4

The solution was magnetically stirred, and its temperature was kept constant within ±0.2 K by means of a constant-temperature bath that had both heating and cooling capabilities (NCB-2500, EYELA, Tokyo, Japan) and was connected to the water jacket of the column.

lines 14-16, page 4

The volumetric flow rate of the gas ($F_{meas}$) was calibrated with a soap-bubble meter for each experimental run. The soap-bubble meter had been calibrated by means of a high-precision film flow meter SF-1U with VP-2U (Horiba, Kyoto, Japan). Errors of $F_{meas}$ are within ±1%.

lines 18-20, page 4

All volumetric gas flows were corrected to prevailing temperature and pressure by Eq. (3) (Krummen et al., 2000). Errors due to this correction are within ±1%. Errors of $F$ are thus within ±1.4%.

lines 14-21, page 5

Hence Eq. (6) was used to deduce $K_{eq}(T)$ from $k_1$. Errors of $T$ are estimated to be within ±0.2 K. These errors of $T$ may give potential systematic bias of ca. ±2% ($\delta K_{eq}/K_{eq}$) where $\delta K_{eq}$ is error of the value of $K_{eq}$. Errors of $F$ are estimated to be less

than 1.4 %, and these errors may give potential systematic bias of less than 1.4 % ($\delta K_{eq}/K_{eq}$). Accordingly, for the IGS methods, values of $K_{eq}$ may have potential systematic bias of ca. ±2%.

If redistribution of $CH_2F_2$ in the headspace to the test solution had occurred, the values determined using Eq. (6) would be overestimated. Errors due to this redistribution are always negative values. Ratio of the errors to the $K_{eq}$ values (%) is $\frac{100k_1V_{head}}{F}$. Values of this ratio increase as values of $K_{eq}$ decrease. Under the experimental conditions here, this ratio is calculated to be from –2.0 % for water at 3.0 °C to −6.5 % for a-seawater at 51.534‰ and 39.5 °C.

lines 14-16, page 8

$$\ln(K_H(T)) = -49.71 + 77.70 \times \left(\frac{100}{T}\right) + 19.14 \times \ln\left(\frac{T}{100}\right) \quad (13)$$

The square-root-of-variance, that is, standard deviation for each fitting coefficient in Eq. (12) is as follows:

$\delta a_1 = 5.5$; $\delta a_2 = 8.3$; $\delta a_3 = 2.8$.

line 2, page 10 - line 3, page 11

This result suggests that $\ln(K_H(T)/{K_{eq}}^S(T))$ varied according to Eq. (18):

$$\ln\left(K_H(T)/{K_{eq}}^S(T)\right) = k_{s1} \times S^{0.5} \quad (18)$$

Values of $k_{s1}$ may be represented by the following function of $T$:

$$k_{s1} = b_1 + b_2 \times \left(\frac{100}{T}\right) \quad (19)$$

Parameterizations of $b_1$ and $b_2$ obtained by fitting all the $\ln(K_H(T)/{K_{eq}}^S(T))$ and $S$ data at each temperature simultaneously by means of the nonlinear least-squares method gives Eq. (20).

$$\ln\left(K_H(T)/{K_{eq}}^S(T)\right) = \left(0.0127 + 0.0099 \times \left(\frac{100}{T}\right)\right) \times S^{0.5} \quad (20)$$

The standard deviation for each fitting coefficient in Eq. (19) is as follows:

$\delta b_1 = 0.0106$; $\delta b_2 = 0.0031$.

Since $2\times\delta b_1 > b_1$, the parameterization by Eq. (19) may be overworked. Accordingly, all the $\ln(K_H(T)/{K_{eq}}^S(T))$ and $S$ data at each temperature are fitted simultaneously using Eq. (21) instead of Eq. (19). The nonlinear least-squares method gives Eq. (22).

$$k_{s1} = b_2 \times \left(\frac{100}{T}\right) \quad (21)$$

$$\ln\left(K_H(T)/{K_{eq}}^S(T)\right) = 0.134 \times \left(\frac{100}{T}\right) \times S^{0.5} \quad (22)$$

The standard deviation for the fitting coefficient in Eq. (21) is as follows: $\delta b_2 = 0.001$. As seen in Fig. 5, Eqs. (21) and (22) reproduced the data well.

$\ln(K_H(T)/{K_{eq}}^S(T))$ depends on $S^{0.5}$ and follows Eq. (22) rather than the Sechenov dependence (Eq. (17)). Table S7 compares values of ${K_{eq}}^S$ calculated by Eq. (22) with those by Eq. (17). The difference between these values of ${K_{eq}}^S$ at 35‰ of

salinity was within 3% of the $K_{eq}^{S}$ value. Decreases in values of $K_{eq}^{S}$ are calculated to be 7–8% and 4%, respectively, by Eqs. (17) and (23) as salinity of a-seawater increases from 30‰ to 40‰ at each temperature.

The reason for this salting-out effect of $CH_2F_2$ solubility in a-seawater is not clear. Specific properties of $CH_2F_2$ –small molecular volume, which results in small work of cavity creation (Graziano, 2004; 2008), and large solute-solvent attractive potential energy in water and a-seawater– may cause deviation from Sechenov relationship (*Supporting Information*).

In Eq. (22), $K_H(T)$ is represented by Eq. (13), as described in Sect. 3.1. Therefore $K_{eq}^{S}(T)$ is represented by Eq. (23):

$$\ln\left(K_{eq}^{S}\right) = -49.71 + (77.70 - 0.134 \times S^{0.5}) \times \left(\frac{100}{T}\right) + 19.14 \times \ln\left(\frac{T}{100}\right) \quad (23)$$

The values calculated with Eq. (23) are indicated by the bold curves in Fig. 4 and are listed in Table 3. Table 3 lists errors at 95% confidence level for the regression. These errors ($error_{23}$) are calculated by Eq. (24):

$$error_{23} = K_{eq}^{S} \times \sqrt{\left(\frac{error_{13}}{K_H}\right)^2 + \left(\frac{error_{22}}{K_{eq}^{S}}\right)^2} \quad (24)$$

where $error_{13}$ represents errors at 95% confidence level for the regression by Eq. (12); $error_{22}$ represents errors at 95% confidence level for the regression by Eq. (21). Table 3 also represents errors due to both errors at 95% confidence level for the regression and potential systematic bias (±2%). Equation (23) reproduced the experimentally determined values of $K_H(T)$ and $K_{eq}^{S}(T)$ within the uncertainty of these experimental runs.

**R2-11----------**

(1) comments from Referee 2

What statistical test for outliers was applied? How many points were removed at each temperature?

(2) author's response

Thank you for the comment. Statistical test for outliers is as follows.

The data with errors being >10% of the data was first excluded. Next, some data were excluded for calculation of the average so that the remaining data were inside the 2σ range. This procedure was iterated until all the data were inside the 2σ range.

The number of them were eight or fewer at each temperature. The maximum number of the data excluded was corrected to be eight although it was described to be six in the original manuscript. Number of the data thus excluded were indicated in Tables 1 and 3 (R1-1).

(3) author's changes in manuscript

lines 19-22, page 7

The data with errors being >10% of the data was first excluded. Next, some data were excluded for calculation of the

average so that the remaining data were inside the 2σ range. This procedure was iterated until all the data were inside the 2σ range. The data points thus excluded was only for $V$ values of 0.350 $dm^3$ and the number of them were eight or fewer at each temperature.

Tables 1 and 3

These tables in the revised manuscript are shown in R1-1.

**R2-12----------**

(1) comments from Referee 2

About Eq (17), for sake of discussion, can a $k_S$ value be given here? And what is the effect of including $k_S$ vs $k_{S1}$, $k_{s2}$ in the model - does it make a difference?

(2) author's response

Thank you for the comment. Parameters of $k_{S1}$, $k_{s2}$ in the original manuscript are replaced by a parameter of $k_{S1}$ in the revised manuscript. I add Table S2. Table S2 lists values of $k_s$ and comparison of the $K_{eq}$ values calculated between by Eq. (17) and by Eq. (22) at salinity of 30, 35 and 40 ‰ and each temperature.

(3) author's changes in manuscript

lines 27-30, page 9

Figure 5 plots $\ln(K_H(T)/K_{eq}^S(T))$ against $S$ at each temperature. Table S2 lists values of $k_s$ determined by fitting the data at each temperature by use of Eq. (17). If the $K_{eq}^S(T)$ values obeyed Eq. (17), the data at each temperature in Fig. 5 would fall on a straight line passing through the origin, but they did not. Figure 5 reveals that the salinity dependence of $CH_2F_2$ solubility in a-seawater cannot be represented by Eq. (17).

lines 18-21, page 10

$\ln(K_H(T)/K_{eq}^S(T))$ depends on $S^{0.5}$ and follows Eq. (22) rather than the Sechenov equation (Eq. (17)). Table S2 compares values of $K_{eq}^S$ calculated by Eq. (22) with those by Eq. (17). The difference between these values of $K_{eq}^S$ at 35‰ of salinity was within 3% of the $K_{eq}^S$ value. Decreases in values of $K_{eq}^S$ are calculated to be 7–8% and 4%, respectively, by Eqs. (17) and (22) as salinity of a-seawater increases from 30‰ to 40‰ at each temperature.

Table S2

**Table S2. Values of $k_s$ (Eq. (17)) and comparison of values of $K_{eq}^{S}$ calculated at each temperature by Eq. (17) with those by Eq. (22).**

| Temperature (°C) | $k_s$ (‰$^{-1}$) | [$K_{eq}^{S}$ from Eq. (17)]/ [$K_{eq}^{S}$ from Eq. (22)] at 30‰ | at 35‰ | at 40‰ | [$K_{eq}^{S}$ at 30‰]/ [$K_{eq}^{S}$ at 40‰] Eq. (17) | Eq. (22) |
|---|---|---|---|---|---|---|
| 3.0 | 0.00811 | 1.027 | 1.008 | 0.988 | 1.084 | 1.043 |
| 5.8 | 0.00785 | 1.033 | 1.014 | 0.995 | 1.082 | 1.042 |
| 10.5 | 0.00768 | 1.033 | 1.016 | 0.997 | 1.080 | 1.042 |
| 15.5 | 0.00718 | 1.044 | 1.028 | 1.012 | 1.074 | 1.041 |
| 20.3 | 0.00728 | 1.037 | 1.020 | 1.003 | 1.076 | 1.040 |
| 25.0 | 0.00704 | 1.040 | 1.024 | 1.008 | 1.073 | 1.039 |
| 29.9 | 0.00731 | 1.027 | 1.010 | 0.992 | 1.076 | 1.039 |
| 34.8 | 0.00713 | 1.029 | 1.012 | 0.995 | 1.074 | 1.038 |
| 39.5 | 0.00709 | 1.026 | 1.010 | 0.992 | 1.073 | 1.038 |

# Experimental determination of Henry's law constants of difluoromethane (HFC-32) and the salting-out effects in aqueous salt solutions relevant to seawater

Shuzo Kutsuna

National Institute of Advanced Industrial Science and Technology (AIST), 16-1 Onogawa, Tsukuba, 305-8569, Japan

*Correspondence to*: S. Kutsuna (s-kutsuna@aist.go.jp)

**Abstract.** Gas-to-water equilibrium coefficients, $K_{eq}^{S}$ (in M atm$^{-1}$) of difluoromethane ($CH_2F_2$), a hydrofluorocarbon refrigerant (HFC-32), in aqueous salt solutions relevant to seawater were determined over a temperature ($T$) range from 276 to 313 K and a salinity ($S$) range up to 51 ‰ by means of an inert-gas stripping method. From the van't Hoff equation, the $K_{eq}^{S}$ value in water, which corresponds to the Henry's law constant ($K_H$), at 298 K was determined to be 0.~~064~~ 065 M atm$^{-1}$. The salinity dependence of $K_{eq}^{S}$ (the salting-out effect), $\ln(K_H/K_{eq}^{S})$, did not obey the ~~Setchenow~~ Sechenov equation but was proportional to~~represented by an equation involving $S$ and~~ $S^{0.5}$. Overall, the $K_{eq}^{S}(T)$ value was expressed by $\ln(K_{eq}^{S}(T)) = -49.71 + (77.70 - 0.134 \times S^{0.5}) \times (100/T) + 19.14 \times \ln(T/100)$~~$= 49.7122 + 77.7018 \times (100/T) + 19.1379 \times \ln(T/100) + [-0.2261 + 0.5176 \times (T/100)] \times S^{0.5} + [0.0362 - 0.1046 \times (T/100)] \times S$~~. By using this equation in a lower tropospheric semi-hemisphere (30° S–90° S) of the Advanced Global Atmospheric Gases Experiment (AGAGE) 12-box model, we estimated that 1 to ~~4~~5 % of the atmospheric burden of $CH_2F_2$ resided in the ocean mixed layer and that this percentage was at least ~~4~~5 % in the winter; dissolution of $CH_2F_2$ in the ocean may partially influence estimates of $CH_2F_2$ emissions from long-term observational data of atmospheric $CH_2F_2$ concentrations.

## 1 Introduction

Hydrofluorocarbons (HFCs) have been developed as replacements for chlorofluorocarbons and hydrochlorofluorocarbons (HCFCs) to protect the stratospheric ozone layer from depletion. In particular, difluoromethane (HFC-32, $CH_2F_2$) has been used as a refrigerant to replace HCFC-22 ($CHClF_2$): azeotropic mixtures of $CH_2F_2$ with HFC-125 ($CHF_2CF_3$) and HFC-134a ($CH_2FCF_3$) have been used as refrigerants for air conditioning and refrigeration for a few decades, and $CH_2F_2$ alone has recently been used as a refrigerant for air conditioning.

However, HFCs can act as greenhouse gases, and thus there is concern about emissions of $CH_2F_2$ and other HFCs to the atmosphere, where they can accumulate and contribute to global warming (IPCC, 2013). Observational data from the Advanced Global Atmospheric Gases Experiment (AGAGE) indicate that the atmospheric concentration of $CH_2F_2$ has been increasing every year since 2004; in 2012, the global mean mole fraction of $CH_2F_2$ was 6.2 ± 0.2 parts per trillion (ppt), and the rate of increase was 1.1 ± 0.04 ppt y$^{-1}$ (17% y$^{-1}$) (O'Doherty et al., 2014). By using AGAGE data in combination with a

chemical transport model such as the AGAGE 12-box model (Cunnold et al., 1994; Rigby et al., 2013) and a value of 5.1 years as the atmospheric lifetime of $CH_2F_2$, O'Doherty et al. (2014) estimated the global emission rate of $CH_2F_2$ in 2012 to be $21 \pm 11$ Gg $y^{-1}$ with an increase rate of $14 \pm 11\%$ $y^{-1}$. Such estimates on the basis of long-term observational data such as the AGAGE and the National Oceanic and Atmospheric Administration Global Monitoring Division (NOAA GMD) network are called top-down estimates and have been shown to provide an independent and effective method for assessing the accuracy of globally and regionally aggregated reductions or increases in emissions of individual HFCs, as well as other greenhouse gases, compiled from national reports to the United Nations Framework Convention on Climate Change (eg. Prinn et al., 2000; Lunt et al., 2015; Montzka et al., 2015).

The atmospheric lifetimes of HFCs are thus related to their estimated emission rates. The currently accepted value of the atmospheric lifetime of $CH_2F_2$, which was revised in 2014 (Carpenter et al., 2014), is 5.4 years. The partial atmospheric lifetime of $CH_2F_2$ with respect to gas-phase reactions with OH in the troposphere is 5.5 years, and that with respect to stratospheric removal processes is 124 years. Other processes, such as dissolution into seawater, are not considered to contribute significantly to atmospheric removal of $CH_2F_2$. Yvon-Lewis and Butler (2002) estimated partial atmospheric lifetimes of some HCFCs and HFCs with respect to irreversible dissolution into seawater by using physicochemical properties such as solubility and aqueous reaction rates, as well as meteorological data such as temperature and wind speed over the ocean in grids. Their estimates indicated that dissolution into seawater is not a significant sink of the HCFCs and HFCs that were evaluated in the study. Because no aqueous reactions of $CH_2F_2$ have yet been observed under environmental conditions, dissolution of $CH_2F_2$ into seawater is considered to be reversible and cannot serve as a sink of $CH_2F_2$. However, because $CH_2F_2$ is more soluble in water than HCFCs and other HFCs (Sander, 2015), even reversible dissolution of $CH_2F_2$ into seawater might influence a top-down estimate of $CH_2F_2$ emission rates.

The objective of the present study is to experimentally determine the seawater solubility of $CH_2F_2$, which is a physicochemical property necessary for estimating the residence ratio of $CH_2F_2$ in the ocean when the ocean mixed layer is at solubility equilibrium with the atmosphere. Specifically, the Henry's law constants, $K_H$ (in M $atm^{-1}$), of $CH_2F_2$ and the salting-out effects of seawater-relevant ions on $CH_2F_2$ solubility were experimentally determined. Values of $K_H$ for $CH_2F_2$ have been reported in some review papers (Sander, 2015; Clever et al., 2005). The largest and smallest values at 298K differ from each other by a factor of approximately 3: 0.87 M $atm^{-1}$ (Sander, 2015; Yaws and Yang, 1992) and 0.30 M $atm^{-1}$ (Clever et al., 2005; Miguel et al., 2000). To the author's knowledge, no data on the salting-out effects of seawater-relevant ions on $CH_2F_2$ solubility have been reported.

First, the values of $K_H$ for $CH_2F_2$ were ~~first~~ determined over the temperature range from 276 to 313 K by means of an inert-gas stripping (IGS) method. The $K_H$ values were also determined over the temperature range from 313 to 353 K by means of a phase ratio variation headspace (PRV-HS) method. The $K_H$ values obtained by the two methods could be fitted by an equation representing the same temperature dependence. Second, salting-out effects on $CH_2F_2$ solubility were determined over the temperature range from 276 to 313 K for test solutions of artificial seawater prepared over the salinity range from 4.5 to 51.5 ‰. The salting-out effects were confirmed for the artificial seawater, but the relationship between $CH_2F_2$

solubility and salinity of the artificial seawater was found to be unusual in that the excessive free energy for dissolution was not proportional to the salinity but rather was represented by an equation involving ~~the salinity and~~ the 0.5 power of the salinity. Over the salinity range relevant to seawater, the solubility of $CH_2F_2$ in the artificial seawater could be represented as a function of both salinity and temperature. Third, on the basis of the solubility of $CH_2F_2$ in seawater determined in this study and a global gridded dataset of monthly mean values of temperature, salinity, and depth of the ocean mixed layer, the amounts of $CH_2F_2$ dissolved in the ocean mixed layer were estimated in each month for each lower tropospheric semi-hemisphere of the AGAGE-12 box model.

## 2 Experimental

### 2.1 Materials

$CH_2F_2$ gas (1010 ppmv or 1000 ppmv in synthetic air) was purchased from Takachiho Chemical Industrial Co. (Tokyo, Japan). Sodium chloride (NaCl, >99.5%), sodium sulfate ($Na_2SO_4$, >99%), magnesium chloride ($MgCl_2 \cdot 6H_2O$, >98%), calcium chloride ($CaCl_2 \cdot 2H_2O$, >99.9%), and potassium chloride (KCl, >99.5%) were purchased from Wako Pure Chemical Industries (Osaka, Japan) and used as supplied. Water was purified with a Milli-Q Gradient A10 system (resistivity > 18 megohm-cm~~>18 MΩ~~).

Synthetic artificial seawater was prepared as described by Platford (1965) and was used to evaluate the salting-out effects on the solubility of $CH_2F_2$ in the ocean. The prepared artificial seawater had the following definite mole ratios: 0.4240 NaCl, 0.0553 $MgCl_2$, 0.0291 $Na_2SO_4$, 0.0105 $CaCl_2$, and 0.0094 KCl. The ionic strength of the artificial seawater was set between 0.089 and 1.026 mol $kg^{-1}$ water, that is, at molality base, with each salt at the aforementioned mole ratio; the salinity (in ‰) of this artificial seawater was between 4.45 and 51.53‰. This artificial seawater is referred to hereafter as a-seawater.

### 2.2 Inert-gas stripping method with a helical plate

An inert-gas stripping (IGS) method (Mackay et al., 1979) was used to determine the solubility of $CH_2F_2$ in water and aqueous salt solutions. A $CH_2F_2$–air-nitrogen mixture (mixing ratio of $CH_2F_2 \sim 10^{-4}$) was bubbled into the aqueous solution for a certain time period (e.g., 5 min), and then nitrogen gas ($N_2$) was bubbled through the resulting aqueous solution containing $CH_2F_2$, which was stripped from the solution into the gas phase.

The gas-to-liquid partition coefficient (in M $atm^{-1}$) at temperature $T$ (in K), $K_{eq}(T)$, was calculated from the rate of decrease of the gas-phase partial pressure according to Eqs. (1) and (2):

$$\ln(P_t/P_0) = -k_1 t \quad (1)$$

$$k_1 = \frac{1}{K_{eq}(T)RT}\frac{F}{V} \quad (2)$$

where $P_t/P_0$ is the ratio of the partial pressure of $CH_2F_2$ at time $t$ to the partial pressure of $CH_2F_2$ at fixed time $t_0$; $k_1$ is the first-order decreasing rate constant (in $s^{-1}$); $F$ is the flow rate of $N_2$ (in $dm^3\ s^{-1}$); $V$ is the volume of water or aqueous salt solution (in $dm^3$); and $R$ is the gas constant (0.0821 $dm^3$ atm $K^{-1}$ $mol^{-1}$). The $K_{eq}(T)$ values in water correspond to the Henry's law constants, $K_H(T)$ in M $atm^{-1}$. The $P_t$ values typically ranged from $10^{-4}$ to $10^{-6}$ atm.

A stripping column apparatus with a helical plate was used to strip $CH_2F_2$. This apparatus was described in detail by Kutsuna and Hori (2008) and is described briefly here. The stripping column consisted of a jacketed Duran glass column (4 cm i.d. × 40 cm height) and a glass gas-introduction tube with a glass helix. Water or a-seawater (0.300 or 0.350 $dm^3$) was added to the column for the test solution. The solution was magnetically stirred, and its temperature was kept constant within ±0.2 K by means of a constant-temperature bath that had both heating and cooling capabilities (NCB-2500, EYELA, Tokyo, Japan) and was connected to the water jacket of the column.

Experiments were conducted at nine temperatures in the range of 276 to 313 K. A $CH_2F_2$–air mixture or $N_2$ was introduced near the bottom of the column through a hole (~1 mm in diameter) in the gas-introduction tube. The bubbles travelled along the underside of the glass helix from the bottom to the top of the column, at which point they entered the headspace of the column. The gas flow was controlled by means of calibrated mass flow controllers (M100 Series, MKS Japan, Inc., Tokyo, Japan) and was varied between $2.2 \times 10^{-4}$ and $4.4 \times 10^{-4}$ $dm^3\ s^{-1}$ (STP).

The volumetric flow rate of the gas ($F_{meas}$) was calibrated with a soap-bubble meter for each experimental run. The soap-bubble meter had been calibrated by means of a high-precision film flow meter SF-1U with VP-2U (Horiba, Kyoto, Japan). Errors of $F_{meas}$ are within ±1%. To prevent water evaporation from the stripping column, the gas was humidified prior to entering the stripping column passage through a vessel containing deionized water. This vessel was immersed in a water bath at the same temperature as the stripping column. All volumetric gas flows were corrected to prevailing temperature and pressure by Eq. (3) (Krummen et al., 2000). Errors due to this correction are within ±1%. Errors of $F$ are thus within ±1.4%.

$$F = F_{meas} \times \frac{P_{meas} - h_{meas}}{P_{hs} - h} \times \frac{T}{T_{meas}} \quad (3),$$

where $P_{meas}$ and $T_{meas}$ are the ambient pressure and temperature, respectively, at which $F_{meas}$ was calibrated; $P_{hs}$ is the headspace total pressure over the test solution in an IGS method experiment with a flow rate of $F$ at temperature of $T$; and $h_{meas}$ is the saturated vapour pressure, in atm, of water at $T_{meas}$; $h$ is the saturated vapor pressure, in atm, of water or a-seawater at $T$. Values of $h_{meas}$ and $h$ were calculated by use of Eq. (4) where $S$ is salinity of a-seawater (Weiss and Price, 1980).

$$h \text{ or } h_{meas} = \exp\left[24.4543 - 67.4509 \times \left(\frac{100}{T}\right) - 4.8489 \times \ln\left(\frac{T}{100}\right) - 0.000544 \times S\right] \quad (4)$$

The purge gas flow exiting from the stripping column was diluted with constant flow of $N_2$ to prevent water vapour from condensing. The $CH_2F_2$ in the purge gas flow thus diluted was determined by means of gas chromatography–mass spectrometry (GC-MS) on an Agilent GC6890N with 5973inert instrument (Agilent Technologies, Palo Alto, CA). A portion

of the purge gas containing $CH_2F_2$ stripped from the test solution was injected into the GC-MS instrument in split mode (split ratio = 1:30) with a six-port sampling valve (VICI AG, Valco International, Schenkon, Switzerland) equipped with a stainless sampling loop (1.0 $cm^3$). Gas was sampled automatically at intervals of 10 to 11 min during an experimental run (which lasted from 2 to 8 h), depending on the decay rate of the partial pressure of $CH_2F_2$. Peaks due to $CH_2F_2$ were measured in selected-ion mode ($m/z$ = 33, $CH_2F^+$). A PoraBOND-Q capillary column (0.32-mm i.d. × 50-m length, Agilent Technologies) was used to separate $CH_2F_2$. The column temperature was kept at 308 K. Helium was used as the carrier gas. The injection port was kept at 383 K.

If $CH_2F_2$ in the headspace over the test solution is redistributed into the test solution, $k_1$ should be represented by Eq. (5) instead of Eq. (2) (Krummen et al., 2000; Brockbank et al., 2013).

$$k_1 = \frac{F}{K_{eq}(T)RTV + V_{head}} \quad (5),$$

where $V_{head}$ is headspace volume over the test solution. In this study, the values of $V_{head}$ were 0.070 and 0.020 $dm^3$ for $V$ values of 0.300 and 0.350 $dm^3$, respectively. Equations (6) and (7) are derived from Eqs. (2) and (5), respectively:

$$K_{eq}(T) = \frac{1}{k_1 RT}\frac{F}{V} \quad (6),$$

$$K_{eq}(T) = \frac{1}{k_1 RT}\frac{F}{V} - \frac{V_{head}}{RTV} \quad (7).$$

As described in *Results and discussion* (Sect. 3.1), $CH_2F_2$ in the headspace over the test solution was not expected to be redistributed into the test solution. Hence Eq. (6) was used to deduce $K_{eq}(T)$ from $k_1$. Errors of $T$ are estimated to be within ±0.2 K. These errors of $T$ may give potential systematic bias of ca. ±1% ($\delta K_{eq}/K_{eq}$) where $\delta K_{eq}$ is error of the value of $K_{eq}$. Errors of $F$ are estimated to be less than 1.4 %, and these errors may give potential systematic bias of less than 1.4 % ($\delta K_{eq}/K_{eq}$). Accordingly, for the IGS methods, values of $K_{eq}$ may have potential systematic bias of ca. ±2%.

If redistribution of $CH_2F_2$ in the headspace to the test solution had occurred, the values determined using Eq. (6) would be overestimated. Errors due to this redistribution are always negative values. Ratio of the errors to the $K_{eq}$ values (%) is $\frac{100k_1V_{head}}{F}$. Values of this ratio increase as values of $K_{eq}$ decrease. Under the experimental conditions here, this ratio is calculated to be from −2.0 % for water at 3.0 °C to −6.5 % for a-seawater at 51.534‰ and 39.5 °C.

### 2.3 Phase ratio variation headspace method

The $K_H$ values of $CH_2F_2$ in water were also determined by means of the phase ratio variation headspace (PRV-HS) method (Ettre et al., 1993) for comparison with the results obtained by the above-described IGS method. The PRV-HS method experiments were performed over the temperature range from 313 to 353 K at 10 K intervals because the headspace

temperature in the equipment used here could not be controlled at less than 313 K. The experimental procedure was the same as that described in detail previously (Kutsuna, 2013) and it is described briefly here.

The determination was carried out by GC-MS on an Agilent GC6890N with 5973inert instrument (Agilent Technologies) equipped with an automatic headspace sampler (HP7694, Agilent Technologies). The headspace samples were slowly and continuously shaken by a mechanical set-up for the headspace equilibration time (1 h; see below), and then the headspace gas (1 $cm^3$) was injected into the gas chromatograph in split mode (split ratio = 1:30). The conditions used for GC-MS were the same as those described in Sect. 2.2.

Headspace samples containing five different amounts of $CH_2F_2$ and six different volumes of water were prepared for an experimental run at each temperature as follows (30 samples total). Volumes ($V_i$) of 1.5, 3.0, 4.5, 6.0, 7.5, and 9.0 $cm^3$ of deionized water were pipetted into six headspace vials with a total volume ($V_0$) of 21.4 $cm^3$ ($V_i/V_0$ = 0.070, 0.140, 0.210, 0.280, 0.350, and 0.421, respectively). Five sets of six headspace vials were prepared and sealed. A prescribed volume ($v_j$) of a standard gas mixture of $CH_2F_2$ and air was added to each set of five vials containing the same volume ($V_i$) of water by means of a gas-tight syringe ($v_j$ = 0.05, 0.10, 0.15, 0.20, or 0.25 $cm^3$). The headspace partial pressure of $CH_2F_2$ thus prepared ranged from $10^{-5}$ to $10^{-6}$ atm.

The time required for equilibration between the headspace and the aqueous solution was determined by analyzing the headspaces over the test samples as a function of time until steady-state conditions were attained. In Fig. S1, the relative signal intensities of the GC-MS peaks for $CH_2F_2$, that is, the ratio of the headspace partial pressure at time $t$ to that at 60 min ($P_t/P_{60}$), are plotted against the time ($t_h$) during which samples were placed in the headspace oven. The plot shows that the peak area did not change after 60 min (Fig. S1). Therefore, the headspace equilibration time was set at 1 h for all the measurements.

If $P_{ij}$ is the equilibrium partial pressure (in atm) of a $CH_2F_2$ sample in a vial with volume $V_0$ (in $cm^3$) containing a volume $V_i$ (in $cm^3$) of water and a volume $v_j$ (in $cm^3$) of a $CH_2F_2$ gas mixture, and if $P_j$ is the equilibrium partial pressure (in atm) of $CH_2F_2$ in a sample containing volume $v_j$ (in $cm^3$) of a $CH_2F_2$ gas mixture without water, then Eq. (8) applies:

$$\frac{P_j V_0}{RT} = K_{\mathrm{eq}}(T) P_{ij} V_i + \frac{P_{ij}(V_0 - V_i)}{RT} \tag{8}$$

Because the signal peak area of $CH_2F_2$ ($S_{ij}$) at partial pressure $P_{ij}$ is expected to be proportional to $v_j$ for each set of samples with the same $V_i$, a plot of $S_{ij}$ versus $v_j$ should be a straight line that intercepts the origin:

$$S_{ij} = L_i v_j \tag{9}$$

The slope of the line, $L_i$, corresponds to $S_{ij}$ at $v_j$ = 1.0 $cm^3$. If $L$ is the slope corresponding to $P_i$ at $V_i$ = 0, then

$$\frac{1}{L_i} = \frac{1}{L} + \frac{RTK_{\mathrm{eq}}(T) - 1}{L} \frac{V_i}{V_0} \tag{10}$$

Plotting $1/L_i$ against $V_i/V_0$ gives an intercept of $1/L$ and a slope of $[RT\,K_{eq}(T) - 1]/L$, and $K_{eq}(T)$ can be obtained from these two values. Therefore, $K_{eq}(T)$ can be determined by recording the peak area $S_{ij}$, deriving $L_i$ from a plot of $S_{ij}$ versus $v_j$, and then applying regression analysis to plots of $1/L_i$ versus $V_i/V_0$ with respect to Eq. (10).

Furthermore, values of $K_{eq}(T)$ and errors of them were ~~determiend~~ determined by nonlinear~~non-liner~~ fitting of the data of $L_i$ and $V_i/V$ by means of Eq. (11), which was obtained from Eq. (10):

$$L_i = \frac{L}{1+(RTK_{eq}(T)-1)\frac{V_i}{V_0}} \quad (11)$$

Errors of $T$ are estimated to be within ca. 2 K. These errors of $T$ may give potential systematic bias of ca. ±4% ($\delta K_{eq}/K_{eq}$) at 313 K and ca. ±3% ($\delta K_{eq}/K_{eq}$) at 353 K. Errors of $V_0$ are estimated to be less than 1 %, and these errors may give potential systematic bias of less than 1 % ($\delta K_{eq}/K_{eq}$). Accordingly, for the PRV-HS methods, values of $K_{eq}$ may have potential systematic bias of ca. ±4%.

## 3 Results and discussion

### 3.1 Determination of Henry's law constants

In the IGS method experiment, an aqueous solution was purged with $N_2$ to strip $CH_2F_2$ from the solution into the $N_2$ purge gas flow, and the partial pressure of $CH_2F_2$ ($P_t$) in the $N_2$ purge gas flow decreased with time. Typically, it took 20–100 min, depending on the purge gas flow rate and the temperature of the solution, for the decrease to show a first-order time profile. From the first-order time profile of $P_t$ for the following period of 2–7 h, during which $P_t$ typically decreased by 2 orders of magnitude, the first-order decreasing rate constant, $k_1$, was calculated according to Eq. (1). Values of $k_1$ were obtained at different volumes of deionized water ($V$), various purge gas flow rate ($F$), and various temperatures. Figure S2 shows an example of time profile of $P_t$ and how to calculate the $k_1$ value.

Figure 1 plots values of $F/(k_1RTV)$, the right side of Eq. 6, against $F$ for $V$ values of 0.350 $dm^3$ and 0.300 $dm^3$ at each temperature $T$ (K). Table 1 lists the average values of $F/(k_1RTV)$ for $V$ values of 0.350 and 0.300 $dm^3$ at each temperature. The data with errors being >10% of the data was first excluded. Next, some~~Some~~ data were excluded for calculation of the average so that the remaining data were inside the 2σ range. This procedure was iterated until all the data were inside the 2σ range. The~~; the~~ data points thus excluded was only for $V$ values of 0.350 $dm^3$ and the number of them were eight~~six~~ or fewer at each temperature.

As is apparent in Fig. 1 and Table 1, the $F/(k_1RTV)$ values for the two $V$ values (0.350 and 0.300 $dm^3$) agreed at each temperature. This agreement strongly suggests that $K_{eq}(T)$ is represented by Eq. (6) rather than by Eq. (7) because, if Eq. (7) were applicable, the $K_{eq}(T)$ values calculated for the $V$ value of 0.300 $dm^3$ would be inconsistent with those for the $V$ value of 0.350 $dm^3$: the former would be smaller than the latter by 0.007–0.008 M $atm^{-1}$. Redistribution of $CH_2F_2$ between the headspace and the test solution was probably negligible under the experimental conditions here; hence, values of $K_{eq}(T)$ should be calculated from Eq. (6) rather than Eq. (7).

The above-mentioned agreement also supports the idea that gas-to-water partitioning equilibrium of $CH_2F_2$ was achieved under the experimental conditions used for the IGS method. As described later, the achievement of gas-to-water partitioning equilibrium was also supported by comparison of these data with $K_{eq}(T)$ values obtained by the PRV-HS method. Hereafter only values of $F/(k_1RTV)$ for the $V$ value of 0.350 $dm^3$ are used to deduce $K_{eq}(T)$ values. Because the $K_{eq}(T)$ values in water correspond to the Henry's law constants, $K_H(T)$ in M $atm^{-1}$, $K_H(T)$ is used instead of $K_{eq}(T)$ in this section.

Figure 2 plots the average $K_H$ values for the $V$ value of 0.350 $dm^3$ against $100/T$. Error bars of the data represent both 2σ for the average and potential systematic bias (±2%). Figure 2 also displays the $K_H(T)$ values obtained by the PRV-HS method. The results of the PRV-HS experiments are described in *Supporting Information* (Fig. S3, Fig. S4 and Table S1). The $K_H$ value obtained by the PRV-HS experiments at each temperature and its error were estimated at 95% confidence level by fitting the two datasets at each temperature (Fig. S4) simultaneously by means of the nonlinear least-squares method with respect to Eq. (11). Error bars of the data by PRV-HS method in Fig. 2 represent both errors at 95% confidence level for the regression and potential systematic bias (±4%).

All the $K_H$ values were regressed with respect to the van't Hoff equation (Eq. (12)) (Clarke and Glew, 1965; Weiss, 1970):

$$K_H(T) = \exp\left(a_1 + a_2 \times \left(\frac{100}{T}\right) + a_3 \times \ln\left(\frac{T}{100}\right)\right) \quad (12).$$

The regression with respect to Eq. (12) gave Eq. (13).

$$\ln\left(K_H(T)\right) = -49.7122 + 77.7018 \times \left(\frac{100}{T}\right) + 19.143794 \times \ln\left(\frac{T}{100}\right) \quad (13).$$

The square-root-of-variance, that is, standard deviation for each fitting coefficient in Eq. (12) is as follows:

$\delta a_1 = 5.5$; $\delta a_2 = 8.3$; $\delta a_3 = 2.8$.

In Fig. 2, the solid curve was obtained by Eq. (13). The $K_H(T)$ values calculated by Eq. (13) are listed in Table 1. Equation (13) can reproduce the average of $K_H$ values at each temperature within an error of 5%. The dashed lines in Fig. 2 represent 95% confidence limits of the regression for fitting the $K_H(T)$ values by Eq. (12). Taking into consideration errors of the $K_H$ values, the $K_H$ values obtained by the two methods were within the 95% confidence limits of the regression by Eq. (12); this result supports the idea that the values determined by the IGS method and the PRV-HS method were accurate.

The Gibbs free energy for dissolution of $CH_2F_2$ into water at temperature $T$ ($\Delta G_{sol}(T)$) and the enthalpy for dissolution of $CH_2F_2$ into water ($\Delta H_{sol}$) can be deduced from $K_H(T)$ by means of Eqs. (14) and (15):

$$\Delta G_{sol}(T) = \mu_l^\circ(T) - \mu_g^\circ(T) = -RT\ln(K_H(T)) \quad (14)$$

$$\Delta H_{sol}(T) = -R\frac{\partial[\ln(K_H(T))]}{\partial(1/T)} \quad (15)$$

where $\mu_l^\circ(T)$ is the chemical potential of $CH_2F_2$ under the standard-state conditions at a concentration of 1 M in aqueous solutions at temperature $T$; and $\mu_g^\circ(T)$ is the chemical potential of $CH_2F_2$ under the standard-state conditions at 1 atm of

partial pressure in the gas phase at temperature $T$. The $K_H(T)$ and $\Delta H_{sol}(T)$ values at 298.15 K were calculated by means of Eqs. (13) and (15) and are listed in Table 2. $K_H(298.15)$ is represented by $K_H^{298}$ hereafter.

Table 2 also lists literature values of $K_H^{298}$ and $\Delta H_{sol}$ at 298.15 K for $CH_2F_2$ reported in two reviews (Clever et al., 2005; Sander, 2015) and by Anderson (2011); the units of the literature data were converted to M atm$^{-1}$ for $K_H^{298}$ and kJ mol$^{-1}$ for $\Delta H_{sol}$. The $K_H^{298}$ value determined in this study was ~~7~~6–~~9~~7% smaller than the values reported by Maaβen (1995), Reichl (1995) and Anderson (2011), whereas the value reported by Yaws and Yang (1992), that reported by Hilal et al. (2008) and that reported by Miguel et al. (2000) were 1.3, 1.~~4~~3 and 0.~~47~~46 times, respectively, as large as the value determined here. The absolute value of $\Delta H_{sol}$ at 298.15 K determined here was by 1.4–3.4 kJ mol$^{-1}$ less than the values determined by Maaβen (1995), Reichl (1995), Kühne et al. (2005) and Anderson (2011), whereas it was by 10 kJ mol$^{-1}$ less than the value reported by Miguel et al. (2000).

### 3.2 Determination of salting-out effects in artificial seawater

The solubility of $CH_2F_2$ in a-seawater (Sect. 2.1) was determined by means of the IGS method (Sect. 2.2). According to Eq. (6), the $K_{eq}(T)$ values at an a-seawater salinity of $S$ in ‰ were obtained by averaging the $F/(k_1RTV)$ values for the $V$ value of 0.350 dm$^3$ at each salinity and temperature in a similar way as described in Sect. 3.1. Figure 3 plots values of $F/(k_1RTV)$ at each temperature against $F$ for $V$ values of 0.350 dm$^3$ at an a-seawater salinity of 36.074‰. Figures S5-S8 represent such plots at an a-seawater salinity of 4.452, 8.921, 21.520 and 51.534 ‰. The $K_{eq}(T)$ value at an a-seawater salinity of $S$ in ‰ is represented by $K_{eq}^S(T)$ hereafter. Table 3 lists the $K_{eq}^S(T)$ values.

Figure 4 plots the $K_{eq}^S(T)$ values against $100/T$. The plots indicate a clear salting-out effect on $CH_2F_2$ solubility in a-seawater: that is, the solubility of $CH_2F_2$ in a-seawater decreased with increasing a-seawater salinity. For example, the solubility of $CH_2F_2$ in a-seawater at a salinity of 36.074‰ was 0.~~73~~74–0.~~79~~78 times the solubility in water at 3.0 to 39.5 °C.

In general, the salting-out effect on nonelectrolyte solubility in an aqueous salt solution of ionic strength $I$ can be determined empirically by means of the ~~Setchenow~~Sechenov equation:

$$\ln(K_H(T)/K_{eq}^I(T)) = k_I I \quad (16)$$

where $K_{eq}^I(T)$ is the $K_{eq}(T)$ at ionic strength $I$ in mol kg$^{-1}$; and $k_I$ is the ~~Setchenow~~ Sechenov coefficient for the molality- and natural logarithm-based ~~Setchenow~~ Sechenov equation and is independent of $I$ (Clegg and Whitfield, 1991). For a-seawater, a similar relationship between $K_{eq}^S(T)$ and $S$ is expected:

$$\ln(K_H(T)/K_{eq}^S(T)) = k_S S \quad (17)$$

where $k_S$ is the ~~Setchenow~~ Sechenov coefficient for the salinity- and natural logarithm-based ~~Setchenow~~ Sechenov equation and is independent of $S$. Figure 5 plots $\ln(K_H(T)/K_{eq}^S(T))$ against $S$ at each temperature. Table S2 lists values of $k_S$ determined by fitting the data at each temperature by use of Eq. (17). If the $K_{eq}^S(T)$ values obeyed Eq. (17), the data at each temperature

in Fig. 5 would fall on a straight line passing through the origin, but they did not. Figure 5 reveals that the salinity dependence of $CH_2F_2$ solubility in a-seawater cannot be represented by Eq. (17).

When the same data were plotted on a log–log graph (Fig. S9), a line with a slope of about 0.5 was obtained by linear regression. This result suggests that $\ln(K_H(T)/K_{eq}^S(T))$ varied according to Eq. (18):

$$\ln\left(K_H(T)/K_{eq}^S(T)\right) = k_{s1} \times S^{0.5} \quad (18)$$

Values of $k_{s1}$ may be represented by the following function of $T$:

$$k_{s1} = b_1 + b_2 \times \left(\frac{100}{T}\right) \quad (19)$$

Parameterizations of $b_1$ and $b_2$ obtained by fitting all the $\ln(K_H(T)/K_{eq}^S(T))$ and $S$ data at each temperature simultaneously by means of the nonlinear least-squares method gives Eq. (20).

$$\ln\left(K_H(T)/K_{eq}^S(T)\right) = \left(0.0127 + 0.0099 \times \left(\frac{100}{T}\right)\right) \times S^{0.5} \quad (20)$$

The standard deviation for each fitting coefficient in Eq. (19) is as follows:

$\delta b_1 = 0.0106$; $\delta b_2 = 0.0031$.

Since $2 \times \delta b_1 > b_1$, the parameterization by Eq. (19) may be overworked. Accordingly, all the $\ln(K_H(T)/K_{eq}^S(T))$ and $S$ data at each temperature are fitted simultaneously using Eq. (21) instead of Eq. (19). The nonlinear least-squares method gives Eq. (22).

$$k_{s1} = b_2 \times \left(\frac{100}{T}\right) \quad (21)$$

$$\ln\left(K_H(T)/K_{eq}^S(T)\right) = 0.134 \times \left(\frac{100}{T}\right) \times S^{0.5} \quad (22)$$

The standard deviation for the fitting coefficient in Eq. (21) is as follows: $\delta b_2 = 0.001$. As seen in Fig. 5, Eqs. (21) and (22) reproduced the data well.

$\ln(K_H(T)/K_{eq}^S(T))$ depends on $S^{0.5}$ and follows Eq. (22) rather than the Sechenov dependence (Eq. (17)). Table S7 compares values of $K_{eq}^S$ calculated by Eq. (22) with those by Eq. (17). The difference between these values of $K_{eq}^S$ at 35‰ of salinity was within 3% of the $K_{eq}^S$ value. Decreases in values of $K_{eq}^S$ are calculated to be 7–8% and 4%, respectively, by Eqs. (17) and (23) as salinity of a-seawater increases from 30‰ to 40‰ at each temperature. ~~$\ln(K_H(T)/K_{eq}^S(T)) = k_{s1} S^{0.5} + k_{s2} S$ (18)~~

~~Values of $k_{s1}$ and $k_{s2}$ may be represented by the following functions of $T$:~~

~~$k_{s1} = a_1 + a_2 \times (100/T)$ (19)~~

~~$k_{s2} = a_3 + a_4 \times (100/T)$ (20)~~

~~Parameterizations of $a_1$, $a_2$, $a_3$ and $a_4$ obtained by fitting all the $\ln(K_H(T)/K_{eq}^S(T))$ and $S$ data simultaneously by means of the nonlinear least squares method (Fig. 5, bold curve) indicated that Eqs. (18), (19) and (20) reproduced the data well. Overall, the $K_{eq}^S(T)$ value for $CH_2F_2$ in a-seawater can be represented by~~

~~$\ln(K_H(T)/K_{eq}^S(T)) = [-0.2261 + 0.5176\times(T/100)] \times S^{0.5} + [0.0362 - 0.1046\times(T/100)] \times S$~~ ~~(21)~~

~~Plots of $k_{s1}$ and $k_{s2}$ against temperature (Fig. S10) indicate that the absolute values of $k_{s1}$ are much larger than those of $k_{s2}$; that is, $\ln(K_H(T)/K_{eq}^S(T))$ depends predominantly on $S^{0.5}$ rather than on $S$.~~

The reason for this salting-out effect of $CH_2F_2$ solubility in a-seawater is not clear. Specific properties of $CH_2F_2$ –small molecular volume, which results in small work of cavity creation (Graziano, 2004; 2008), and large solute-solvent attractive potential energy in water and a-seawater– may cause deviation from Sechenov relationship (*Supporting Information*).

In Eq. (~~21~~22), $K_H(T)$ is represented by Eq. (13), as described in Sect. 3.1. Therefore $K_{eq}^S(T)$ is represented by Eq. (~~22~~23):.

$$\ln(K_{eq}^S) = -49.71 + (77.70 - 0.134 \times S^{0.5}) \times \left(\frac{100}{T}\right) + 19.14 \times \ln\left(\frac{T}{100}\right) \quad (23)$$

~~$\ln(K_{eq}^S(T)) = -49.7122 + 77.7018\times(100/T) + 19.1379\times\ln(T/100) + [-0.2261 + 0.5176\times(T/100)] \times S^{0.5}$~~
~~$+ [0.0362 - 0.1046\times(T/100)] \times S$~~ ~~(22)~~

The values calculated with Eq. (~~22~~23) are indicated by the bold curves in Fig. 4 and are listed in Table 3. Table 3 lists errors at 95% confidence level for the regression. These errors ($error_{23}$) are calculated by Eq. (24):

$$error_{23} = K_{eq}^S \times \sqrt{\left(\frac{error_{13}}{K_H}\right)^2 + \left(\frac{error_{22}}{K_{eq}^S}\right)^2} \quad (24)$$

where $error_{13}$ represents errors at 95% confidence level for the regression by Eq. (12); $error_{22}$ represents errors at 95% confidence level for the regression by Eq. (21). Table 3 also lists errors due to both errors at 95% confidence level for the regression and potential systematic bias (±2%). Equation (~~22~~23) reproduced the experimentally determined values of $K_H(T)$ and $K_{eq}^S(T)$ within the uncertainty of these experimental runs.

### 3.3 Dissolution of $CH_2F_2$ in the ocean mixed layer and its influence on estimates of $CH_2F_2$ emissions

The solubility of $CH_2F_2$ in a-seawater can be represented as a function of temperature and salinity relevant to the ocean (Eq. (~~22~~23)). Monthly averaged equilibrium fractionation values of $CH_2F_2$ between the atmosphere and the ocean ($R_m$ in Gg patm$^{-1}$, where patm is $10^{-12}$ atm) in that the ocean mixed layer is at solubility equilibrium with the atmosphere is estimated as follows. If we divide the global ocean into 0.25°×0.25° grids, $R_m$ can be estimated from the sum of the equilibrium fractionation values from the gridded cells:

$$R_m = \frac{m_{d,m}}{P_a} = Q \sum_{i=-360}^{i=360} \sum_{j=-720}^{j=720} K_{eq}^S(T) d_{i,j,m} A_{i,j,m} \quad (~~23~~25)$$

where $m_{d,m}$, in Gg, is the amount of $CH_2F_2$ dissolved in the ocean mixed layer; $p_a$, in $10^{-12}$ atm, is the $CH_2F_2$ partial pressure in the air; $d_{i,j,m}$ is the monthly mean depth, in m, of the ocean mixed layer in each grid cell; $A_{i,j,m}$ is the oceanic area, in m$^2$, in each grid cell; $Q$ is a conversion factor (with a value of 52); $m$ is the month index; and $i$ and $j$ are the latitude and longitude

indices. We obtained monthly 0.25°×0.25° gridded sea surface temperatures and sea surface salinities from WOA V2 2013 data collected at 10 m depth from 2005 to 2012 (https://www.nodc.noaa.gov/OC5/woa13/woa13data.html; Boyer et al., 2013) and monthly 2° × 2° gridded mean depths of the ocean mixed layer from Mixed layer depth climatology and other related ocean variables in temperature with a fixed threshold criterion (0.2°C) (http://www.ifremer.fr/cerweb/deboyer/mld/Surface_Mixed_Layer_Depth.php; de Boyer Montégut et al., 2004). Values of $A_{i,j,m}$ were estimated to be equal to the area of each grid cell in which both gridded data were unmasked.

Figure 6 shows the $R_m$ values for the global and the semi-hemispheric atmosphere. Values of $R_m$ for the global atmosphere are between 0.057 and 0.096 Gg patm$^{-1}$. Because $10^{-12}$ atm of $CH_2F_2$ in the global atmosphere corresponds to 9.4 Gg of atmospheric burden of $CH_2F_2$, 0.6 to 1.0 % of the atmospheric burden resides in the ocean mixed layer when that layer is at solubility equilibrium with the atmosphere. The magnitude of "buffering" of the atmospheric burden of $CH_2F_2$ by the additional $CH_2F_2$ in ocean surface waters is therefore realistically limited to only about 1 % globally. However, such buffering would be more effective in each lower tropospheric semi-hemisphere of the AGAGE 12-box model, which has been used for a top-down estimate of $CH_2F_2$ emissions. The right vertical axis of Fig. 6 represents the residence ratios of $CH_2F_2$ dissolved in the ocean mixed layer for each lower tropospheric semi-hemispheric atmosphere of the AGAGE 12-box model. The residence ratios were calculated on the assumption that $10^{-12}$ atm of $CH_2F_2$ corresponds to 1.2 Gg of atmospheric burden of $CH_2F_2$ in each lower tropospheric semi-hemisphere. As seen in Figure 6, in the southern semi-hemispheric lower troposphere (30° S–90° S), at least 5 % of the atmospheric burden of $CH_2F_2$ would reside in the ocean mixed layer in the winter, and the annual variance of the $CH_2F_2$ residence ratio would be 4%. These ratios are, in fact, upper limits because $CH_2F_2$ in the ocean mixed layer may be undersaturated. It takes days to a few weeks after a change in temperature or salinity for oceanic surface mixed layers to come to equilibrium with the present atmosphere, and equilibration time increases with depth of the surface mixed layer (Fine, 2011). In the estimation using the gridded data here, >90 % of $CH_2F_2$ in the ocean mixed layer would reside in less than 300 m depth (Tables ~~S3~~S4, ~~S4~~S5, ~~S5~~ S6 and ~~S6~~S7).

Haine and Richards (1995) demonstrated that seasonal variation in ocean mixed layer depth was the key process which affected undersaturation and supersaturation of chlorofluorocarbon 11 (CFC-11), CFC-12 and CFC-113 by use of a one-dimensional slab mixed model. As described above, >90 % of $CH_2F_2$ in the ocean mixed layer is expected to reside in less than 300 m depth. According to the model calculation results by Haine and Richards (1995), saturation of $CH_2F_2$ would be >0.9 for the ocean mixed layer with less than 300 m depth. The saturation of $CH_2F_2$ in the ocean mixed layer is thus estimated to be at least 0.8. In the southern semi-hemispheric lower troposphere (30° S–90° S), therefore, at least 4 % of the atmospheric burden of $CH_2F_2$ would reside in the ocean mixed layer in the winter, and the annual variance of the $CH_2F_2$ residence ratio would be 3%.

In the Southern Hemisphere, $CH_2F_2$ emission rates are much lower than in the Northern Hemisphere. Hence, dissolution of $CH_2F_2$ in the ocean, even if dissolution is reversible, may influence estimates of $CH_2F_2$ emissions derived from long-term observational data on atmospheric concentrations of $CH_2F_2$; in particular, consideration of dissolution of $CH_2F_2$ in the ocean may affect estimates of $CH_2F_2$ emissions in the Southern Hemisphere and their seasonal variability because of slow rates of

inter-hemispheric transport and small portion of the $CH_2F_2$ emissions in the Southern Hemisphere to the total emissions.

## 4 Conclusion

The solubility of $CH_2F_2$ in aqueous salt solutions relevant to seawater can be represented as a function of temperature and salinity, as shown in Eq. (~~22~~23). The relationship between $CH_2F_2$ solubility and the salinity of the artificial seawater was found to be unusual in that the excessive free energy for dissolution depended predominantly on the 0.5 power of salinity. By using the solubility of $CH_2F_2$ determined in this study, the magnitude of buffering of the atmospheric burden of $CH_2F_2$ by the additional $CH_2F_2$ in ocean surface waters is estimated to be realistically limited to only about 1 % globally; however, in a southern semi-hemispheric lower troposphere (30° S–90° S) of the AGAGE 12-box model, the atmospheric burden of $CH_2F_2$ is estimated to reside in the ocean mixed layer by at least ~~5~~ 4 % in the winter and by 1 % in the summer. Hence, it may be necessary that dissolution of $CH_2F_2$ in the ocean be taken into consideration to derive $CH_2F_2$ emissions in the Southern Hemisphere and their seasonal variability from long-term observational data on atmospheric concentrations of $CH_2F_2$.

## Supplement link

Supporting information is attached.

## Competing interests

The authors declare that they have no conflict of interest.

## References

Anderson, G. K.: A thermodynamic study of the (difluoromethane + water) system, J. Chem. Thermodynamics, 43, 1331-1335, doi:10.1016/j.jct.2011.03.020, 2011.

Boyer, T.P., Antonov, J. I., Baranova, O. K., Coleman, C., Garcia, H. E., Grodsky, A., Johnson, D. R., Locarnini, R. A., Mishonov, A. V., O'Brien, T. D., Paver, C. R., Reagan, J. R., Seidov, D., Smolyar, I. V. and Zweng, M. M.: World Ocean Database 2013, NOAA Atlas NESDIS 72, S. Levitus, Ed., A. Mishonov, Technical Ed.; Silver Spring, MD, 209 pp., 2013. http://doi.org/10.7289/V5NZ85MT.

Brockbank, S. A., Russon, J. L., Giles, N. F., Rowley, R. L., and Wilding, W. V.: Infinite dilution activity coefficients and Henry's law constants of compounds in water using the inert gas stripping method, Fluid Phase Equil., 348, 45-51, doi:10.1016/j.fluid.2013.03.023, 2013.

Carpenter, L. J., Reimann (Lead Authors), S., Burkholder, J. B., Clerbaux, C., Hall, B. D., Hossaini, R., Laube, J. C., and Yvon-Lewis, S. A.: Ozone-Depleting Substances (ODSs) and Other Gases of Interest to the Montreal Protocol, Chapter 1, in Scientific Assessment of Ozone Depletion: 2014, Global Ozone Research and Monitoring Project, 55, World Meteorological Organization, Geneva, Switzerland, 2014.

Clarke, E. C. W. and Glew, D. N.: Evaluation of thermodynamic functions from equilibrium constants. Trans. Faraday Soc., 134, 539-547, doi:10.1039/TF9666200539, 1965.

Clegg, S. L. and Whitfield, M.: Activity coefficients in natural waters, Chapter 6, in Pitzer, K. S. (Ed.), Activity coefficients in electrolyte solutions, 2nd ed. CRC Press, Boca Raton, FL, pp. 279-434, 1991.

Clever, H.L., Battino, R., Clever, H.L., Jaselskis, B., Clever, H.L., Yampol'skii, Y.P., Jaselskis, B., Scharlin, and P., Young, C.L.: IUPAC-NIST Solubility Data Series. 80. Gaseous fluorides of boron, nitrogen, sulfur, carbon, and silicon and solid xenon fluorides in all solvents. J. Phys. Chem. Ref. Data, 34, 201-438, doi:10.1063/1.1794762, 2005.

Cunnold, D. M., Fraser, P. J., Weiss, R. F., Prinn, R. G., Simmonds, P. G., Miller, B. R., Alyea, F. N., and Crawford, A. J.: global trends and annual releases of $CCl_3F$ and $CCl_2F_2$ estimated from ALE/GAGE and other measurements from July 1978 to June 1991. J. Geophys. Res., 99, 1107-1126, doi: 10.1029/93JD02715, 1994.

de Boyer Montégut, C., Madec, G., Fischer, A. S., Lazar, A., Iudicone, D.: Mixed layer depth over the global ocean: an examination of profile data and a profile-based climatology. J. Geophys. Res., 109, C12003, doi:10.1029/2004JC002378, 2004.

Ettre, L., Welter, C., Kolb, B.: Determination of gas-liquid partition coefficients by automatic equilibrium headspace-gas chromatography utilizing the phase ratio variation method. Chromatographia, 35, 73-84, doi:10.1007/BF02278560, 1993.

Fine, R. A.: Observations of CFCs and $SF_6$ as ocean tracers. Annual Review of Marine Science, 3, 173-195, doi:10.1146/annurev.marine.010908.163933, 2011.

Graziano, G.: Case study of enthalpy–entropy noncompensation. Journal of Chemical Physics, 120, 4467-4471, doi: 10.1063/1.1644094, 2004.

Graziano, G.: Salting out of methane by sodium chloride: A scaled particle theory study. Journal of Chemical Physics, 129, 084506, doi: 10.1063/1.2972979, 2008.

Haine, T. W. N., and Richards, K. J.: The influence of the seasonal mixed layer on oceanic uptake of CFCs. Journal of Geophysical Research, 100, 10727-10744, doi:10.1029/95JC00629, 1995.

Hilal, S. H., Ayyampalayam, S. N. and Carreira, L. A.: Air-liquid partition coefficient for a diverse set of organic compounds: Henry's law constant in water and hexadecane. Environ. Sci. Technol., 42, 9231-9236, doi:10.1021/es8005783, 2008.

IPCC, 2013: Climate change 2013: the physical science basis. Contribution of Working group I to the fifth assessment report of the Intergovernmental panel on climate change [Stocker, T. F., Qin, D., Plattner, G.-K., Tignor, M., Allen, S. K., Boschung, J., Nauels, A., Xia, Y. Bex V. and Midgley, P. M. (eds.)], Cambridge University Press, Cambridge, United Kingdom and New York, NY, USA, 1535 pp.

Krummen, M., Gruber, D., and Gmehling, J.: Measurement of activity coefficients at infinite dilution in solvent mixtures using the dilutor technique. Ind. Eng. Chem. Res., 39, 2114-2123, doi:10.1021/ie990830p, 2000.

Kutsuna, S.: Determination of rate constants for aqueous reactions of HCFC-123 and HCFC-225ca with $OH^-$ along with Henry's law constants of several HCFCs. Int. J. Chem. Kinet., 45, 440-451, doi:10.1002/kin.20780, 2013.

Kutsuna, S., and Hori, H.: Experimental determination of Henry's law constant of perfluorooctanoic acid (PFOA) at 298K by means of an inert-gas stripping method with a helical plate, Atmos. Environ., 42, 8883-8892, doi:10.1016/j.atmosenv.2008.09.008, 2008.

Kühne, R., Ebert, R.-U., and Schüürmann, G.: Prediction of the temperature dependency of Henry's law constant from chemical structure, Environ. Sci. Technol., 39, 6705–6711, doi:10.1021/es050527h, 2005.

Lunt, M.F., Rigby, M., Ganesan, A.L., Manning, A.J., Prinn, R.G., O'Doherty, S., Mühle, J., Harth, C.M., Salameh, P.K., Arnold, T., Weiss, R.F., Saito, T., Yokouchi, Y., Krummel, P.B., Steele, L.P., Fraser, P.J., Li, S., Park, S., Reimann, S., Vollmer, M.K., Lunder, C., Hermansen, O., Schmidbauer, N., Maione, M., Arduini, J., Young, D., Simmonds, P.G.: Reconciling reported and unreported HFC emissions with atmospheric observations. Proceedings of the National Academy of Sciences 112, 5927-5931, doi: 10.1073/pnas.1420247112, 2015.

Maaβen, S., 1995, Experimentelle Bestimmung und Korrelierung von Verteilungskoeffizienten in verdünnten Lösungen, Ph.D. thesis, Technische Universität Berlin, Germany.

Mackay, D., Shiu, W. Y., and Sutherland, R. P.: Determination of air-water Henry's law constants for hydrophobic pollutants, Environ. Sci. Technol., 13, 333-337, doi:10.1021/es60151a012, 1979.

Miguel, A. A. F., Ferreira, A. G. M., and Fonseca, I. M. A.: Solubilities of some new refrigerants in water. Fluid Phase Equil. 173, 97-107, doi:10.1016/S0378-3812(00)00390-3, 2000.

Montzka, S. A., McFarland, M., Andersen, S. O., Miller, B. R., Fahey, D. W., Hall, B. D., Hu, L., Siso, C., and Elkins, J. W.: Recent trends in global emissions of hydrochlorofluorocarbons and hydrofluorocarbons: reflecting on the 2007 Adjustments to the Montreal Protocol. J. Phys. Chem. A, 119, 4439-4449, doi:10.1021/jp5097376, 2015.

O'Doherty, S., Rigby, M., Mühle, J., Ivy, D.J., Miller, B.R., Young, D., Simmonds, P.G., Reimann, S., Vollmer, M.K., Krummel, P.B., Fraser, P.J., Steele, L.P., Dunse, B., Salameh, P.K., Harth, C.M., Arnold, T., Weiss, R.F., Kim, J., Park, S., Li, S., Lunder, C., Hermansen, O., Schmidbauer, N., Zhou, L.X., Yao, B., Wang, R.H.J., Manning, A.J., and Prinn, R.G.: Global emissions of HFC-143a ($CH_3CF_3$) and HFC-32 ($CH_2F_2$) from in situ and air archive atmospheric observations. Atmos. Chem. Phys. 14, 9249-9258, doi: 10.5194/acp-14-9249-2014, 2014.

Platford, R.F.: The activity coefficient of sodium chloride in seawater. J. Marine Res., 23, 55-62, 1965.

Prinn, R.G., Weiss, R.F., Fraser, P.J., Simmonds, P.G., Cunnold, D.M., Alyea, F.N., O'Doherty, S., Salameh, P., Miller, B.R., Huang, J., Wang, R.H.J., Hartley, D.E., Harth, C., Steele, L.P., Sturrock, G., Midgley, P.M., McCulloch, A.: A history of chemically and radiatively important gases in air deduced from ALE/GAGE/AGAGE. J. Geophys. Res.-Atmos., 105, 17751-17792, doi:10/1029/2000JD900141, 2000. Website: http://agage.mit.edu

Reichl, A., 1995, Messung und Korrelierung von Gaslöslichkeiten halogenierter ohlenwasserstoffe, Ph.D. thesis, Technische Universität Berlin, Germany.

Rigby, M., Prinn, R. G., O'Doherty, S., Montzka, S. A., McCulloch, A., Harth, C. M., Műhle, J. Salameh, P. K., Weiss, R. F., Young, D., Simmonds, P. G., Hall, B. D., Dutton, G. S., Nance, D., Mondeel, D. J., Elkins, J. W., Krummel, P. B., Steele, L. P., and Fraser, P. J.: Re-evaluation of the lifetimes of the major CFCs and $CH_3CCl_3$ using atmospheric trends, Atmos. Chem. Phys., 13, 2691-2702, doi: 10.5194/acp-13-2691-2013, 2013.

Sander, R.: Compilation of Henry's law constants (version 4.0) for water as solvent, Atmos. Chem. Phys., 15, 4399-4981, doi:10.5194/acp-15-4399-2015, 2015.

Weiss, R. F.: The solubility of nitrogen, oxygen and argon in water and seawater, Deep-Sea Res., 17, 721-735, doi:10.106/0011-7471(70)90037-9, 1970.

Weiss, R. F. and Price, B. A.: Nitrous oxide solubility in water and seawater, Marine Chem., 8, 347-359, doi:10.1016/0304-4203(80)90024-9, 1980.

Yaws, C.L., Yang, H.-C., 1992. Chapter 11, Henry's law constant for compound in water, in: Yaws, C.L. (Ed.), Thermodynamic and Physical Property Data. Gulf Publishing, Houston, TX, pp. 181-206.

Yvon-Lewis, S.A. and Butler, J.H.: Effect of oceanic uptake on atmospheric lifetimes of selected trace gases. J. Geophys. Res.-Atmos., 107, 4414, doi:10.1029/2001JD001267, 2002.

~~**Table 1. The average of values of $F/(k_1RTV)$ obtained for $V$ value of 0.350 dm$^3$ and 0.300 dm$^3$ and the $K_H(T)$ value derived from Eq. (13) at each temperature. $N$ represents number of experimental runs for the average.**~~

| $T$ (K) | $F/(k_1RTV)$ | | | | $K_H(T)$ (M atm$^{-1}$) |
|---|---|---|---|---|---|
| | $V$ = 0.350 | | $V$ = 0.300 | | |
| | average [a] | $N$ | average [a] | $N$ | From Eq. (13) [b] |
| 276.15 | 0.119 ± 0.006 | 21 | 0.117 ± 0.006 | 11 | 0.118 ± 0.003 |
| 278.35 | 0.107 ± 0.005 | 18 | 0.110 ± 0.005 | 14 | 0.108 ± 0.002 |
| 283.65 | 0.093 ± 0.003 | 27 | 0.092 ± 0.001 | 5 | 0.094 ± 0.002 |
| 288.65 | 0.082 ± 0.006 | 41 | 0.084 ± 0.006 | 12 | 0.082 ± 0.002 |
| 293.45 | 0.071 ± 0.001 | 15 | 0.071 ± 0.001 | 5 | 0.072 ± 0.002 |
| 298.15 | 0.064 ± 0.002 | 30 | 0.067 ± 0.005 | 12 | 0.064 ± 0.002 |
| 303.05 | 0.057 ± 0.003 | 16 | 0.056 ± 0.005 | 4 | 0.058 ± 0.002 |
| 307.95 | 0.051 ± 0.001 | 12 | 0.054 ± 0.004 | 10 | 0.052 ± 0.002 |
| 312.65 | 0.046 ± 0.001 | 13 | 0.047 ± 0.001 | 4 | 0.048 ± 0.001 |

~~a. Errors are 2σ for the average only.; b. Errors are 95% confidence level for the regression only.~~

**Table 1. The average of values of $F/(k_1RTV)$ obtained for $V$ value of 0.350 dm$^3$ and 0.300 dm$^3$ and the $K_H(T)$ value derived from Eq. (13) at each temperature. $N$ represents number of experimental runs for the average.**

| $T$ (K) | $F/(k_1RTV)$ | | | | $K_H(T)$ (M atm$^{-1}$) |
|---|---|---|---|---|---|
| | $V$ = 0.350 | | $V$ = 0.300 | | |
| | average [a, b] | $N$ [c] | average [a] | $N$ [c] | From Eq. (13) [d, e] |
| 276.15 | 0.119 ± 0.006 (0.008) | 21 (2) | 0.117 ± 0.006 (0.008) | 11 (0) | 0.119 ± 0.003 (0.005) |
| 278.35 | 0.107 ± 0.005 (0.007) | 18 (3) | 0.110 ± 0.005 (0.007) | 14 (0) | 0.111 ± 0.002 (0.004) |
| 283.65 | 0.093 ± 0.003 (0.005) | 27 (5) | 0.092 ± 0.001 (0.003) | 5 (0) | 0.094 ± 0.002 (0.004) |
| 288.65 | 0.082 ± 0.006 (0.008) | 41 (5) | 0.084 ± 0.006 (0.008) | 12 (0) | 0.082 ± 0.002 (0.004) |
| 293.45 | 0.071 ± 0.001 (0.002) | 15 (8) | 0.071 ± 0.001 (0.002) | 5 (0) | 0.072 ± 0.002 (0.003) |
| 298.15 | 0.064 ± 0.002 (0.003) | 30 (6) | 0.067 ± 0.005 (0.006) | 12 (0) | 0.065 ± 0.002 (0.003) |
| 303.05 | 0.057 ± 0.003 (0.004) | 16 (0) | 0.056 ± 0.005 (0.006) | 4 (0) | 0.058 ± 0.002 (0.003) |
| 307.95 | 0.051 ± 0.001 (0.002) | 12 (6) | 0.054 ± 0.004 (0.005) | 10 (0) | 0.052 ± 0.002 (0.003) |
| 312.65 | 0.046 ± 0.001 (0.002) | 13 (3) | 0.047 ± 0.001 (0.002) | 4 (0) | 0.048 ± 0.001 (0.002) |

a. Errors are 2σ for the average only.; b. Number in parenthesis represents an error reflecting both 2σ for the average and potential systematic bias (±2%).; c. Number in parenthesis represents number of experimental runs excluded for the average.; d. Errors are 95% confidence level for the regression only.; e. Number in parenthesis represents an error reflecting both errors at 95% confidence level for the regression and potential systematic bias (±2%).

**Table 2. $K_H^{298}$ and $\Delta H_{sol}$ values derived from Eqs. (11′) and (13), along with literature data for $K_H^{298}$ and $\Delta H_{sol}$**

| $K_H^{298}$ (M atm$^{-1}$) | $\Delta H_{sol}$ (kJ mol$^{-1}$) | |
|---|---|---|
| 0.~~064~~065 | −17.2 | This work |
| 0.070 | −20 | Maaβen (1995)[a] |
| 0.070 | −19 | Reichl (1995)[a] |
| 0.069[c] | −20.6 | Anderson (2011) |
| 0.085 | | Hilal et al. (2008)[a] |
| | −18.6, −19.7 | Kühne et al. (2005)[a] |
| 0.087 | | Yaws (1999)[a] |
| 0.087 | | Yaws and Yang (1992)[a] |
| 0.030 | −27.2 | Miguel et al. (2000)[b] |

[a] Reviewed by Sander (2015); [b] Reviewed by Clever et al. (2005)

[c] The value was obtained by extrapolation of the data reported at 284.15-296.15 K (Supplementary data in Anderson (2011)) with respect to the van't Hoff equation.

**Table 3. The average of values of $F/(k_1RTV)$ obtained for $V$ value of 0.350 dm$^3$ and the $K_{eq}^{S}(T)$ value derived from Eq. (22) at each salinity and temperature. $N$ represents number of experimental runs for the average.**

| $T$ (K) | $K_{eq}^{S}$ (M atm$^{-1}$) | | | | | | | | |
|---|---|---|---|---|---|---|---|---|---|
| | salinity, 4.452 ‰ | | | salinity, 8.921 ‰ | | | salinity, 21.520 ‰ | | |
| | average[a] | $N$ | Eq. (22) | average[a] | $N$ | Eq. (22) | average[a] | $N$ | Eq. (22) |
| 276.15 | 0.108 ± 0.006 | 8 | 0.108 | 0.103 ± 0.006 | 21 | 0.104 | 0.095 ± 0.006 | 20 | 0.095 |
| 278.35 | 0.099 ± 0.004 | 12 | 0.099 | 0.095 ± 0.006 | 26 | 0.095 | 0.087 ± 0.005 | 22 | 0.087 |
| 283.65 | 0.086 ± 0.003 | 9 | 0.085 | 0.083 ± 0.007 | 24 | 0.082 | 0.075 ± 0.004 | 15 | 0.076 |
| 288.65 | 0.075 ± 0.004 | 12 | 0.074 | 0.072 ± 0.005 | 33 | 0.071 | 0.066 ± 0.004 | 20 | 0.066 |
| 293.45 | 0.065 ± 0.002 | 10 | 0.065 | 0.063 ± 0.003 | 27 | 0.062 | 0.058 ± 0.003 | 14 | 0.058 |
| 298.15 | 0.058 ± 0.002 | 13 | 0.058 | 0.056 ± 0.004 | 26 | 0.056 | 0.052 ± 0.003 | 20 | 0.052 |
| 303.05 | 0.052 ± 0.001 | 8 | 0.052 | 0.049 ± 0.004 | 14 | 0.050 | 0.046 ± 0.003 | 16 | 0.046 |
| 307.95 | 0.047 ± 0.002 | 13 | 0.047 | 0.046 ± 0.004 | 23 | 0.045 | 0.042 ± 0.003 | 16 | 0.042 |
| 312.65 | 0.042 ± 0.001 | 7 | 0.042 | 0.040 ± 0.003 | 12 | 0.041 | 0.038 ± 0.002 | 16 | 0.038 |

| $T$ (K) | $K_{eq}^{S}$ (M atm$^{-1}$) | | | | | |
|---|---|---|---|---|---|---|
| | salinity, 36.074 ‰ | | | salinity, 51.534 ‰ | | |
| | average[a] | $N$ | Eq. (22) | average[a] | $N$ | Eq. (22) |
| 276.15 | 0.088 ± 0.005 | 21 | 0.088 | 0.081 ± 0.003 | 10 | 0.082 |
| 278.35 | 0.079 ± 0.006 | 20 | 0.081 | 0.077 ± 0.003 | 15 | 0.076 |
| 283.65 | 0.069 ± 0.002 | 18 | 0.071 | 0.067 ± 0.001 | 9 | 0.066 |
| 288.65 | 0.062 ± 0.004 | 19 | 0.062 | 0.059 ± 0.002 | 14 | 0.058 |
| 293.45 | 0.054 ± 0.002 | 19 | 0.055 | 0.052 ± 0.001 | 7 | 0.052 |
| 298.15 | 0.049 ± 0.002 | 24 | 0.049 | 0.047 ± 0.002 | 15 | 0.047 |
| 303.05 | 0.044 ± 0.002 | 16 | 0.044 | 0.042 ± 0.001 | 8 | 0.042 |
| 307.95 | 0.040 ± 0.002 | 15 | 0.040 | 0.038 ± 0.002 | 12 | 0.039 |
| 312.65 | 0.036 ± 0.002 | 16 | 0.037 | 0.036 ± 0.001 | 7 | 0.036 |

a. Errors are 2σ for the average only.

**Table 3. The average of values of $F/(k_1RTV)$ obtained for $V$ value of 0.350 dm$^3$ and the $K_{eq}^S(T)$ value derived from Eq. (23) at each salinity and temperature. $N$ represents number of experimental runs for the average.**

| $T$ (K) | $K_{eq}^S$ (M atm$^{-1}$) | | | | | |
|---|---|---|---|---|---|---|
| | salinity, 4.452 ‰ | | | salinity, 8.921 ‰ | | |
| | average [a, b] | $N$ [c] | Eq. (23) [d, e] | average [a, b] | $N$ [c] | Eq. (23) [d, e] |
| 276.15 | 0.108 ± 0.006 (0.008) | 8 (0) | 0.107 ± 0.003 (0.005) | 0.103 ± 0.006 (0.008) | 21 (0) | 0.103 ± 0.003 (0.005) |
| 278.35 | 0.099 ± 0.004 (0.006) | 12 (0) | 0.100 ± 0.002 (0.005) | 0.095 ± 0.006 (0.008) | 26 (1) | 0.096 ± 0.002 (0.004) |
| 283.65 | 0.086 ± 0.003 (0.005) | 9 (0) | 0.085 ± 0.002 (0.004) | 0.083 ± 0.007 (0.009) | 24 (0) | 0.082 ± 0.002 (0.004) |
| 288.65 | 0.075 ± 0.004 (0.006) | 12 (0) | 0.074 ± 0.002 (0.003) | 0.072 ± 0.005 (0.006) | 33 (0) | 0.071 ± 0.001 (0.002) |
| 293.45 | 0.065 ± 0.002 (0.003) | 10 (0) | 0.066 ± 0.002 (0.003) | 0.063 ± 0.003 (0.004) | 27 (5) | 0.063 ± 0.002 (0.003) |
| 298.15 | 0.058 ± 0.002 (0.003) | 13 (0) | 0.059 ± 0.002 (0.003) | 0.056 ± 0.004 (0.005) | 26 (2) | 0.056 ± 0.002 (0.003) |
| 303.05 | 0.052 ± 0.001 (0.002) | 8 (0) | 0.053 ± 0.002 (0.003) | 0.049 ± 0.004 (0.005) | 14 (6) | 0.051 ± 0.001 (0.002) |
| 307.95 | 0.047 ± 0.002 (0.003) | 13 (1) | 0.048 ± 0.001 (0.002) | 0.046 ± 0.004 (0.005) | 23 (1) | 0.046 ± 0.001 (0.002) |
| 312.65 | 0.042 ± 0.001 (0.002) | 7 (0) | 0.044 ± 0.001 (0.002) | 0.040 ± 0.003 (0.004) | 12 (8) | 0.042 ± 0.001 (0.002) |

| $T$ (K) | $K_{eq}^S$ (M atm$^{-1}$) | | | | | |
|---|---|---|---|---|---|---|
| | salinity, 21.520 ‰ | | | salinity, 36.074 ‰ | | |
| | average [a, b] | $N$ [c] | Eq. (23) [d, e] | average [a, b] | $N$ [c] | Eq. (23) [d, e] |
| 276.15 | 0.095 ± 0.006 (0.008) | 20 (0) | 0.095 ± 0.003 (0.005) | 0.088 ± 0.005 (0.007) | 21 (0) | 0.089 ± 0.002 (0.004) |
| 278.35 | 0.087 ± 0.005 (0.007) | 22 (0) | 0.088 ± 0.002 (0.004) | 0.079 ± 0.006 (0.008) | 20 (3) | 0.083 ± 0.002 (0.004) |
| 283.65 | 0.075 ± 0.004 (0.006) | 15 (1) | 0.076 ± 0.001 (0.003) | 0.069 ± 0.002 (0.003) | 18 (2) | 0.071 ± 0.001 (0.002) |
| 288.65 | 0.066 ± 0.004 (0.005) | 20 (0) | 0.066 ± 0.001 (0.002) | 0.062 ± 0.004 (0.005) | 19 (4) | 0.062 ± 0.001 (0.002) |
| 293.45 | 0.058 ± 0.003 (0.004) | 14 (0) | 0.058 ± 0.001 (0.002) | 0.054 ± 0.002 (0.003) | 19 (4) | 0.055 ± 0.001 (0.002) |
| 298.15 | 0.052 ± 0.003 (0.004) | 20 (0) | 0.052 ± 0.001 (0.002) | 0.049 ± 0.002 (0.003) | 24 (4) | 0.049 ± 0.001 (0.002) |
| 303.05 | 0.046 ± 0.003 (0.004) | 16 (0) | 0.047 ± 0.001 (0.002) | 0.044 ± 0.002 (0.003) | 16 (0) | 0.044 ± 0.001 (0.002) |
| 307.95 | 0.042 ± 0.003 (0.004) | 16 (0) | 0.043 ± 0.001 (0.002) | 0.040 ± 0.002 (0.003) | 15 (2) | 0.040 ± 0.001 (0.002) |
| 312.65 | 0.038 ± 0.002 (0.003) | 16 (0) | 0.039 ± 0.001 (0.002) | 0.036 ± 0.002 (0.003) | 16 (0) | 0.037 ± 0.001 (0.002) |

| $T$ (K) | $K_{eq}^S$ (M atm$^{-1}$) | | |
|---|---|---|---|
| | salinity, 51.534 ‰ | | |
| | average [a, b] | $N$ [c] | Eq. (23) [d, e] |
| 276.15 | 0.081 ± 0.003 (0.005) | 10 (0) | 0.084 ± 0.002 (0.004) |
| 278.35 | 0.077 ± 0.003 (0.005) | 15 (0) | 0.078 ± 0.002 (0.004) |
| 283.65 | 0.067 ± 0.001 (0.003) | 9 (1) | 0.067 ± 0.001 (0.002) |
| 288.65 | 0.059 ± 0.002 (0.003) | 14 (1) | 0.059 ± 0.001 (0.002) |
| 293.45 | 0.052 ± 0.001 (0.002) | 7 (3) | 0.052 ± 0.001 (0.002) |
| 298.15 | 0.047 ± 0.002 (0.003) | 15 (0) | 0.047 ± 0.001 (0.002) |
| 303.05 | 0.042 ± 0.001 (0.002) | 8 (0) | 0.042 ± 0.001 (0.002) |
| 307.95 | 0.038 ± 0.002 (0.003) | 12 (0) | 0.038 ± 0.001 (0.002) |
| 312.65 | 0.036 ± 0.001 (0.002) | 7 (1) | 0.035 ± 0.001 (0.002) |

a. Errors are 2σ for the average only.; b. Number in parenthesis represents an error reflecting both 2σ for the average and potential systematic bias (±2%).; c. Number in parenthesis represents number of experimental runs excluded for the average.; d. Errors are 95% confidence level for the regression only.; e. Number in parenthesis represents an error reflecting both errors at 95% confidence level for the regression and potential systematic bias (±2%).

**Figure captions**

Figure 1. Plots of values of $F/(k_1RTV)$ against $F$ at each temperature for 0.350 $dm^3$ and 0.300 $dm^3$ of deionized water. Error bars represent 2σ due to errors of values of $k_1$ as described in Sect. S2 in Supporting Information. Grey symbols represent the data excluded for calculating the average.

Figure 2. van't Hoff plot of the $K_H$ values obtained by the IGS method and the PRV-HS method. Bold curve displays the fitting of the data obtained by the IGS method and the PRV-HS method (Eq. (13)). Dashed curves display upper and lower 95% confidence limit of the above fitting by Eq. (12). Error bars of the data by the IGS method represent both 2σ for the average and potential systematic bias (±2%). Error bars of the data by PRV-HS method represent both errors at 95% confidence level for the regression and potential systematic bias (±4%).

Figure 3. Plots of values of $F/(k_1RTV)$ against $F$ at each temperature for 0.350 $dm^3$ of a-seawater at 36.074‰. Error bars represent 2σ due to errors of values of $k_1$ as described in Sect. S2 in Supporting Information. Grey symbols represent the data excluded for calculating the average.

Figure 4. van't Hoff plot of the $K_{eq}^S$ values for a-seawater at each salinity. Dashed curve represents the $K_H$ values by Eq. (13). Bold curves represent the fitting obtained by Eq. (23). Error bars of the data represent both 2σ for the average and potential systematic bias (2%). ~~(22).~~

Figure 5. Plots of $\ln(K_H(T)/$~~$K_H^S$~~$K_{eq}^S(T))$ vs. salinity in a-seawater at each temperature. Bold curves represent the fitting obtained by Eq. (22). Error bars represent errors reflecting both 2σ for the average and potential systematic bias (2%) of $K_{eq}^S$. ~~(21).~~

Figure 6. Plots of monthly averaged equilibrium fractionation of $CH_2F_2$ between atmosphere and ocean, $R_m$ (Gg $patm^{-1}$) in the global and the semi-hemispheric atmosphere. Right vertical axis represents the residence ratio of $CH_2F_2$ in the ocean, instead of $R_m$, for each lower tropospheric semi-hemisphere of the AGAGE 12-box model.

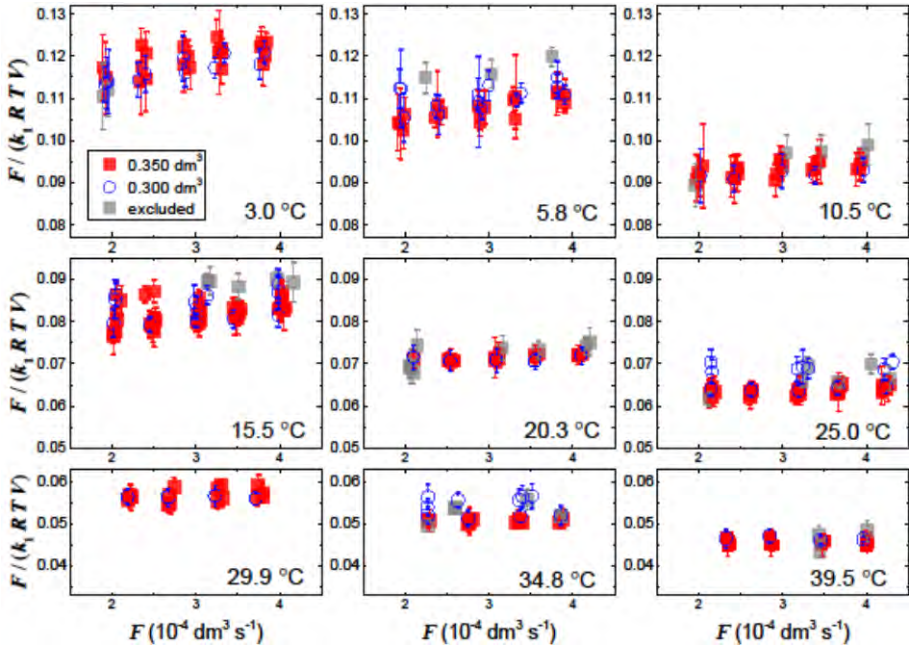


**Figure 1. Plots of values of $F/(k_1RTV)$ against $F$ at each temperature for 0.350 dm$^3$ and 0.300 dm$^3$ of deionized water. Error bars represent 2σ due to errors of values of $k_1$ as described in Sect. S2 in Supporting Information. Grey symbols represent the data excluded for calculating the average.**

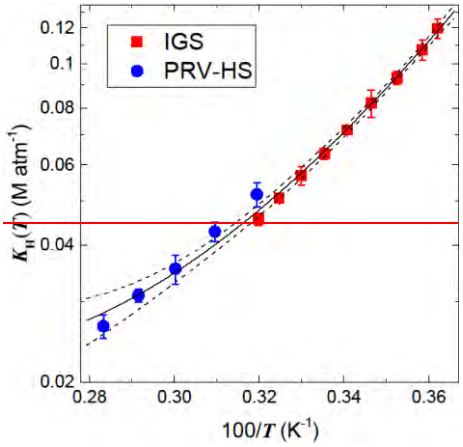


~~**Figure 2. van't Hoff plot of the $K_H$ values obtained by the IGS method and the PRV-HS method. Bold curve displays the fitting of the data obtained by the IGS method and the PRV-HS method (Eq. (13)). Dashed curves display upper and lower 95% confidence limit of the above fitting by Eq. (12).**~~

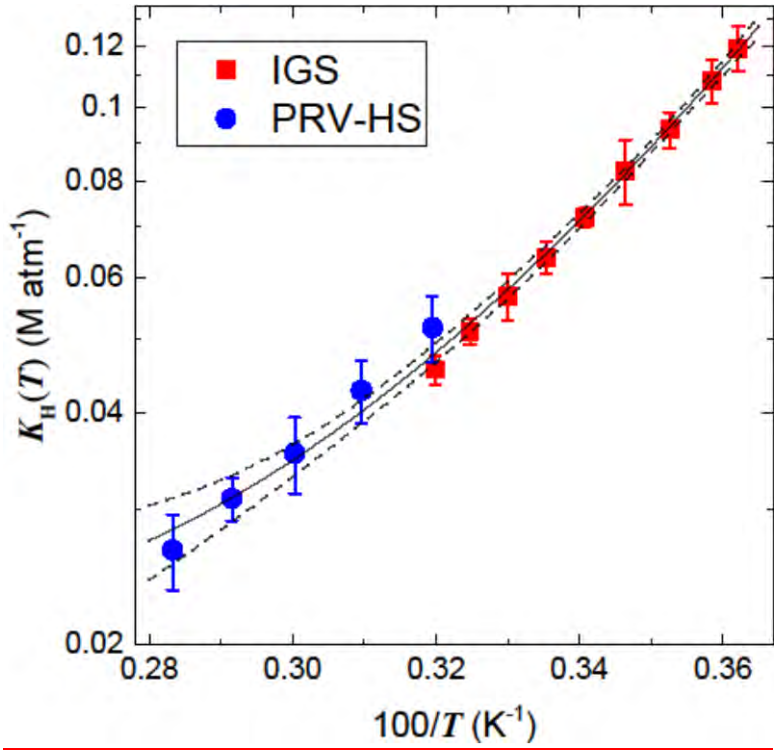


**Figure 2. van't Hoff plot of the $K_H$ values obtained by the IGS method and the PRV-HS method. Bold curve displays the fitting of the data obtained by the IGS method and the PRV-HS method (Eq. (13)). Dashed curves display upper and lower 95% confidence limit of the above fitting by Eq. (12). Error bars of the data by the IGS method represent both 2σ for the average and potential systematic bias (±2%). Error bars of the data by PRV-HS method represent both errors at 95% confidence level for the regression and potential systematic bias (±4%).**

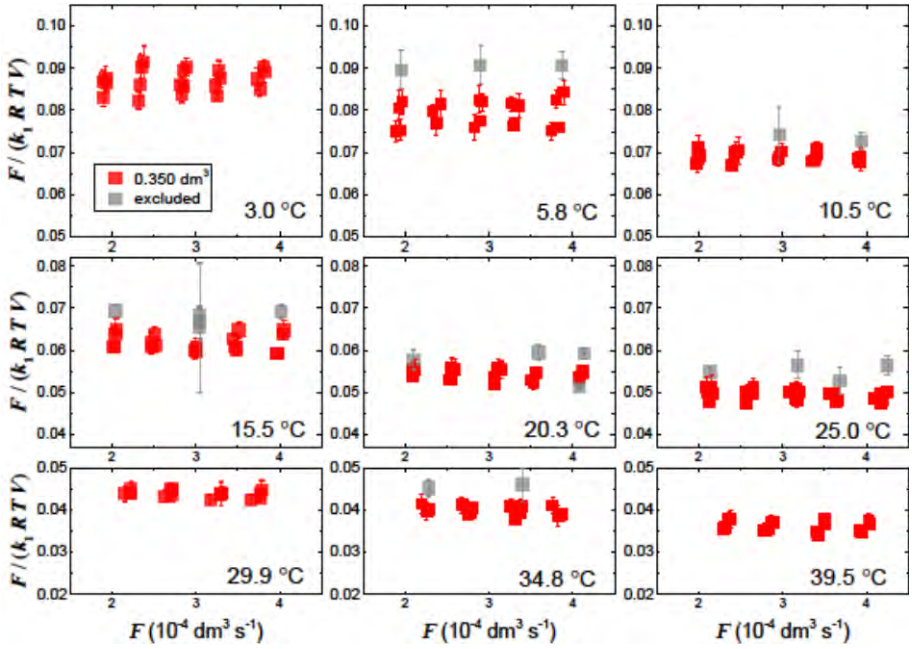


**Figure 3. Plots of values of $F/(k_1RTV)$ against $F$ at each temperature for 0.35 dm$^3$ of a-seawater at 36.074‰. Error bars represent 2σ due to errors of values of $k_1$ as described in Sect. S2 in Supporting Information. Grey symbols represent the data excluded for calculating the average.**

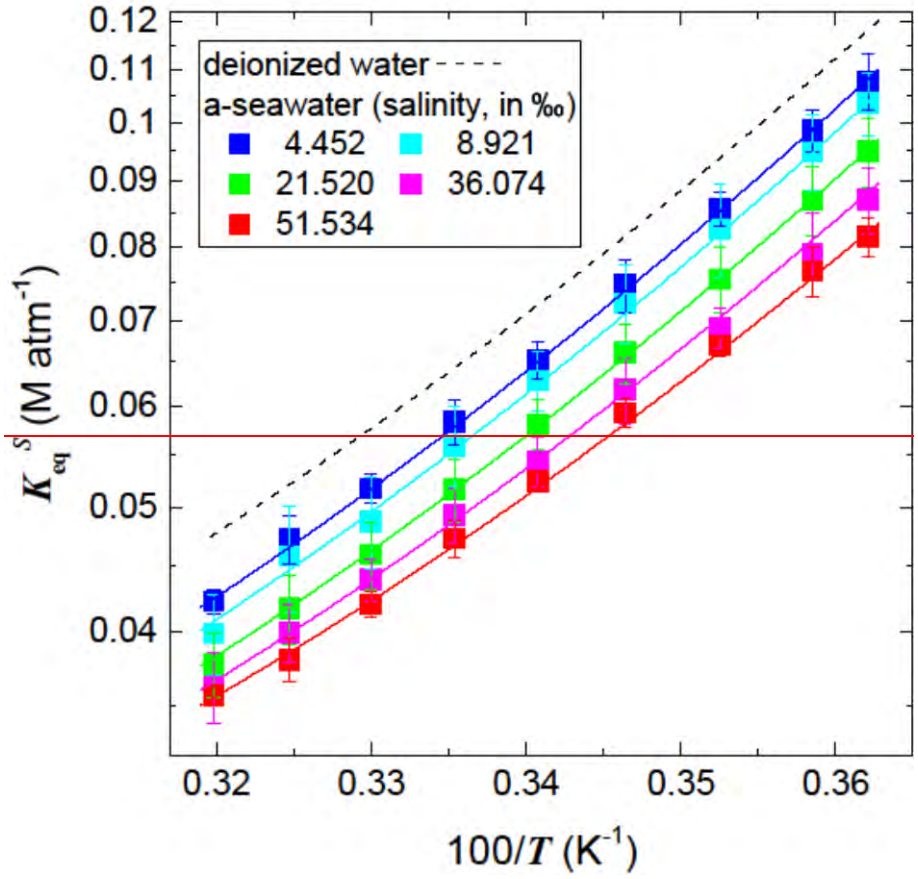


~~**Figure 4. van't Hoff plot of the $K_{eq}^{s}$ values for a-seawater at each salinity. Dashed curve represents the $K_H$ values by Eq. (13). Bold curves represent the fitting obtained by Eq. (22).**~~

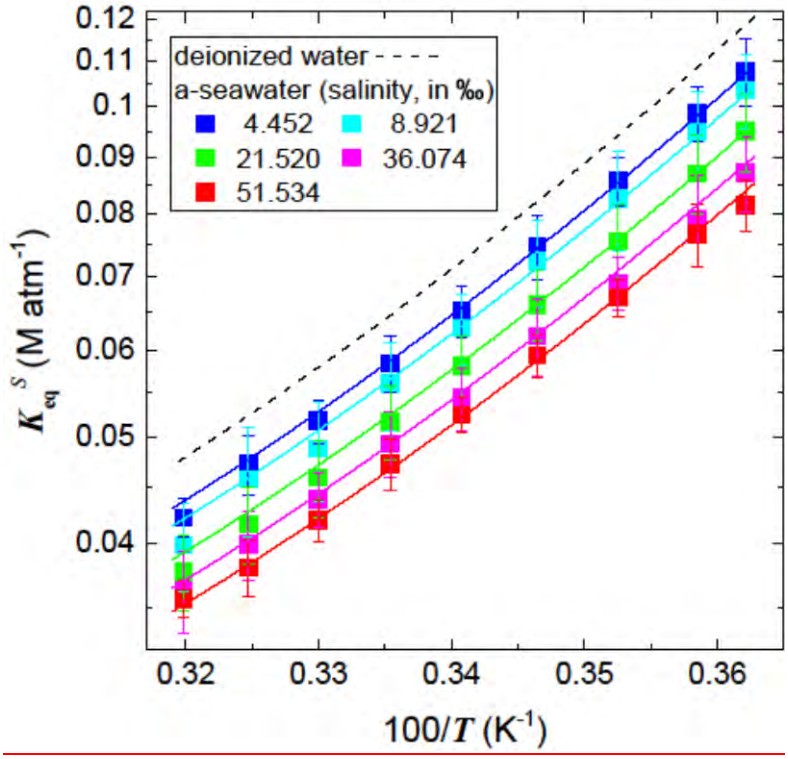


**Figure 4. van't Hoff plot of the $K_{eq}^{S}$ values for a-seawater at each salinity. Dashed curve represents the $K_H$ values by Eq. (13). Bold curves represent the fitting obtained by Eq. (23). Error bars of the data represent both 2σ for the average and potential systematic bias (±2%).**

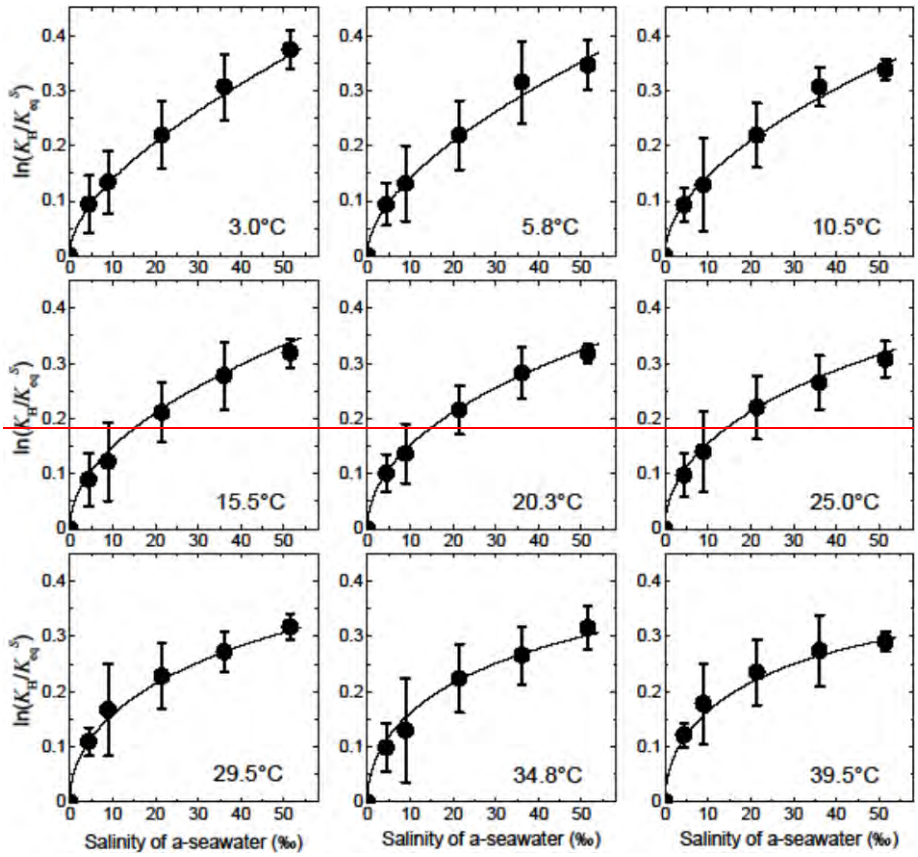


~~**Figure 5. Plots of $\ln(K_H(T)/K_H^S(T))$ vs. salinity in a-seawater at each temperature. Bold curves represent the fitting obtained by Eq. (21).**~~

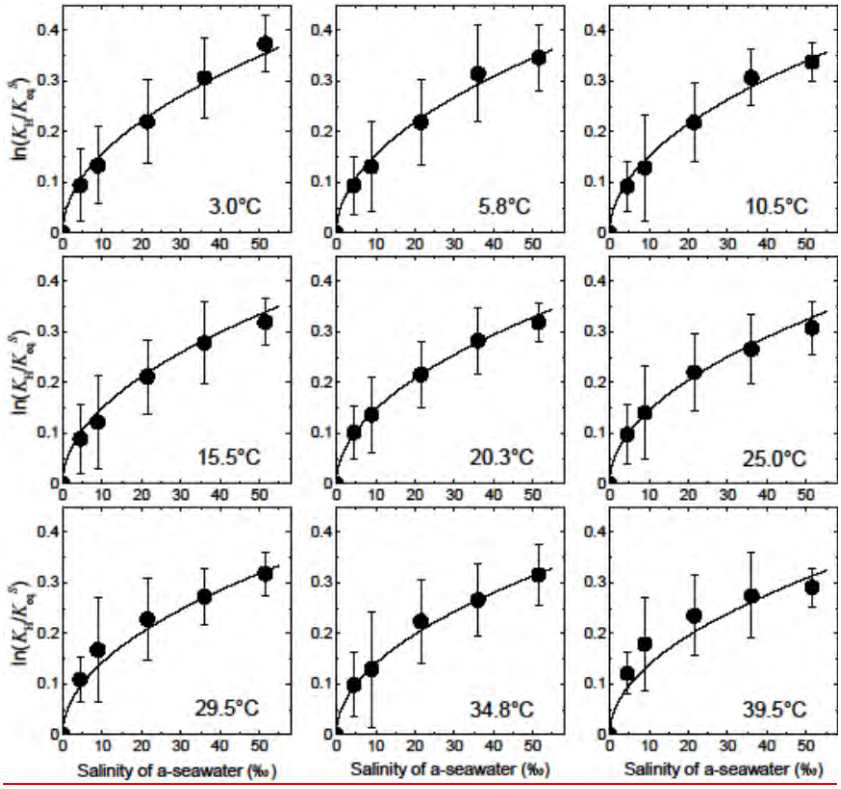


**Figure 5. Plots of $\ln(K_H(T)/K_{eq}^S(T))$ vs. salinity in a-seawater at each temperature. Bold curves represent the fitting obtained by Eq. (22). Error bars represent errors reflecting both 2σ for the average and potential systematic bias (±2%) of $K_{eq}^S$.**

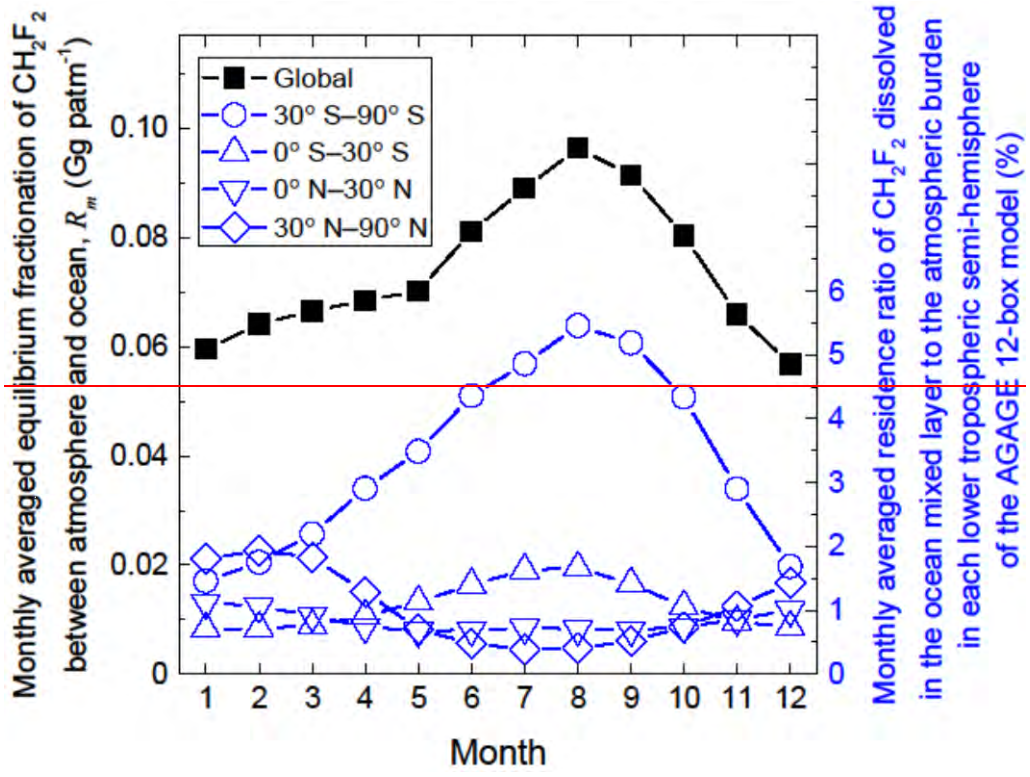


**~~Figure 6. Plots of monthly averaged equilibrium fractionation of $CH_2F_2$ between atmosphere and ocean, $R_m$ (Gg patm$^{-1}$) in the global and the hemispheric atmosphere. Right vertical axis represents monthly averaged residence ratio of $CH_2F_2$ dissolved in the ocean mixed layer to the atmospheric burden for each lower tropospheric semi-hemisphere of the AGAGE 12-box model.~~**

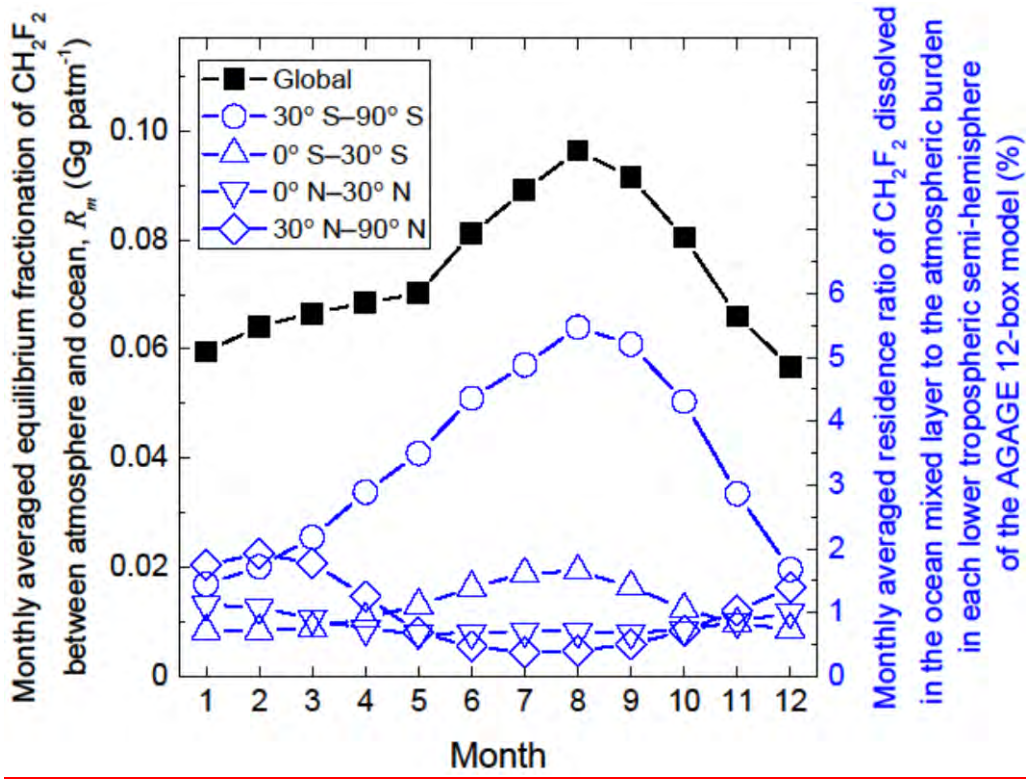


**Figure 6. Plots of monthly averaged equilibrium fractionation of $CH_2F_2$ between atmosphere and ocean, $R_m$ (Gg patm$^{-1}$) in the global and the semi-hemispheric atmosphere. Right vertical axis represents monthly averaged residence ratio of $CH_2F_2$ dissolved in the ocean mixed layer to the atmospheric burden for each lower tropospheric semi-hemisphere of the AGAGE 12-box model.**

# Supporting information

# Experimental determination of Henry's law constants of difluoromethane ($CH_2F_2$) and the salting-out effects in aqueous salt solutions relevant to seawater

S. Kutsuna

[1]National Institute of Advanced Industrial Science and Technology (AIST), 16-1 Onogawa, Tsukuba, 305-8569, Japan

*Correspondence to*: S. Kutsuna (s-kutsuna@aist.go.jp)

## S1. Equilibrium time for the PRV-HS method experiments

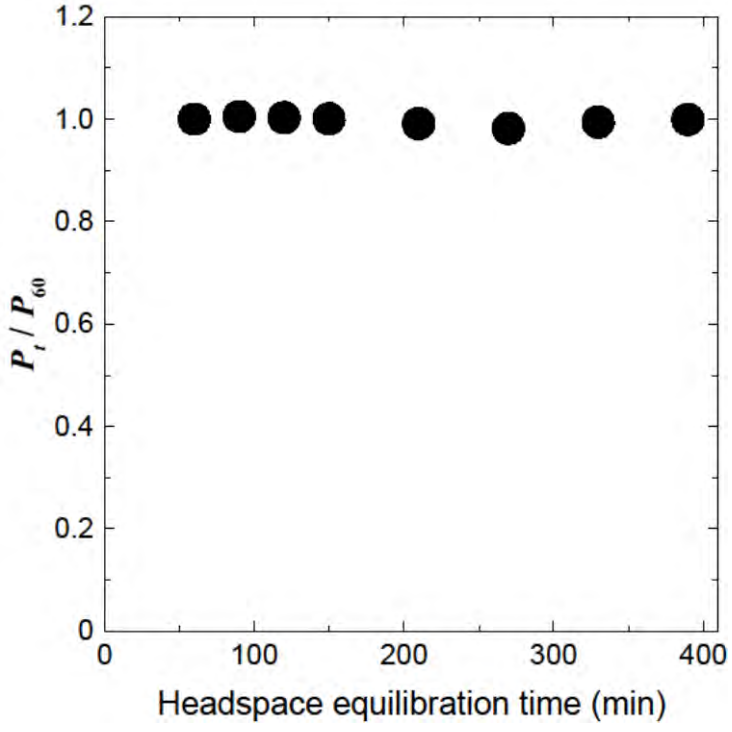


**Figure S1. Relative areas of GC-MS peaks for $CH_2F_2$ versus headspace time duration for equilibration of 9.0 $cm^3$ of aqueous $CH_2F_2$ at 353 K.**

**S2. An example of the IGS method experiments**

Figure S2 shows an example of time profile of $P_t$ and how to calculate the $k_1$ value for the IGS method experiments. The $k_1$ value at each time was calculated by fitting nearest three data of $P_t$ for each time. The average of the $k_1$ values is given as the $k_1$ value for the experimental run. Two standard deviation of the $k_1$ values gives errors of the $k_1$ value for the experimental run.

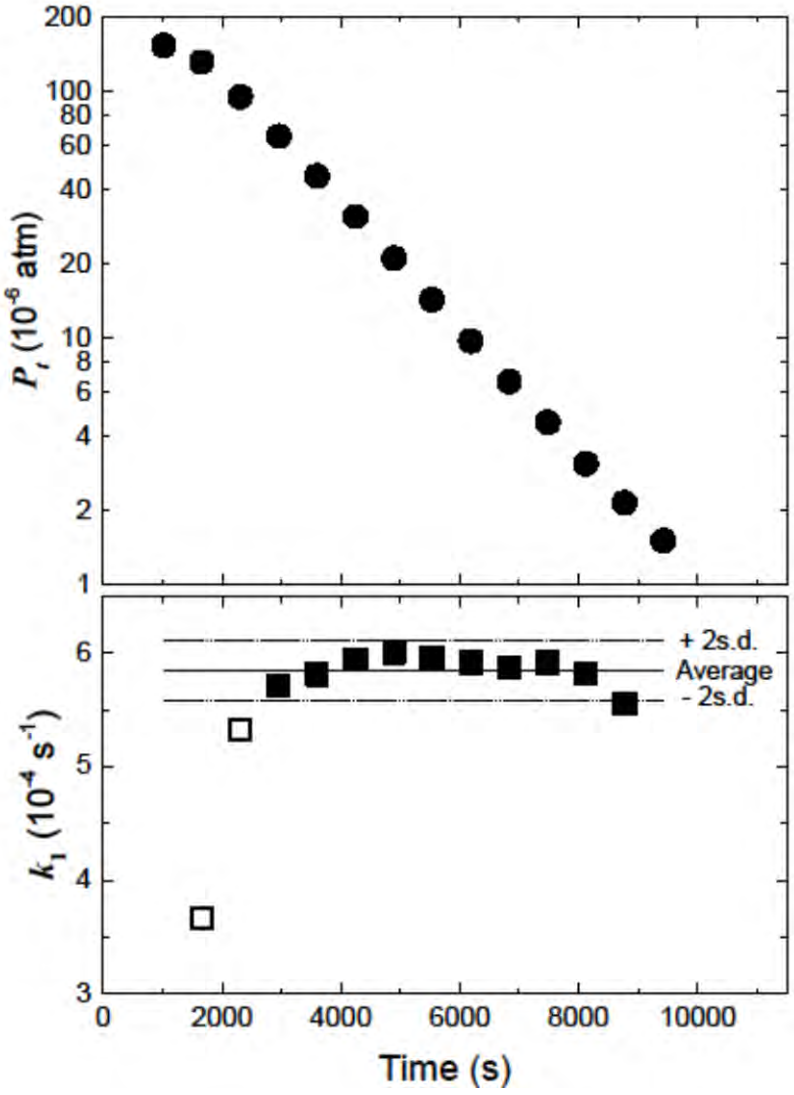


**Figure S2. An IGS experimental result for $V$ = 0.350 $dm^3$ and $F = 3.32\times10^{-4}$ $dm^3$ $s^{-1}$ at 25°C. (upper panel) time profile of $P_t$; (lower panel) values of $k_1$ calculated by fitting nearest three data of $P_t$ for each time with respect to Eq. (1).**

## S3. Results of the PRV-HS method experiments

Figure S3 illustrates the results of a PRV-HS experiment at 313 K. In panel A, peak area ($S_{ij}$) is plotted against the volume of the $CH_2F_2$ gas mixture added ($v_j$) for $V_i$ = 9.0, 7.5, 6.0, 4.5, 3.0, and 1.5 $cm^3$. For each $V_i$, the data form a straight line intersecting the origin, indicating that $S_{ij}$ is proportional to $v_j$ for vials with the same value of $V_i$. The slope ($L_i$) of each line is obtained by linear regression with respect to Eq. (8), and the reciprocal of the slope ($L_i^{-1}$) is plotted against the phase ratio ($V_i/V_0$) in panel B of Fig. S3. Plots of $L_i^{-1}$ and $V_i/V_0$ obey Eq. (9). Table S1 lists the values of $L_i^{-1}$, the slopes and the intercepts for linear regression with respect to Eq. (9), and the $K_H(T)$ values calculated from the slopes and the intercepts. Two measurements of $K_H(T)$ were carried out at each temperature.

Furthermore, the $K_H(T)$ values, along with errors of them at 95% confidence level, were also estimated by non-liner fitting of the two datasets simultaneously at each temperature by use of Eq. (11) (Fig. S4). The $K_H(T)$ values and their errors thus estimated are plotted in Fig. 2 and are listed in Table S1.

**Table S1. $L_i$ values for various $V_i/V_0$ ratios at various temperatures, slopes and intercepts for linear regression with respect to Eq. (10), $K_H(T)$ values calculated from the slopes and intercepts, and $K_H(T)$ values and the errors at 95% confidence level estimated by non-linear fitting the two datasets simultaneously at each temperature (Fig. S4) with respect to Eq. (11).**

| $T$ (K) | $L_i$ (a.u.) [*a] | | | | | | Eq. (10) Intercept | Eq. (10) Slope | $K_H$ ($M\ atm^{-1}$) | | |
|---|---|---|---|---|---|---|---|---|---|---|---|
| | $V_i/V$ = 0.421 | 0.351 | 0.280 | 0.210 | 0.140 | 0.070 | | | Eq. (10) | Eq. (11)[**b,c] | Eq. (13)[**b] |
| 353 | 3.226±0.002 | 3.270±0.026 | 3.330±0.004 | 3.391±0.008 | 3.462±0.014 | 3.526±0.009 | 3.581 | –0.870 | 0.026 | 0.027 ±0.002 (±0.003) | 0.03102 8 ±0.003 |
| | 2.044±0.006 | 2.050±0.012 | 2.112±0.010 | 2.132±0.009 | 2.186±0.021 | 2.209±0.011 | 2.248 | –0.513 | 0.027 | | |
| 343 | 3.000±0.018 | 3.025±0.009 | 3.070±0.008 | 3.089±0.015 | 3.117±0.015 | 3.148±0.018 | 3.179 | –0.423 | 0.031 | 0.031 ±0.001 (±0.002) | 0.033031 ±0.002 |
| | 1.949±0.004 | 1.955±0.005 | 1.968±0.003 | 1.998±0.004 | 2.020±0.002 | 2.030±0.009 | 2.050 | –0.258 | 0.031 | | |
| 333 | 3.247±0.018 | 3.234±0.018 | 3.243±0.015 | 3.241±0.010 | 3.247±0.009 | 3.223±0.013 | 3.231 | 0.034 | 0.037 | 0.036 ±0.003 (±0.004) | 0.037035 ±0.002 |
| | 3.080±0.009 | 3.044±0.006 | 3.082±0.005 | 3.127±0.009 | 3.113±0.008 | 3.134±0.014 | 3.149 | –0.213 | 0.034 | | |
| 323 | 3.208±0.011 | 3.190±0.008 | 3.133±0.010 | 3.134±0.011 | 3.092±0.008 | 3.093±0.006 | 3.055 | 0.355 | 0.042 | 0.043 ±0.002 (±0.004) | 0.042040 ±0.001 |
| | 3.357±0.010 | 3.289±0.014 | 3.275±0.005 | 3.233±0.004 | 3.226±0.016 | 3.160±0.001 | 3.135 | 0.496 | 0.044 | | |
| 313 | 3.245±0.018 | 3.185±0.013 | 3.100±0.015 | 3.022±0.012 | 2.995±0.012 | 2.915±0.011 | 2.848 | 0.935 | 0.052 | 0.052 ±0.003 (±0.005) | 0.049047 ±0.001 |
| | 2.162±0.031 | 2.134±0.010 | 2.060±0.014 | 2.029±0.018 | 1.992±0.010 | 1.925±0.018 | 1.896 | 0.612 | 0.052 | | |

[*] a. Errors are 2σ for the regression only.; [**] b. Errors are those at 95% confidence level for the regression only. ; c. Number in parenthesis represents both errors at 95% confidence level for the regression and potential systematic bias (±4%).

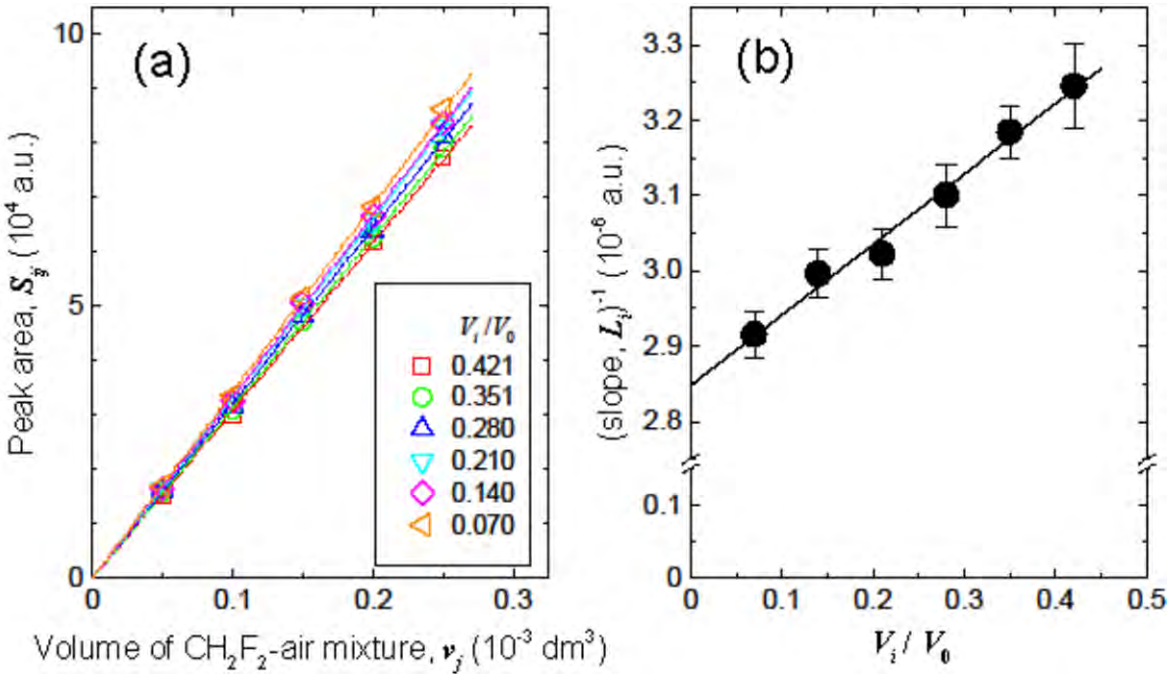


**Figure S3. Headspace GC-MS measurements for six series of test samples containing water ($V_i$ in cm$^3$) to which a $CH_2F_2$–air mixture was added ($v_j$ in cm$^3$) at 313 K. (a) Plot of peak area ($S_{ij}$) versus $v_j$ for test samples containing volume $V_i$ of water. Slope ($L_i$) was obtained by linear fitting of the data to Eq. (8) for samples of the same $V_i$. (b) Plot of $L_i^{-1}$ versus $V_i/V_0$ fitted to Eq. (10).**

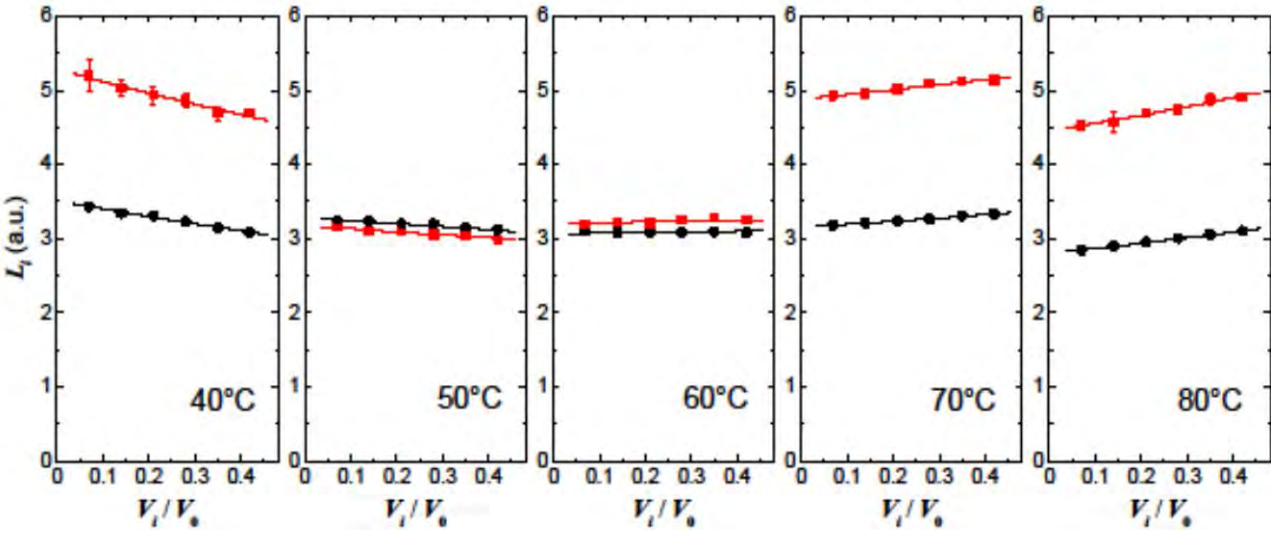


**Figure S4. Plot of $L_i$ versus $V_i/V_0$ for the PRV-HS measurements at each temperature. Bold curves represent the simultaneous fitting of the two datasets at each temperature by Eq. (11).**

## S4. Determination of salting-out effects in artificial seawater

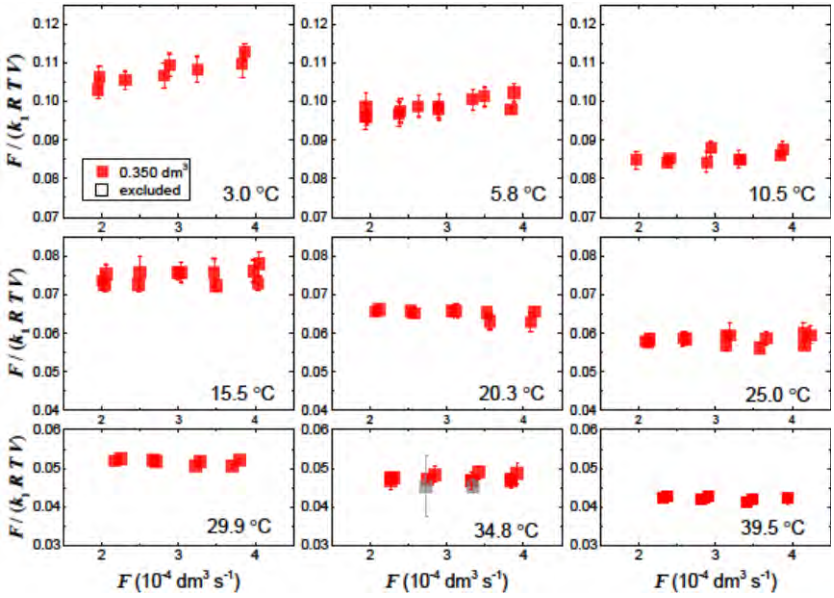


**Figure S5. Plots of values of $F/(k_1RTV)$ against $F$ at each temperature for 0.35 dm$^3$ of a-seawater at 4.452‰. Error bars represent 2σ due to errors of values of $k_1$ as described in Sect. S2. Grey symbols represent the data excluded for calculating the average.**

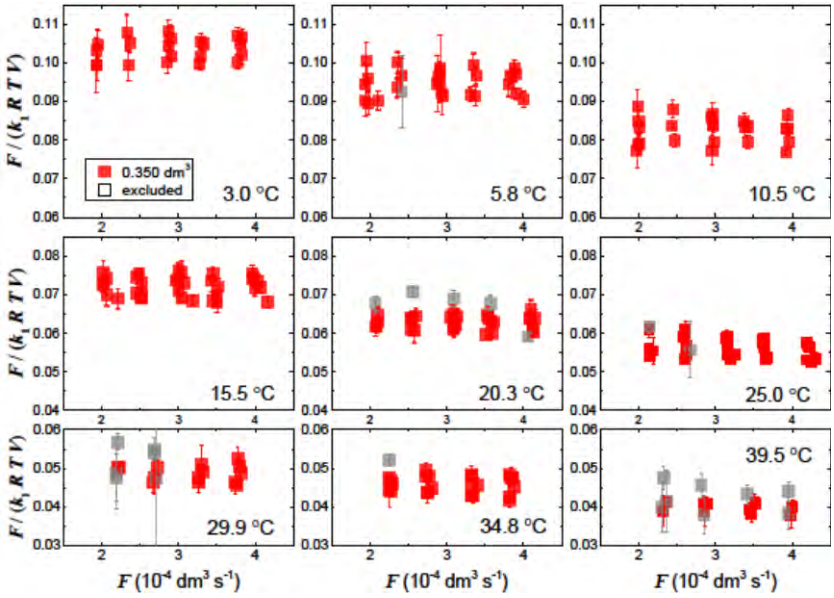


**Figure S6. Plots of values of $F/(k_1RTV)$ against $F$ at each temperature for 0.35 dm$^3$ of a-seawater at 8.921‰. Error bars represent 2σ due to errors of values of $k_1$ as described in Sect. S2. Grey symbols represent the data excluded for calculating the average.**

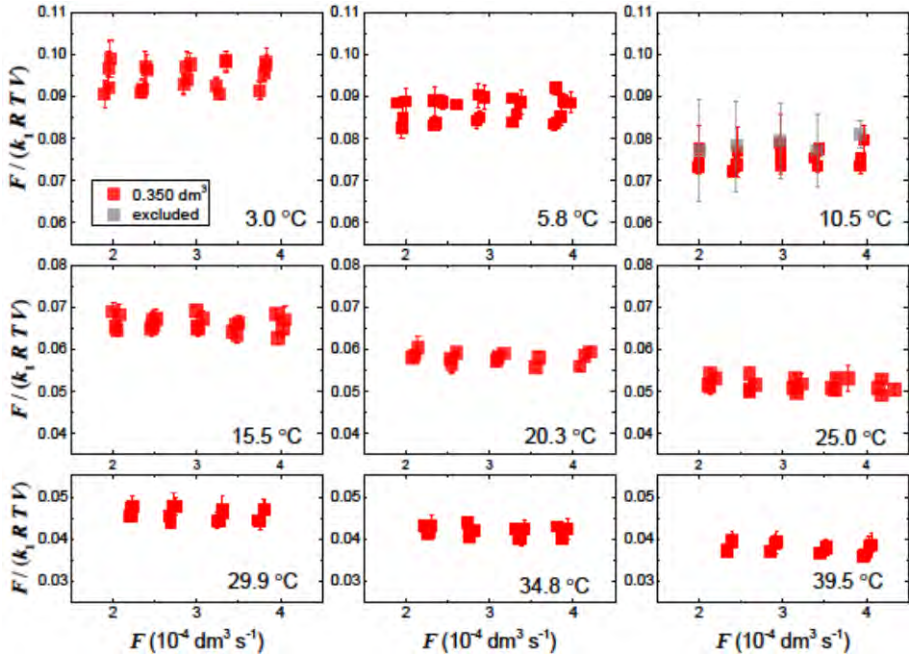


**Figure S7. Plots of values of $F/(k_1RTV)$ against $F$ at each temperature for 0.35 dm$^3$ of a-seawater at 21.520‰. Error bars represent 2σ due to errors of values of $k_1$ as described in Sect. S2. Grey symbols represent the data excluded for calculating the average.**

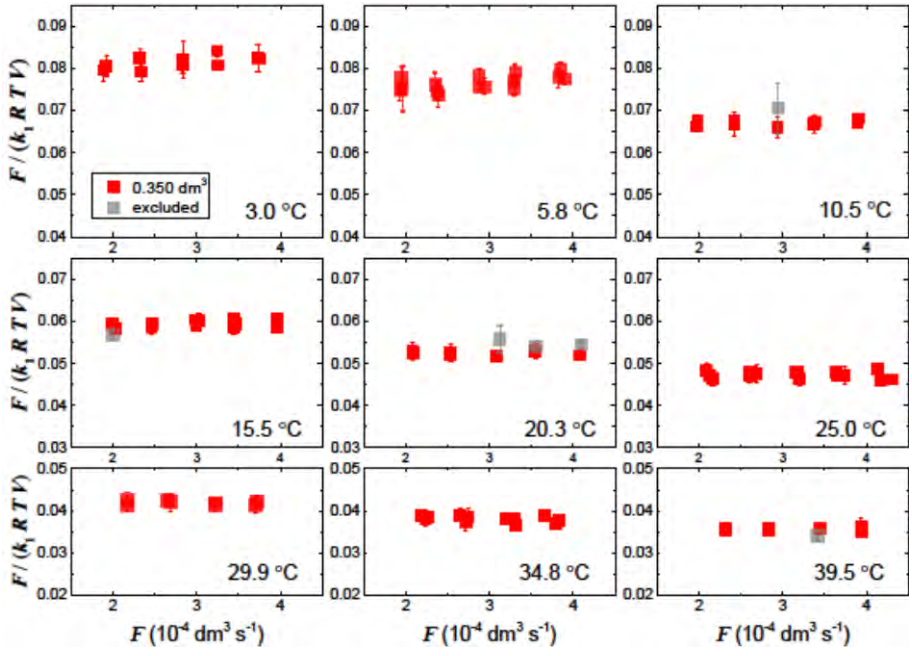


**Figure S8. Plots of values of $F/(k_1RTV)$ against $F$ at each temperature for 0.35 dm$^3$ of a-seawater at 51.534‰. Error bars represent 2σ due to errors of values of $k_1$ as described in Sect. S2. Grey symbols represent the data excluded for calculating the average.**

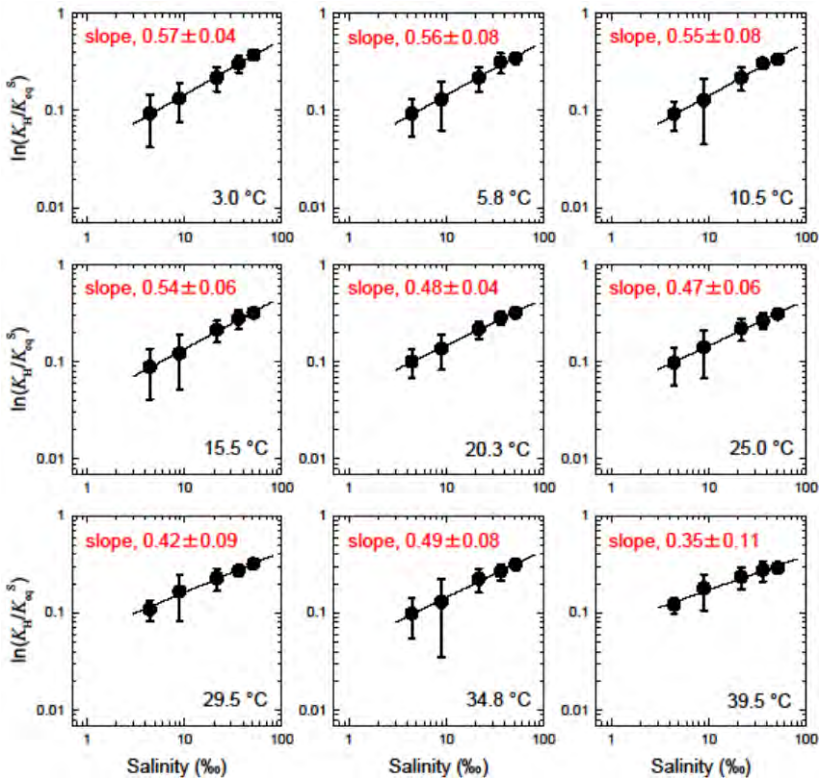


**Figure S9. log-log plots for $\ln(K_H(T)/$~~$K_H$~~ $^S\underline{K}_{eq}{}^S(T))$ vs. salinity in a-seawater at each temperature. Bold lines represent the fitting obtained by a liner regression. Errors are those at 95% confidence level for the regression only.**

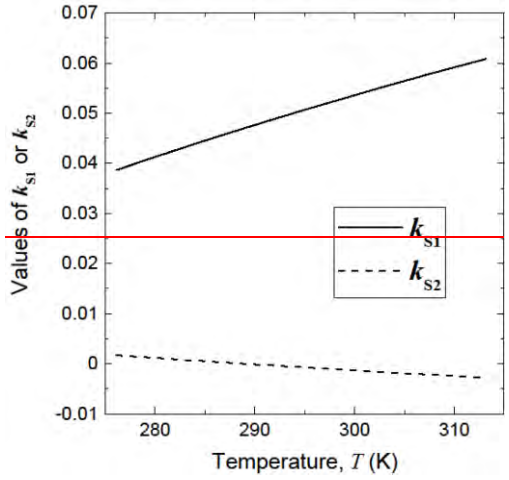


~~**Figure S10. Plots of $k_{s1}$ and $k_{s2}$ (coefficients in Eq. (18)) against temperature.**~~

**Table S2. Values of $k_s$ (Eq. (17)) and comparison of values of $K_{eq}^S$ calculated at each temperature by Eq. (17) with those by Eq. (22).**

| Temperature (°C) | $k_s$ (‰$^{-1}$) | [$K_{eq}^S$ from Eq. (17)]/ [$K_{eq}^S$ from Eq. (22)] | | | [$K_{eq}^S$ at 30‰]/ [$K_{eq}^S$ at 40‰] | |
|---|---|---|---|---|---|---|
| | | at 30‰ | at 35‰ | at 40‰ | Eq. (17) | Eq. (22) |
| 3.0 | 0.00811 | 1.027 | 1.008 | 0.988 | 1.084 | 1.043 |
| 5.8 | 0.00785 | 1.033 | 1.014 | 0.995 | 1.082 | 1.042 |
| 10.5 | 0.00768 | 1.033 | 1.016 | 0.997 | 1.080 | 1.042 |
| 15.5 | 0.00718 | 1.044 | 1.028 | 1.012 | 1.074 | 1.041 |
| 20.3 | 0.00728 | 1.037 | 1.020 | 1.003 | 1.076 | 1.040 |
| 25.0 | 0.00704 | 1.040 | 1.024 | 1.008 | 1.073 | 1.039 |
| 29.9 | 0.00731 | 1.027 | 1.010 | 0.992 | 1.076 | 1.039 |
| 34.8 | 0.00713 | 1.029 | 1.012 | 0.995 | 1.074 | 1.038 |
| 39.5 | 0.00709 | 1.026 | 1.010 | 0.992 | 1.073 | 1.038 |

**S5. Discussion of potential reason for this salting-out effect of $CH_2F_2$ solubility in a-seawater (deviation from Sechenov relationship)**

The reason that the salting-out effect of $CH_2F_2$ solubility in a-seawater depends on $S^{0.5}$ is not clear. Specific properties of $CH_2F_2$ –small molecular volume, which results in small work of cavity creation (Graziano, 2004; 2008), and large solute-solvent attractive potential energy in water and a-seawater− may cause deviation from Sechenov relationship. This possibility may be discussed here.

I calculate Ben-Naim standard Gibbs energy $\Delta G^{\bullet}$, enthalpy $\Delta H^{\bullet}$, and entropy $\Delta S^{\bullet}$ changes for dissolution of $CH_2F_2$ in water because these values correspond to the values for the transfer from a fixed position in the gas phase to a fixed position in water. Values of $\Delta G^{\bullet}$, $\Delta H^{\bullet}$, and $\Delta S^{\bullet}$ are calculated on the basis of the Ostwald solubility coefficient, $L(T)$, as follows.

$$\ln(L(T)) = \ln\left(RTK_{\mathrm{eq}}{}^{S}(T)\right) \quad \text{(B1)}$$

$$\Delta G^{\cdot} = R'T\ln(L(T)) \quad \text{(B2)}$$

$$\Delta H^{\cdot} = -\frac{\partial}{\partial(1/T)}\left(\frac{\Delta G^{\cdot}}{T}\right) \quad \text{(B3)}$$

$$\Delta S^{\cdot} = \frac{\Delta H^{\cdot} - \Delta G^{\cdot}}{T} \quad \text{(B4)}$$

where both $R$ and $R'$ represent gas constant but their units are different: $R$ = 0.0821 in atm dm$^3$ K$^{-1}$ mol$^{-1}$; $R'$ = 8.314 in J K$^{-1}$ mol$^{-1}$.

Combining Eqs. (B1), (B2), (B3), and (B4) with Eqs. (14) and (15), $\Delta G^{\bullet}$ (kJ mol$^{-1}$), $\Delta H^{\bullet}$ (kJ mol$^{-1}$), and $\Delta S^{\bullet}$ (J mol$^{-1}$ K$^{-1}$) are represented by $\Delta G_{\mathrm{sol}}$ and $\Delta H_{\mathrm{sol}}$ as follows:

$$\Delta G^{\cdot} = \Delta G_{\mathrm{sol}} + R'T\ln(RT) \quad \text{(B5)}$$

$$\Delta H^{\cdot} = \Delta H_{\mathrm{sol}} + R'T \quad \text{(B6)}$$

$$\Delta S^{\cdot} = \frac{\Delta H_{\mathrm{sol}} - \Delta G_{\mathrm{sol}}}{T} + R' - R'\ln(RT) \quad \text{(B7)}$$

Values of $\Delta G^{\bullet}$, $\Delta H^{\bullet}$, and $\Delta S^{\bullet}$ calculated at 298 K are listed in Table S3. Table S3 also lists values of $\Delta G^{\bullet}$, $\Delta H^{\bullet}$, and $\Delta S^{\bullet}$ reported for $CH_3F$ and $C_2H_6$ (Graziano, 2004) and $CH_4$ (Graziano, 2008) at 298 K. The chemicals, which having a methyl group, in Table S3 are classified into two groups ($CH_2F_2$ and $CH_3F$; $CH_4$ and $C_2H_6$) according to $\Delta G^{\bullet}$.

Table S3 lists values of $\Delta G_c$, $E_a$ and $\Delta H^h$ deduced using a scaled particle theory (Granziano, 2004; 2008). $\Delta G_c$ is the work of cavity creation to insert a solute in a solvent. $E_a$ is a solute-solvent attractive potential energy and accounts for the solute-solvent interactions consisting of dispersion, dipole-induced dipole, and dipole-dipole contributions. $\Delta H^h$ is enthalpy of solvent molecules reorganization caused by solute insertion. The solvent reorganization mainly involves a rearrangement of H-bonds.

$\Delta G_c$ is entropic in nature in all liquids, being a measure of the excluded volume effect due to a reduction in the spatial configurations accessible to liquid molecules upon cavity creation. Hence, $C_2H_6$ has larger value of $\Delta G_c$ than $CH_3F$ and $CH_4$. $\Delta G_c$, $E_a$, and $\Delta H^h$ are related to $\Delta G^{\bullet}$ and $\Delta H^{\bullet}$ as follows (Graziano, 2008):

$$\Delta G^{\cdot} = \Delta G_c + E_a \quad \text{(B8)}$$

$$\Delta H^{\cdot} = E_a + \Delta H^h \quad \text{(B9)}$$

Table S3 thus suggests that smaller value of $\Delta G^{\bullet}$ of $CH_3F$ than $CH_4$ is due to large solute-solvent attractive potential energy ($-E_a$) of $CH_3F$.

**Table S3. Ben-Naim standard hydration Gibbs energy $\Delta G^{\bullet}$, enthalpy $\Delta H^{\bullet}$, and entropy $\Delta S^{\bullet}$ changes for dissolution of $CH_2F_2$ at 298 K determined here and the corresponding values and values of $\Delta G_c$, $E_a$ and $\Delta H^h$ reported for $CH_3F$ and $C_2H_6$ (Granziano, 2004) and $CH_4$ (Graziano, 2008).**

| | $\Delta G^{\cdot}$ (kJ mol$^{-1}$) | $\Delta H^{\cdot}$ (kJ mol$^{-1}$) | $\Delta S^{\cdot}$ (J K$^{-1}$ mol$^{-1}$) | $\Delta G_c$ (kJ mol$^{-1}$) | $E_a$ (kJ mol$^{-1}$) | $\Delta H^h$ (kJ mol$^{-1}$) |
|---|---|---|---|---|---|---|
| $CH_2F_2$ | −1.1 | −14.7 | −45.4 | | | |
| $CH_3F$ | −0.9 | −15.8 | −50.0 | 23.3 | −24.3 | 8.5 |
| $CH_4$ | 8.4 | −10.9 | −64.7 | 22.9 | −14.5 | 3.7 |
| $C_2H_6$ | 7.7 | −17.5 | −84.5 | 28.4 | −20.7 | 3.2 |

Graziano (2008) definitively explained the salting-out of $CH_4$ by sodium chloride at molecular level on the basis of a scaled particle theory. He explained that $\Delta G_c$ increase was linearly related to the increase in the volume packing density of the solutions ($\xi_3$) with adding NaCl. Such an increase of $\Delta G_c$ is probably the case for salting-out of $CH_2F_2$ by a-seawater observed in this study. He also explained that $E_a$ was linearly related to the increase in $\xi_3$ assuming that a fraction of the dipole-induced dipole attractions could be taken into account by the parameterization of the dispersion contribution.

I think the possibility that $E_a$ may be nonlinearly related to the increase in $\xi_3$ because of dipole-dipole interaction between $CH_2F_2$ and solvents. Temperature dependence in Eq. (22) suggests that salting-out effect of $CH_2F_2$ by a-seawater is enthalpic. Eqs. (22) and (B9) thus suggests that the salting-out of $CH_2F_2$ is mostly related to change in $E_a$. $CH_2F_2$ has relatively small value of $\Delta G_c$ because of its small molecular volume compared to other chemicals such as $C_2H_6$. Accordingly, $\Delta G^{\bullet}$, that is, solubility of $CH_2F_2$ would depend on $E_a$ rather than $\Delta G_c$. Therefore, I think that specific properties of $CH_2F_2$ – small molecular volume, which results in small work of cavity creation (Graziano, 2004; 2008), and large solute-solvent attractive potential energy in water and a-seawater– may cause deviation from Sechenov relationship.

## References


Graziano, G.: Case study of enthalpy–entropy noncompensation. Journal of Chemical Physics, 120, 4467-4471, doi: 10.1063/1.1644094, 2004.

Graziano, G.: Salting out of methane by sodium chloride: A scaled particle theory study. Journal of Chemical Physics, 129, 084506, doi: 10.1063/1.2972979, 2008.

## S6. Estimated results (Sect. 3.3) for monthly amount of $CH_2F_2$ dissolved in the ocean mixed layer at solubility equilibrium with the atmospheric $CH_2F_2$ (1 patm) and the depth distribution of the $CH_2F_2$ dissolved in each semi-hemisphere

**Table S4. Monthly amount of $CH_2F_2$ dissolved in the ocean mixed layer at solubility equilibrium with the atmospheric $CH_2F_2$ (partial pressure, 1 patm) and the depth distribution of the $CH_2F_2$ dissolved in the southern semi-hemisphere (90° S - 30° S).**

| | Amount (Gg patm$^{-1}$) | Distribution of the amount of $CH_2F_2$ dissolved in the ocean mixed layer with respect to the ocean mixed layer depth (%) | | | | | |
|---|---|---|---|---|---|---|---|
| | | 10 - 100 m | 100 - 200 m | 200 - 300 m | 300 - 400 m | 400 - 500 m | 500 - 600 m |
| January | 0.0169 | 94.9 | 2.9 | 1.0 | 0.5 | 0.3 | 0.3 |
| February | 0.0201 | 92.1 | 3.6 | 2.9 | 1.0 | 0.3 | 0.0 |
| March | 0.0255 | 87.8 | 9.2 | 1.7 | 0.7 | 0.2 | 0.4 |
| April | 0.0338 | 66.5 | 31.8 | 1.1 | 0.2 | 0.1 | 0.2 |
| May | 0.0409 | 48.5 | 48.1 | 2.2 | 0.8 | 0.3 | 0.0 |
| June | 0.0510 | 26.8 | 62.7 | 8.0 | 1.7 | 0.8 | 0.1 |
| July | 0.0571 | 14.1 | 69.3 | 12.2 | 3.3 | 0.9 | 0.1 |
| August | 0.0640 | 8.5 | 65.8 | 17.0 | 6.2 | 2.3 | 0.2 |
| September | 0.0609 | 13.5 | 61.0 | 14.6 | 8.2 | 2.7 | 0.0 |
| October | 0.0504 | 24.7 | 58.6 | 12.1 | 2.9 | 1.4 | 0.3 |
| November | 0.0335 | 60.4 | 30.5 | 4.6 | 2.2 | 2.3 | 0.1 |
| December | 0.0196 | 95.1 | 4.3 | 0.4 | 0.2 | 0.0 | 0.0 |

**Table S5. Monthly amount of $CH_2F_2$ dissolved in the ocean mixed layer at solubility equilibrium with the atmospheric $CH_2F_2$ (partial pressure, 1 patm) and the depth distribution of the $CH_2F_2$ dissolved in the southern semi-hemisphere (30° S - 0° S).**

| | Amount (Gg patm$^{-1}$) | Distribution of the amount of $CH_2F_2$ dissolved in the ocean mixed layer with respect to the ocean mixed layer depth (%) | | | | | |
|---|---|---|---|---|---|---|---|
| | | 10 - 100 m | 100 - 200 m | 200 - 300 m | 300 - 400 m | 400 - 500 m | 500 - 600 m |
| January | 0.0084 | 99.6 | 0.4 | 0 | 0 | 0 | 0 |
| February | 0.0084 | 99.7 | 0.3 | 0 | 0 | 0 | 0 |
| March | 0.0089 | 100.0 | 0 | 0 | 0 | 0 | 0 |
| April | 0.0106 | 100.0 | 0 | 0 | 0 | 0 | 0 |
| May | 0.0131 | 100.0 | 0 | 0 | 0 | 0 | 0 |
| June | 0.0163 | 97.1 | 2.9 | 0 | 0 | 0 | 0 |
| July | 0.0189 | 80.1 | 19.9 | 0 | 0 | 0 | 0 |
| August | 0.0193 | 73.1 | 26.9 | 0 | 0 | 0 | 0 |
| September | 0.0165 | 82.2 | 17.8 | 0 | 0 | 0 | 0 |
| October | 0.0124 | 94.6 | 5.4 | 0 | 0 | 0 | 0 |
| November | 0.0097 | 99.9 | 0.1 | 0 | 0 | 0 | 0 |
| December | 0.0087 | 100.0 | 0 | 0 | 0 | 0 | 0 |

**Table S6. Monthly amount of $CH_2F_2$ dissolved in the ocean mixed layer at solubility equilibrium with the atmospheric $CH_2F_2$ (partial pressure, 1 patm) and the depth distribution of the $CH_2F_2$ dissolved in the northern semi-hemisphere (0° N - 30° N).**

| | Amount (Gg patm$^{-1}$) | Distribution of the amount of $CH_2F_2$ dissolved in the ocean mixed layer with respect to the ocean mixed layer depth (%) | | | | | |
|---|---|---|---|---|---|---|---|
| | | 10 - 100 m | 100 - 200 m | 200 - 300 m | 300 - 400 m | 400 - 500 m | 500 - 600 m |
| January | 0.0132 | 96.4 | 3.6 | 0 | 0 | 0 | 0 |
| February | 0.0126 | 95.9 | 4.1 | 0 | 0 | 0 | 0 |
| March | 0.0107 | 98.7 | 1.3 | 0 | 0 | 0 | 0 |
| April | 0.0087 | 99.8 | 0.2 | 0 | 0 | 0 | 0 |
| May | 0.0079 | 100.0 | 0 | 0 | 0 | 0 | 0 |
| June | 0.0080 | 100.0 | 0 | 0 | 0 | 0 | 0 |
| July | 0.0084 | 100.0 | 0 | 0 | 0 | 0 | 0 |
| August | 0.0082 | 100.0 | 0 | 0 | 0 | 0 | 0 |
| September | 0.0080 | 100.0 | 0 | 0 | 0 | 0 | 0 |
| October | 0.0086 | 100.0 | 0 | 0 | 0 | 0 | 0 |
| November | 0.0100 | 100.0 | 0 | 0 | 0 | 0 | 0 |
| December | 0.0118 | 100.0 | 0 | 0 | 0 | 0 | 0 |

**Table S7. Monthly amount of $CH_2F_2$ dissolved in the ocean mixed layer at solubility equilibrium with the atmospheric $CH_2F_2$ (partial pressure, 1 patm) and the depth distribution of the $CH_2F_2$ dissolved in the northern semi-hemisphere (30° N - 90° N).**

| | Amount (Gg patm$^{-1}$) | Distribution of the amount of $CH_2F_2$ dissolved in the ocean mixed layer with respect to the ocean mixed layer depth (%) | | | | | |
|---|---|---|---|---|---|---|---|
| | | 10 - 100 m | 100 - 200 m | 200 - 300 m | 300 - 400 m | 400 - 500 m | 500 - 600 m |
| January | 0.0205 | 41.3 | 50.1 | 7.0 | 1.4 | 0.2 | 0.0 |
| February | 0.0225 | 34.5 | 55.3 | 7.1 | 2.3 | 0.6 | 0.2 |
| March | 0.0208 | 49.7 | 42.3 | 4.9 | 1.7 | 0.7 | 0.6 |
| April | 0.0147 | 79.7 | 17.6 | 1.7 | 0.4 | 0.0 | 0.6 |
| May | 0.0081 | 90.1 | 9.9 | 0 | 0 | 0 | 0 |
| June | 0.0055 | 97.7 | 2.3 | 0 | 0 | 0 | 0 |
| July | 0.0045 | 96.6 | 3.4 | 0 | 0 | 0 | 0 |
| August | 0.0048 | 94.4 | 5.6 | 0 | 0 | 0 | 0 |
| September | 0.0059 | 97.7 | 2.3 | 0 | 0 | 0 | 0 |
| October | 0.0084 | 99.6 | 0.4 | 0 | 0 | 0 | 0 |
| November | 0.0121 | 89.6 | 10.4 | 0.1 | 0 | 0 | 0 |
| December | 0.0163 | 71.0 | 26.1 | 2.9 | 0 | 0 | 0 |